

KATHOLIEKE UNIVERSITEIT LEUVEN
FACULTEIT INGENIEURSWETENSCHAPPEN
DEPARTEMENT CHEMISCHE INGENIEURSTECHNIEKEN
W. de Croylaan 46 - 3001 Leuven (Belgium)

INFLUENCE OF PROCESSING CONDITIONS ON THE STRUCTURE DEVELOPMENT IN PEBAX®

Promotoren:
Prof. J. MEWIS
Prof. P. VAN PUYVELDE
Prof. T. HASHIMOTO

Proefschrift voorgedragen tot
het behalen van het doctoraat
in de ingenieurswetenschappen
door
Bruno TAVERNIER

Jan 2009



KATHOLIEKE UNIVERSITEIT LEUVEN
FACULTEIT INGENIEURSWETENSCHAPPEN
DEPARTEMENT CHEMISCHE INGENIEURSTECHNIEKEN
W. de Croylaan 46 - 3001 Leuven (Belgium)

INFLUENCE OF PROCESSING CONDITIONS ON THE STRUCTURE DEVELOPMENT IN PEBAX®

Jury:
Prof. Y. Willems, voorzitter
Prof. J. Mewis, promotor
Prof. P. Van Puyvelde, promotor
Prof. T. Hashimoto, promotor
Prof. P. Moldenaers
Prof. B. Goderis
Prof. G. Peters
Prof. J. Degrève

Proefschrift voorgedragen tot
het behalen van het doctoraat
in de ingenieurswetenschappen

door

Bruno TAVERNIER

UDC 66.095.26 Jan 2009

© Katholieke Universiteit Leuven - Faculteit Ingenieurswetenschappen
Arenbergkasteel, B-3001 Leuven (Belgium)

Alle rechten voorbehouden. Niets uit deze uitgave mag worden vermenigvuldigd en/of openbaar gemaakt worden door middel van druk, fotocopie, microfilm, elektronisch of op welke andere wijze zonder voorafgaandelijke schriftelijke toestemming van de uitgever.

All rights reserved. No part of the publication may be reproduced in any form by print, photoprint, microfilm or any other means without written permission from the publisher.

D/2009/7515/5

ISBN 978-94-6018-022-4

Acknowledgments

I would like to thank all the people who contributed, directly or indirectly, to the completion of this thesis.

My gratitude will first go to my promotors, Prof. Jan Mewis, Prof. Takeji Hashimoto and Prof. Peter Van Puyvelde, for their support and for sharing their experience and knowledge.

I am also grateful to my assessors, specially Prof. Bart Goderis, for in-depth reading of this manuscript and for their useful suggestions.

I would like to acknowledge Arkema for funding my research, its research staff for their helpful discussions, and K.U. Leuven for providing scholarship for additional five months to complete this work.

I am thankful to all my colleagues from the applied rheology laboratory at KU Leuven and from the polymer mechanics laboratory at Kyoto University for the pleasant work atmosphere. I am especially grateful to Basavaraja Madivala and Satoshi Akasaka who have provided assistance in numerous ways.

Enfin, du fond du coeur, un grand merci à mes parents et à mes frères sans qui je ne serais jamais allé aussi loin dans mes études.

Bruno Tavernier

Abstract

Industrial processing of polymers can involve complex conditions and materials. Therefore, prediction and control of the properties are not always well understood. It sometimes happens that unwanted phenomena occur in the final product. In order to minimize as much as possible such problems, investigation of the conditions leading to various morphologies is required. In this thesis, the focus is on the delamination phenomenon which causes a peeling of injected pieces. Here, we seek to understand what kind of morphology is responsible for delamination in injected pieces. Various techniques such as X-ray and light scattering, optical and electron microscopy, rheology and calorimetry have been used to investigate the different length scales of matter organization. The material under consideration is a polyamide/polytetramethylene-glycol copolymer with a high content of polyamide.

The first approach consists in studying the morphologies of that material as a function of temperature and shear. Two kinds of organized states were observed. The first one results from the natural tendency of the different segments to segregate leading to a microphase separation in the molten state. A microphase separation in the molten state is observed. However, the time required for such an organization to appear is so large that this morphology is very unlikely to be involved in the delamination phenomenon. On the other hand, the semi-crystalline state which originates from the fast crystallization of the polyamide segments may play a role. A comparative study of the crystallization after applying flow to the neat polyamide and to the multiblock shows that the latter is not very sensitive to the imposed shear. As a consequence, no large changes in crystalline morphology are expected during injection and hence trans-crystallinity is not likely to be a source of decohesion and hence of delamination.

The second approach takes into account that the real material used during injection molding is in a fact a mixture of two chemically similar multiblocks. For practical reasons, additives such as antimony oxide (flame retardant), carbon black (enhanced electroconductivity), dyes (coloration), zinc oxide (prevents the photo-oxidation) are required to produce performance materials. In the case of the

polymer investigated, the additives are introduced via the use of a soft multiblock. It was observed that the two materials are partially miscible and it was predicted that with the conditions imposed during injection, fibrils made of the dispersed phase are expected to be present in the final pieces. This was confirmed by the observation of injected pieces by means of transmission electron microscopy. Such a morphology is very likely to be responsible for the delamination since it produces a discontinuity in the piece over a large scale. A relatively simple experiment in real injection conditions is suggested to confirm the previous assumption. Finally, based on this study, suggestions are made to suppress or diminish the probability of producing delaminating pieces.

Table of contents

1 State of the art **16**

1.1 Thermoplastic elastomers 16

1.2 Pebax ® block copolymers 20

1.3 Delamination 21

1.4 Flow-induced crystallization 24

1.4.1 Homopolymers 24

1.4.2 Copolymers 29

1.5 Two-phase flows 30

1.5.1 Deformation 31

1.5.2 Break-up 31

1.5.3 Coalescence 32

2 Materials and methods **34**

2.1 Materials 34

2.1.1 7033 SA - Multiblock copolymer 34

2.1.2 PA12 - Homopolymer 35

2.1.3 3533 SA - Multiblock copolymer 36

2.2 Methods 37

2.2.1 X-ray scattering 37

2.2.2 Rheology 38

2.2.3 Optical experiments 39

2.2.4 Differential scanning calorimetry 39

2.2.5 Transmission electron microscopy 41

3 Influence of thermal history 42

3.1 Transition temperatures 42
3.2 Morphology in the ordered states 48
3.3 Investigation of the morphologies 53
3.4 Structural interpretation 63
3.5 Conclusions 65

4 Influence of thermomechanical history 67

4.1 Extracting data from small angle light scattering 67
4.1.1 Stein-Wilson theory [170] 68
4.2 Use of the Stein-Wilson model 72
4.3 Quiescent crystallization 79
4.3.1 Effect of temperature - Optical microscopy 79
4.3.2 Effect of temperature - Small angle light scattering 85
4.3.3 Discussion on quiescent crystallization of PA12 and 7033 SA 88
4.4 Crystallization under shear 90
4.4.1 Effect of shear - Optical microscopy 91
4.4.2 Effect of shear - Small Angle Light Scattering 96
4.4.3 Conclusions on the effect of shear on crystallization of PA12 and 7033 SA 97

5 Study of 7033 SA blends 100

5.1 Brief material description 100
5.2 Probing the blend character by means of rheology 101
5.2.1 Probing the blend character 101
5.2.2 Droplet relaxation 104
5.2.3 Viscosity ratio measurements 107
5.3 Direct observation of the blends 115
5.3.1 Discrimination of dispersed phase 115
5.3.2 Observation of the blends 116
5.3.3 Observation of a sheared sample 116
5.4 Conclusions 119

6 General conclusions **121**

The bibliography **126**

List of symbols

Symbol	*Description*	*Units*
B	radius of a fibril	[m]
B_0	constant in eq. 1.2	[K]
C_a	capillary number	[-]
d	domain spacing	[m]
d_c	lamellar thickness	[m]
G'	storage modulus	[Pa]
G''	loss modulus	[Pa]
G^*	complex modulus	[Pa]
h_c	critical thickness	[m]
I	intensity	[$e^2.nm^{-3}$]
I_0	intensity scaling factor	[$e^2.nm^{-3}$]
I_m	intensity of the maximum of scattering	[$e^2.nm^{-3}$]
k_B	Boltzmann constant	[$J.K^{-1}$]
K	temperature scaling factor	[K]
L	long semi-axis of an ellipsoid	[m]
M_N	number average molecular weight	[$g.mol^{-1}$]
M_W	weight average molecular weight	[$g.mol^{-1}$]
N	degree of polymerization	[-]
p	viscosity ratio	[-]

Symbol	*Description*	*Units*
q	scattering vector	[m^{-1}]
q_m	position of the maximum of scattering	[m^{-1}]
Q_η	density invariant	[-]
Q_δ	orientation invariant	[-]
r	distance	[m]
R	radius	[m]
R	gas constant	[$J.K^{-1}.mol^{-1}$]
R_g	radius of gyration	[m]
t	time	[s]
$t_{1/2}$	half-time of crystallization	[s]
T	temperature	[K]
T_A	activation temperature	[K]
T_c	crystallization temperature	[K]
T_g	glass transition temperature	[K]
T_m	melting temperature	[K]
T_{m0}	equilibrium melting temperature	[K]
T_{ODT}	order-disorder transition temperature	[K]
T_V	Vogel-Fulcher temperature	[K]

Greek Symbol	*Description*	*Units*
α	crystalline form	[-]
α'	crystalline form	[-]
α	polarizability	[C.m^2.V^{-1}]
$\overline{\alpha}$	mean polarizability	[C.m^2.V^{-1}]
β	crystalline form	[-]
γ	deformation	[-]
γ	crystalline form	[-]
γ'	crystalline form	[-]
$\dot{\gamma}$	shear rate	[s^{-1}]
δ	anisotropy	[-]
$\overline{\delta}$	mean anisotropy	[-]
η	mean polarizability fluctuation	[C^2.m^2.J^{-1}]
η	viscosity	[Pa.s]
η_0	Newtonian viscosity	[Pa.s]
η_d	dispersed phase viscosity	[Pa.s]
η_m	matrix viscosity	[Pa.s]
θ	scattering angle	[°]
ϑ	monomer volume	[m^3]
λ	wave length	[m]
ξ	correlation length	[m]
ρ	electronic density	[C.m^{-3}]
σ	standard deviation in eq. 3.4	[m]
σ	excess of free energy per unit area	[J.m^{-2}]
τ	relaxation time	[s]
τ	shear stress	[Pa]
ϕ	volume fraction	[-]
χ	Flory-Huggins parameter	[-]
ω	frequency	[rad.s^{-1}]
Γ	interfacial tension	[N.m^{-1}]
Δ_m^f	heat of fusion per monomer	[J.g^{-1}]
Ω	constant in eq. 5.12	[-]

Introduction

Polymeric materials are used in a wide range of products ranging from very simple decorative objects to highly technological applications such as chips manufacturing or medical prostheses. In a permanent drive towards quality improvement, two approaches are commonly followed. The first one consists of synthesizing new monomers that provide new properties or combinations of properties. Although this approach is efficient, it is most often not feasible economically, considering the cost of developing and introducing a new polymer. For this reason, a second approach seems to be more attractive. Starting from well known monomers, new materials can be obtained by combining two or more polymers. This is practically done by either blending or by creating copolymers. The thus formed materials will have properties dependent on the nature of the molecules used, their ratio and their relative position. The morphology formed by the multiphasic structure is strongly related to the relative amount of the components. The organization of matter adds features to the material that are not present in the separate components alone. However, mixing of polymers does not only provide advantages. Sometimes, the morphology can be seen as a defect or a weakness in a given application. This could range from undesired gas permittivity to unacceptable weakening of the bulk. Therefore, the morphology that is formed during processing should be investigated carefully.

Objectives

In this work, the focus is on a particular polyamide-poly(tetramethylene-glycol) multiblock copolymer. Since the polyamide block is able to crystallize, structures that form at high temperatures may be altered or frozen when the material crystallizes at lower temperatures. Hence, external stresses, which have a temporary effect in a molten material, might have a permanent effect on the final morphology. Therefore, the combined study of flow and temperature will be important since these are the main two parameters involved in the processing of polymers. Attention will be given to:

- the morphology as a function of temperature;
- the morphology generated under shear conditions;
- the morphology resulting from the blending of the copolymer with a given amount of another copolymer. This is especially important when considering the compounding with a masterbatch carrier.

This investigation will result in the description of the structure formation and its kinetics. The understanding of the morphology development is of importance since it might allow to bring a solution for an industrial problem. Indeed, when performing injection molding on the material under study, it has been observed that sometimes delamination occurs. Since this phenomenon clearly depends on the morphology, it is hoped that this study will shed some light on the underlying mechanisms responsible for this problem.

Approach

This study is performed on a commercial polymer. This is a serious drawback if one wants to generate generic information about the morphology development. Clearly, commercial materials contain various impurities/additives and the molecular structure is not always well defined. To overcome this drawback, various experimental techniques to probe various length scales in the material can be used to obtain a general picture of the structure generation. Such an approach will indeed be followed throughout this study.

This work is organized as follows. The state of the art describes the global properties of the polymers used. Current knowledge of the phenomena encountered in polymers and their blends is briefly reviewed. Chapter 2 presents the materials as well as details of the experimental methods. In chapter 3, the effect of temperature on the morphology of the multiblock copolymer and its kinetics is studied. In chapter 4, the crystallization of the multiblock copolymer is investigated. The influence of shear on the kinetics and on the final morphology is discussed as well. Chapter 5 deals with the two-phase character of the structure, when a mixture with a masterbatch carrier is used. Finally, the conclusions drawn from this work, and solutions to the delamination problem are summarized in chapter 6.

Chapter 1

State of the art

In this chapter, thermoplastic elastomers are reviewed. The problem of delamination is presented and its possible causes highlighted. Basically, two major causes can be put forth: the first one is related to the creation of a heterogeneous structure due to the flow-induced crystallization. A second possible reason is related to a two-phase structure that might be present when Pebax ® is processed with its masterbatch-carrier. These two potential causes are briefly touched upon.

1.1 Thermoplastic elastomers

Definition

Historically, the first commercial thermoplastic elastomers (TPE's), based on styrenic block copolymers, became available in 1965 and since this time a plethora of new variations of such materials have become available. The formal definition of a thermoplastic rubber or elastomer is a polymer blend or compound which exhibits a thermoplastic character above its melting temperature that enables it to be processed as a melt. In addition, such material possesses an elastomeric behavior within its design temperature range. The crosslinking process is reversible and hence the products can be reprocessed. For that reason, TPE's are also called 'virtually cross-linked polymers' [1, 2]. When considering multiblock copolymers as TPE's, the thermodynamic incompatibility between the different blocks leads to peculiar structures.

Phase behavior

Multiblock copolymers are often made of chemically different soft and hard segments, linked together by covalent bonds. The soft segment can be an amorphous or a semi-crystalline polymer that exhibits elastomer-like properties at service temperature whereas the hard segment component for instance consists of a crystallisable material. The hard segments take care of the cohesion of the bulk, playing the role of physical crosslinking points. The polymers under consideration here can be remelted because of the non-permanent character of the crosslinking in contrast to for instance thermoset materials. Such multiblock copolymers are therefore called thermoplastic elastomers (TPE).

Because dissimilar block components are usually incompatible with one another, they will tend to segregate. However, instead of a macrophase separation, i.e. a phase separation at a large scale (micrometer and above), the segregation can only take place on a local scale (of the order of the size of the blocks) since the blocks are linked by a covalent bond. This type of phase separation is called 'microphase separation'.

The degree of microphase separation is often expressed by the so-called segregation power. The latter can be approximated by χ^{N} in which χ represents the Flory interaction parameter of the block materials and N the degree of polymerization (i.e. the total length of the molecule). This approach has been used by many authors to calculate the phase diagram of block copolymers [3–7]. Especially in the case of diblocks, detailed information about structure formation is available. An example of a phase diagram as a function of the volume fraction of one component A is shown in Figure 1.1. As can be seen in this figure, a broad variety of morphologies can be generated, depending on the temperature and relative size of the blocks. The knowledge of the phase diagram is important from a practical point of view, since the structural organization will determine to a large extent the final properties of the material. In the case of multiblocks, the calculation of the phase diagram becomes more complicated but the fundamentals remain the same [8, 9].

Temperature dependence

The morphology of the material, and hence its properties, strongly depend on the ratio of the constitutive segments. Typically, the stiffness of the material can be tuned by changing the ratio of hard/soft phases. The higher the hard phase content, the harder will be the TPE. However, not only the ratio but also the choice of a particular polymer will influence the final mechanical properties of the designed TPE. Important parameters, such as transition temperatures, depend on the nature of the constituents themselves. Two temperatures are usually considered. The

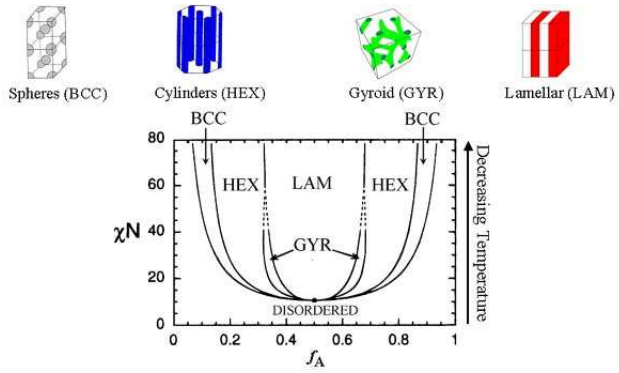


Figure 1.1: Phase diagram of a diblock copolymer as a function of the volume fraction f_A of block A [10]

first one is the glass transition T_g below which long range molecular movements are impossible. The other important temperature, in the case of semi-crystalline polymers, is the melting temperature T_m.

The existence of these two temperatures implies that the flexural modulus of TPE's, when measured over a range of temperatures, will exhibit three distinct regions (see Figure 1.2). At very high temperatures, both elastomer and hard phase are molten. At intermediate temperatures the hard phase is 'frozen' because of the crystallization. And finally, at very low temperatures both components are below their glass transition temperature, leading to a stiff material. Therefore, TPEs have two service temperatures, the T_g of the elastomer phase and the T_m of the hard phase.

Aside from the glass transition temperature (T_g) and the melting temperature (T_m), another transition temperature can be detected in block copolymers [11]. Since multiblocks are by definition made of different segments, it is possible to find structures formed by segregation of the segments. This situation can even be achieved when the temperature is raised above the melting temperature of the hard phase. This implies that a local structure is present even when the material is molten. Obviously, the stability of such kind of morphology has some limits and above a certain temperature, due to thermal agitation, the segments can mix and form a single disordered phase. This temperature is called the order-disorder transition temperature (T_{ODT}) [12]. Knowing this transition temperature is of importance since it indicates where a material can be structured, even if in the molten state. It is thus relevant for investigating the morphologies of the material, as well as for defining the kind of properties one can expect. The T_{ODT} can be detected by means of several techniques such as rheology, DSC and X-ray

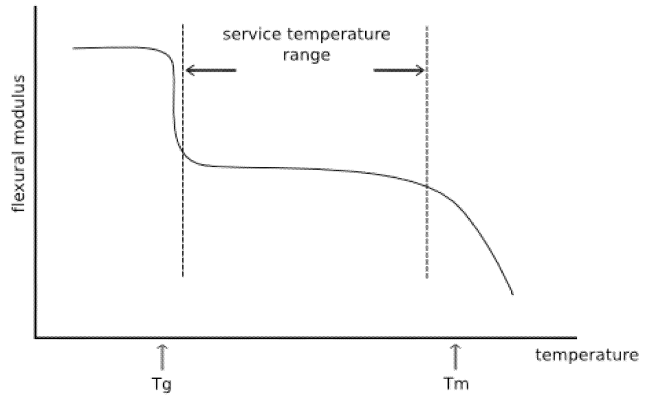


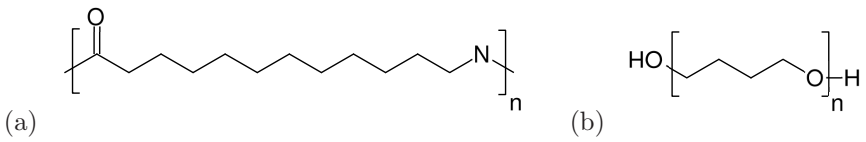
Figure 1.2: Stiffness of thermoplastic elastomer as a function of temperature

scattering [13–18]. A brief overview of the different techniques is given below.

When the ordered state is well defined, a simple way to estimate the T_{ODT} consists in recording the SAXS profile during a slow temperature scan. In the ordered state, a clear peak is observed, and in the disordered state this peak should vanish. Hence, the temperature at which the change occurs can be considered to be the T_{ODT} [19].

It is also possible to determine the T_{ODT} using rheology. The method is based on the response of an ordered material to flow versus the one of its disordered counterpart. More precisely, plots of G' vs. G" as a function of temperature should coincide in the disordered state and when a structure appears, a deviation is expected to occur. The temperature at which curves of G' vs. G" cease to be independent of temperature can therefore be regarded as T_{ODT}. This method was initially proposed by Han et al. [15] and has proven to be in agreement with the SAXS determination for other multiblock copolymers, such as for instance poly(ether-ester) multiblock copolymers (see [20–22]).

DSC allows to measure the position of T_{ODT} in a similar way as T_m. Starting from an ordered state, increasing gradually the temperature will at some point result in a mixing of the phases, i.e. the material will be in a disordered state. In such an experiment, the energy required to destroy the ordered state is observed as an endotherm. The position of this endotherm is then associated with the T_{ODT} [14, 23, 24].



(a) (b)

Figure 1.3: (a) PA12 molecule (b) PTMG molecule

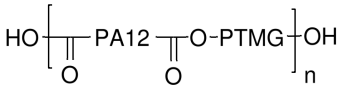


Figure 1.4: Pebax ® molecule

1.2 Pebax ® block copolymers

Pebax ®, the commercial material under study in this work, is an example of a thermoplastic elastomer [25]. The hard segments consist of polyamide 12 (PA12) and the soft segments of poly(tetra-methylene glycol) (PTMG) (see Figures 1.3 and 1.4). The usual application temperature is well above the glass transition temperature of PTMG which hence provides the flexibility of the material. At room temperature, PA12 is in a semi-crystalline state and its crystals act as virtual cross-links, ensuring the cohesion of the material. At high temperatures, however, PA12 crystals will melt. Hence, it is possible to obtain an amorphous melt that can be easily processed using conventional polymer processing machines. Therefore, this combination of hard and soft segments gives a class of materials with unique properties that can be tuned by adjusting the chemical structure of the polymers and by controlling the multiphase structure during processing.

Figure 1.5 represents a schematic overview of the production process. Pebax ® is prepared by means of a molten state polycondensation reaction [26]. Dicarboxylic polyamide, coming from a prepolymerization reaction is fed to a reactor in which it is catalytically reacted with poly(ether)diol. The final molecular properties of the resulting Pebax ® are to a large extent determined by the OH/COOH ratio. The reaction is conducted under vacuum conditions in order to remove H_2O, a side product of the polycondensation, from the mixture. More details about the impact of the synthesis on the material properties are given in the Materials and methods chapter. After granulation, the pellets are mixed in a vacuum dryer with a small amount of another polymer ($\backsim$3.5% in mass) containing all necessary additives. This polymer carrying the additives is called the masterbatch carrier.

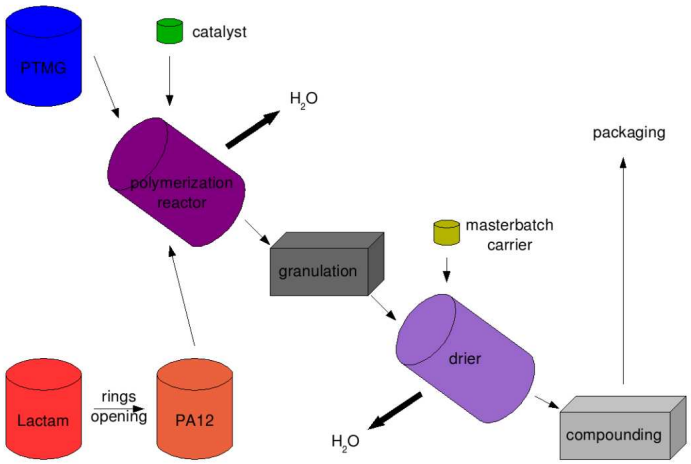


Figure 1.5: Processes leading to the commercially available Pebax

Finally, the dry mixture is compounded in order to evenly distribute the additives in the Pebax ®.

It needs to be stressed that, since additives are much easier to add (diffusion is faster) into soft grade materials, the masterbatch carrier is most often a low molar Pebax ® which serves as a 'general' carrier for most of the Pebax ® grades. For that reason, when a hard grade Pebax ® is produced, the final product is a mixture of hard grade Pebax ® (96.5% in mass) and a small amount of soft grade. The question arises whether this low molar mass carrier is fully compatible with its higher molar mass equivalent. This issue is of critical importance since properties of the material may be different if macrophase separation occurs. The blend character of such mixtures as well as the resulting structure are discussed in Chapter 5. Another important aspect of the process must be highlighted. Since the reaction of the prepolymers is catalytic, the final product will unavoidably contain catalyst traces. The influence of such impurities on the crystallization behavior will be touched upon in Chapter 4.

1.3 Delamination

Pebax ® is widely used in sport and leisure applications. It is easy to color, easy to process, and has very good mechanical properties. More precisely, Pebax ®

is intensively used in sport shoe soles as an impact cushioner. Such pieces are usually processed by injection molding. Therefore, the material experiences high shear and rapid temperature changes. Hence, the structure/organization formed in the polymer is induced by both temperature and shear conditions. Usually, injected parts are relatively thin (about 1 mm) and it is sometimes found that a thin layer can be peeled off. This phenomenon is called delamination, and in injection-molded parts it refers to the splitting or peeling off from regions of the surface. This phenomenon is well known in the injection molding community and is typically attributed to two possible causes. The inadequate bonding might be caused by excessive shearing of a relatively cold melt, in combination with intensive cooling. In the case of semi-crystalline polymers, this might give rise to formation of layers having different crystal structures. A second reason is often associated with a contamination of the resin by another undesirable material.

Delamination can also occur in Pebax ® under certain injection molding conditions. An image, taken by optical microscopy, of a delaminating injected piece is shown in Figure 1.6. As can clearly be observed, voids are present, leading to the delamination phenomenon. The latter observation is closely related to the flow profile in an injection molded part, as schematically shown in Figure 1.7. When a polymer melt is injected in a cold mold, the layers in contact with the walls will solidify almost instantaneously and will form a skin layer. The material flows in a so-called fountain flow profile. Figure 1.7 shows the shear rate profile ($d\gamma/dt$). As can be seen on this figure, the shear rate reaches a maximum in the liquid layer in the neighborhood of the skin layer. Depending on the injection molding conditions (injection speed, T_{wall}, T_{melt}), the position of this maximum might vary. The presence of the void is typically observed in this region, pointing towards the importance of flow induced phenomena. Taking these considerations into account, two hypotheses can be put forth to explain the delamination in Pebax ®.

- Shear-induced crystallization

As explained above, the typical explanation of delamination is related to excessive shearing that might lead to variations in crystalline structures throughout the thickness of the part. Shear is known to interfere with the crystallization process [28]. Indeed, in homopolymers, shear has been found to increase the kinetics of the process (see section 1.4). In addition, shear can also affect the crystalline structure. Extremely high shear conditions, as the ones obtained in injection molding might even lead to the formation of shish-kebabs. In this hypothesis, it remains to be verified to what extent shear will have an influence on the behavior of Pebax ® during solidification.

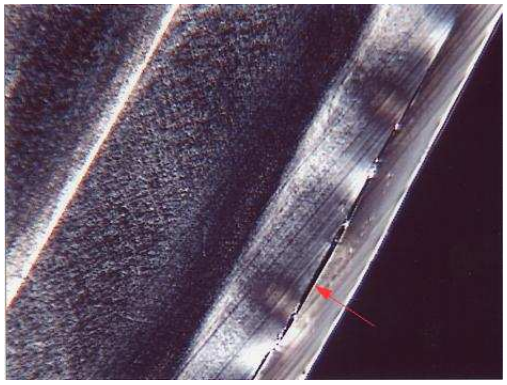


Figure 1.6: Delamination in injected pieces [27]

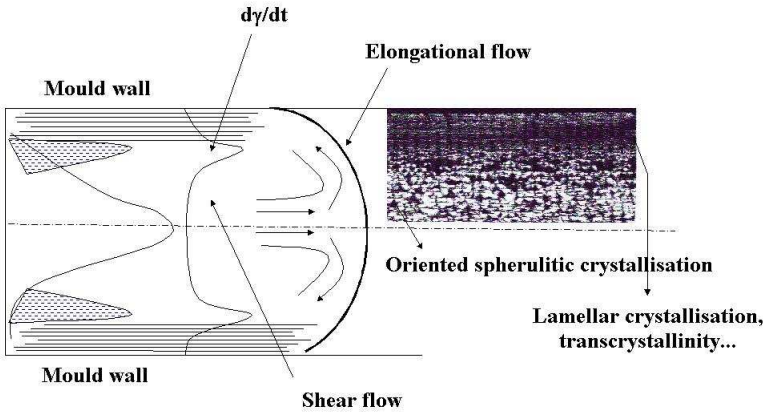


Figure 1.7: Velocity and shear profile during injection [27]

- Two-phase flow

The second hypothesis is related to the contamination argument. Indeed, the masterbatch carrier being a 'soft' Pebax ®, it is assumed that this is fully compatible with the virgin material. However, this statement cannot be made a priori and it might be anticipated that the incorporation of the masterbatch carrier leads to a two-phasic structure blend. During injection molding, a high shear might lead to fibrillation of the dispersed phase which may weaken the material.

In the next paragraphs, a brief literature review of the above two aspects will be given. In this context, a full description of flow-induced crystallization or structure development in polymer blends is not required and only the important issues related to the experimental data will be mentioned.

1.4 Flow-induced crystallization

One hypothesis of the origin of the delamination phenomenon is the shear-induced crystallization. It is thought that during injection molding the high shear rate affects the crystallization. Hence, peculiar crystals are supposed to be formed in the high shear region. For some reason, these crystals do not have a good cohesion with their neighbors and hence it might become possible to peel apart two layers of the injected piece. A summary of the effect of shear on crystallization of homopolymers and block copolymers is given below.

1.4.1 Homopolymers

Before addressing the effect of flow on homopolymers, a description of the crystallization process is required. It is a complex process that can be summarized in three steps as follows [29, 30]:

- Step 1: starting from a molten disordered state, when the polymer is cooled down in between its glass transition temperature and its melting temperature, some density fluctuations are supposed to appear throughout the volume.

- Step 2: some of these high density regions become large enough so that the energy gained during the creation of crystals overwhelm the energy penalty paid for increase of the surface. They are called nuclei.

- Step 3: polymer chains crystallize at the surface of nuclei.

Coming from a molten state to a temperature at which a polymer can crystallize, a rapid development of density fluctuations is observed. This phenomenon seems to be a prerequisite for crystallization [31, 32]. Since crystal density is higher than the amorphous density, a higher packing of chains is needed in order to initiate crystallization. Such condition is fulfilled when some regions of space undergo a density increase. In these dense zones, there is a higher probability to find chains packed/organized in such way that crystallization is initiated. The number of nuclei is found to depend on the temperature and on the material itself (M_w, etc.). The mechanisms that induce this primary nucleation were recently investigated [33–35]. However, the debate about the appearance of nuclei is still going on.

Nucleation and growth [36]

As mentioned before, only cooling of a disordered melt below the melting point is considered here. However, this is not a very restrictive limitation since it is the most often encountered case in practical applications.

Crystallization experiments show that a certain induction time is required before any nucleus can be observed. Furthermore, the time at which nuclei appear varies from one to another. Additionally, the nuclei are found to be randomly distributed in space. For these reasons, nucleation is often considered from a statistical point of view. Once a nucleus is activated, a 3-dimensional structure is formed due to the growth of the lamellae and the random branching of the semi-crystalline phases. This structure develops into a spherulite. The spherulite size will increase constantly until two spherulites come into contact. Once the volume is filled up with spherulites, crystallization within the remaining amorphous regions might occur, however its kinetics is very slow. Crystallization is a slow process at the beginning when a few spherulites are present and also at the end when the whole space is occupied by spherulites. The evolution of the rate of crystallinity with time is hence usually described by a sigmoid.

Concerning the effect of temperature on the kinetics, the higher the degree of supercooling, i.e. the lower below the melting point, the smaller the induction time will be. This is true for both types of nucleation, i.e. homogeneous and heterogeneous nucleation. The former one consists in the spontaneous nucleation of the polymers chains and as such depends on the nature of material. As a consequence, the spherulites appear randomly dispersed throughout the bulk. Hence, it is called homogeneous. On the contrary, heterogeneous nucleation is the result of impurities, which come either uncontrolled, or deliberately as nucleating agents. Indeed, in that case, the energy barrier to form nuclei becomes lower as no initial chain packing is needed. This tremendously facilitates the nucleation and more spherulites are therefore generated. Because many different type of particles can

induce heterogeneous nucleation, the conditions required for nucleation may vary from a site to another. Therefore, the spherulites do not appear at the same time, and their dispersion is related to one of the impurities.

In the case of homogeneous nucleation, the nucleation rate v_{rate} is related to T by [36]:

$$v_{rate} \sim \exp(-\frac{A\ \sigma^3 \vartheta_m}{kT(\Delta_m^f)^2(T_{m0}-T)^2}) \tag{1.1}$$

where σ is the excess of free energy per unit area, ϑ_m the monomer volume, Δ_m^f the heat of fusion per monomer and A a constant dependent on the geometrical form of the nucleus. T_{m0} is the equilibrium melting temperature, above which no crystal is stable. This Equation shows that the nucleation rate is enhanced by a lower temperature.

It is also expected that a high degree of supercooling will accelerate the growth of crystalline lamellae. The equation of spherulite growth rate as a function of temperature is given by [36]:

$$u \sim \exp(-\frac{T_A}{T-T_V}) \exp(-\frac{B_0}{T_{m0}-T}) \tag{1.2}$$

with T_A an 'activation temperature' usually of the order of 1000 K, and B_0 a constant. T_V is the Vogel-Fulcher temperature, which is related to the 'frictional force' experienced by the segments. T_V is usually located around the glass transition temperature. This Equation shows that for low temperatures above and close to T_V and hence T_g, i.e. when the segmental mobility is greatly reduced, the growth rate decreases rapidly. At high temperatures, relatively close to T_m, the growth rate is also considerably slowed down since the Equation 1.2 tends to zero. The physical explanation being that the thermal agitation becomes so large that the crystals are less stable, and hence the formation of nuclei is less likely. The kinetics and the thermodynamic effects are thus acting in opposite directions. It also implies the existence of a temperature, located between T_g and T_m, at which the growth rate will be optimal, and a plot of the growth rate as a function of temperature looks like a Gaussian shape [37] (see Figure 1.8).

The lamellar thickness d_c also depends on the degree of supercooling. The closer the temperature is to the melting point, the thicker a lamella should be or else thermal agitation will destroy it. The thickness of a lamella follows Equation 1.3.

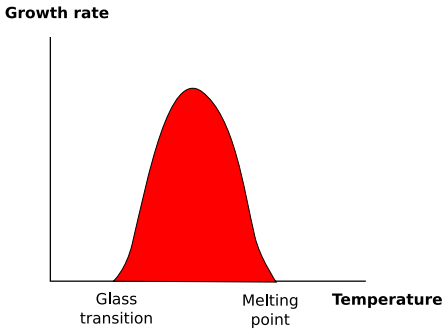


Figure 1.8: The spherulites growth rate as a function of temperature

$$d_c = \frac{A}{T_m - T} + B \tag{1.3}$$

with A and B two constants, T the temperature and T_m the melting temperature.

Semi-crystalline morphology

In the quiescent state, crystallization is usually described as a nucleation and growth process [38, 39] and more attention has been given to the growth process [40–42]. Starting from nuclei, the polymer chains (smallest scale) crystallize under the form of lamellae (medium scale), and these lamellae grow uniaxially, filling in all directions of space. The morphology observed in absence of flow is spherulitic (largest scale). An overview of the different length scales of the crystalline structure is shown in Figure 1.9.

Techniques used to probe crystallization

The description of the crystallization phenomena requires a careful evaluation over the relevant parameters. In particular, the effect of thermomechanical history can make the analyzes difficult. Therefore, although far from being able to reproduce industrial conditions, specific devices like rotary shear are used. [43–53]. Such devices allow to control both shear stress or strain over a limited range, as well as temperature. Studies of elongational flow are also available [54–61]. Additionally, since any flow tends to dissipate heat, it was also verified that the heat released during shear experiments is not enough to disturb crystallization [48, 62]. Finally, the effect of pressure was also investigated [63] and it seems to be decoupled from

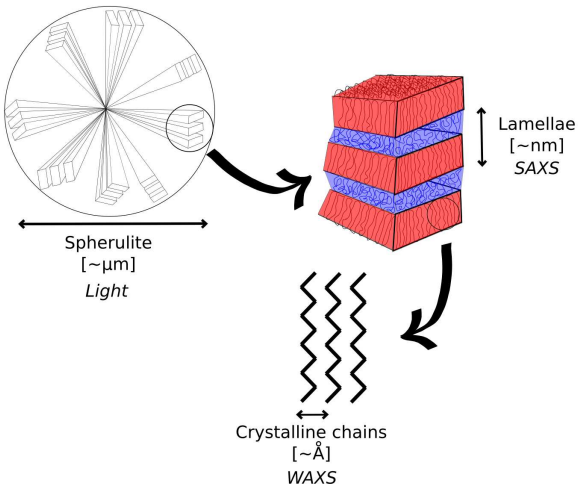


Figure 1.9: Crystalline structure at different length scales

that of flow. A high pressure does increase the supercooling, i.e. the nucleation density is enhanced.

As shown in Figure 1.9, crystallization involves various length scales. Hence, depending on the scale (crystalline lattice, lamella, spherulite, etc.), different monitoring techniques should be used. For instance, shear devices and modern rheometers allow to study the material in-situ. To such techniques, other investigation tools can also be coupled: DSC [64] for the study of the phase transition, X-rays [65–81] and light [53–60, 82–84] scattering for crystal lattice and spherulitic organization respectively, rheology [43, 45–48, 50, 60, 85–89] and dilatometry [49] for bulk behavior, and surface probes such as AFM [90] for direct observation of very small scales.

Effect of shear

In the molten state, entanglements with the neighboring chains slow down the relaxation. Therefore, the conformation of a chain remains modified for a relatively long time after the application of an external stress field. For this reason, semi-crystalline polymers are very sensitive to flow applied during or before crystallization.

In fact, under flow, the slow relaxation of polymer molecules causes a persistent distortion of the coil conformation. In industrial processes, the Weissenberg number

(relaxation × deformation rate) is typically higher than 1. Hence, the polymer material very often crystallizes from a deformed state [91]. The crystallization process usually happens to be modified, and the basic effects observed are the following:

- The nucleation density is known to be increased, i.e. more spherulites are observed [82]. As discussed above, nucleation will occur when chains are in a more favorable conformation as compared to the quiescent state. The application of flow tends to align the chains with the flow direction, bringing the polymer molecules in a more 'ready to crystallize' conformation. It practically lowers the energy barrier that the system has to overcome in order to crystallize. As a result, the number of crystals increases.
- Flow can also affect the final crystal morphology. For instance, when the shear or the elongation rate is really high, anisotropic morphologies such as shish-kebabs are obtained [64, 65, 92–98]. They consist of fibrils resulting from the flow-induced orientation of chains, on which lamellae will grow in the perpendicular direction. In fact, it is found that the chains of higher molecular weight are responsible for such behavior, even if their amount is relatively small [96, 99]. At relatively high shear or elongation rates, so-called row nucleation is sometimes observed. It also involves high molecular weight chains that align with the flow and serve further as a backbone for nucleation. This ends up in the formation of a row of spherulites in the axis of the strain [100–102]. Compared to the shish-kebab it seems that such a morphology only appears if the degree of orientation is not too high [103].

1.4.2 Copolymers

Crystallization of block copolymers is very similar to the crystallization of homopolymers. Both homogeneous and heterogeneous nucleation can occur and crystallization is governed by the same rules. However, some extra features are observed [104].

First, for a block copolymer, the maximum amount of crystallization depends on the polydispersity of the segments. If A is the crystallizable segment and B the amorphous one, two A segments are more likely to crystallize fully when their length matches. Therefore, as a general rule, a distribution in segment sizes will always decrease the total crystallinity [105]. Nevertheless, it should be mentioned that monodispersity of the crystallizable segment, does not guarantee a complete crystallization of all the segments. A crystallizable segment is not necessarily fully involved in the crystalline structure.

Presence of non-crystallizable segments will hinder the crystallization. As a consequence, the thermal stability of the copolymer crystals is lower than that of their

homopolymer counterpart, and hence the T_m of the copolymers are lower. The kinetics is also modified, and for a given diblock the kinetics is found to be slower than that of the homopolymer [106–109]. It is also observed that the kinetics of crystallization follows a nucleation and growth process, both when the melt is disordered or ordered [110, 111].

Concerning the influence of flow, some changes are expected due to the multimodal relaxation behavior. Unfortunately, the resulting behavior is hardly predictable since it strongly depends on the constituents and their interaction. Nevertheless, at low temperatures an expected feature is observed. For an already crystallized material, its stretching can induce a crystallization of the segments found to be amorphous at this temperature. Indeed, in the case of the block copolymer the soft segments have to sustain part of the stress because of its covalent links with hard crystallized segments. Therefore, the amorphous segments will also be stretched along the shear direction and eventually these oriented segments will be able to crystallize if sufficiently regular [112, 113].

Finally, the most important feature is linked to the ability of block copolymers to form microdomains. Indeed, in the melt, when below the order-disorder transition temperature, segments of different nature tend to segregate. This results in the formation of various morphologies. Even multiblocks, where the number of block per chain is large, exhibit similar phase diagrams [3, 4, 114]. However, as expected, due to the segment polydispersity, the long range order is substantially limited. Compared to homopolymers, copolymers have the opportunity to crystallize from this pre-ordered states. In a system where the microdomain structure is weakly segregated [107, 111, 115, 116], which usually occurs for copolymers whose order-disorder transition temperature is close to the melting temperature, the crystallization destroys the microdomains as initially present in the melt. No noticeable effects of the initial state are observed on the final morphology, and hence the crystallization process is similar to homopolymers. On the other hand, for microdomains that are strongly segregated (T_{ODT} much higher than T_m [106, 110, 117–119]), the crystallization may not affect the structure and occurs within the domains [120–122].

1.5 Two-phase flows

In the case of blends consisting of Newtonian components, the evolution of the microstructure during flow is relatively well understood. These results are reported in several recent review articles [123, 124]. However, it needs to be stressed that effects of elasticity are at present not completely understood. In this paragraph, we will highlight some of the basic phenomena that govern the morphology development in immiscible systems in shear flow.

1.5.1 Deformation

When shear flow is applied on a polymer blend consisting of a droplet/matrix structure, the droplets will deform due to the application of the hydrodynamic force. For Newtonian components, this deformation is governed by two dimensionless quantities. The first important parameter is the viscosity ratio:

$$p = \frac{\eta_d}{\eta_m} \tag{1.4}$$

where η_d and η_m are the viscosity of the dispersed and matrix phase respectively. The second one is the capillary number Ca [125, 126]:

$$Ca = \frac{\eta_m \dot{\gamma} R}{\Gamma} \tag{1.5}$$

where η_m is the viscosity of the matrix, $\dot{\gamma}$ the shear rate, Γ the interfacial tension and R the radius of the droplet. The capillary number expresses the ratio of the deforming force ($\eta_m \dot{\gamma}$ is the hydrodynamic stress) over the restoring interfacial stress (Γ/R).

Depending on the value of p, the droplet deformation proceeds differently as can be seen in Figure 1.10. For a high viscosity ratio, the droplet deforms uniformly to an ellipsoidal shape. On the contrary, at low value of p the deformation is concentrated on the center of the droplet which gradually necks. Due to the orientation induced by the flow, the shape looks like a sigmoid. It is important to note that for a small deformation, the process is reversible since after cessation of shear, the droplets recover their spherical shape.

1.5.2 Break-up

When the capillary number exceeds a certain critical value, the so-called critical capillary number, the droplet becomes unstable and will break. The mode of break-up is found to be related to the viscosity ratio [128]. The dependence of this Ca_{crit} on p was mapped out by Grace [124] (see continuous line in Figure 1.10). At a low value of p, the droplet deforms to a sigmoidal shape and finally breaks in the middle. This movement is accompanied by the release of small droplets at the tips. For a relatively high value of p, the droplet necks until it breaks into two daughter droplets, plus satellite droplets in between.

It needs to be stressed that this Grace curve is only valid for relatively gentle changes in flow. In real processing operations however, the flow conditions can be well above the critical capillary number. The deformation mechanism is then different: the droplets will be elongated into long fibrils that - depending on the

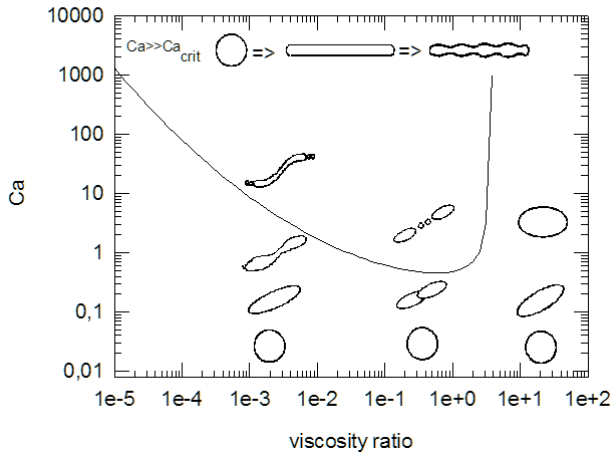


Figure 1.10: Scheme of droplets deformation and break-up as function of viscosity ratio and capillary number [127]

cooling time scale - will break up in a series of smaller droplets by means of Rayleigh instabilities [129, 130].

1.5.3 Coalescence

Whereas a high shear rate tends to break up droplets into smaller ones, at low shear rates (low capillary number) the droplet size can be increased by coalescence. When two droplets collide, a thin and flat interface of matrix fluid is formed in between the two droplets. If this interface thickness becomes less than a critical value h_c, mutual attraction between the droplets because of van der Waals forces will cause a disruption of the film and hence the droplets coalesce (see Figure 1.11). The smaller the droplets are, the easier they coalesce, since the liquid in between is more easily drained. Since it increases the droplet size, coalescence counterbalances the break-up phenomenon. Big droplets are easy to break and difficult to coalesce, and the reverse applies for small droplets. The final morphology is thus obtained by the balance between coalescence and break-up phenomena.

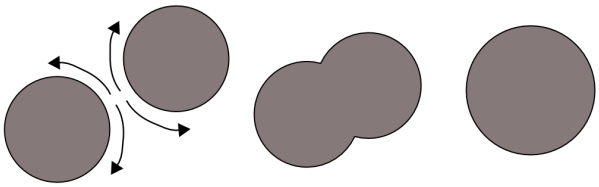


Figure 1.11: Scheme of droplets coalescence

Chapter 2

Materials and methods

In this chapter, the various materials that will be used throughout this work will be described. In addition, the different techniques applied in this thesis will be presented.

2.1 Materials

2.1.1 7033 SA - Multiblock copolymer

7033 SA Pebax ® (Arkema), is a multiblock copolymer consisting of an alternation of polyamide 12 (PA12) segments and polytetra-methylene glycol (PTMG) segments. The grade number (7033) refers to the hardness of the material. SA refers to the fact that no additives are present in the material. PA12, also known as nylon 12 (Figure 1.3a), is a semi-crystalline polymer with a glass transition temperature (T_g) of 36°C and a melting temperature (T_m) of 182°C (values obtained by differential scanning calorimetry). Pure PTMG (Figure 1.3b) is found to be amorphous. Its T_g is around -85°C [131].

The nylon 12 monomer is obtained by opening of a lactame ring, which is subsequently reacted with adipic acid. Hence, the PA12 segments are functionalized at the two ends with a carboxylic acid group. The PTMG segments contain alcohol groups, they are expected to have a certain polydispersity in molecular weight, however no information is available concerning its value. The purpose of the functional segments is to ensure reactivity between the two polymers. The chemical reaction is thus a classical esterification reaction (see Figure 2.1). In order to enhance the speed of the reaction, a catalyst is used. Active stirring is required to

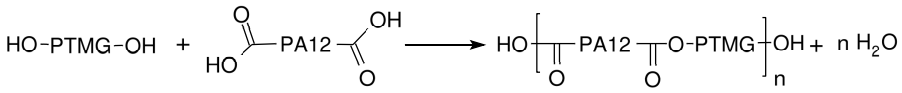


Figure 2.1: Synthesis of Pebax ® molecule by polycondensation

Polymer	M_n PA12	M_n PTMG	average PA12 monomers/segment	average PTMG monomers/segment
3533 SA	850	2000	4.3	19.2
7033 SA	5000	650	25.0	6.3

Table 2.1: Molar masses of 7033 SA Pebax ® [27]

increase the probability of PA12 to come in contact with PTMG since they do not mix well.

Since the 7033 grade is synthesized by polycondensation of PTMG and PA12, a polydispersity of 2 is expected. Because of the polydispersity of PTMG, it is also supposed that, for a given molecular mass, two molecules of 7033 may have a different composition. In one case for instance, a molecule of 7033 can consist of short PTMG segments that diffused quickly to the interface with PA12 during chemical reaction. In an other case, the 7033 molecule could be made of relatively long PTMG segments that diffused slowly to the interface with PA12. The first type of molecule is believed to be formed during the early stages of the polycondensation while the second type would be obtained near the end of it. The number average molecular weight (M_n) and the weight average molecular weight (M_w) of the 7033 molecule are found to be about 20 000 g.mol^{-1} and 40 000 g.mol^{-1} respectively. The M_n of the PA12 segments is equal to 5 000 whereas the M_n of the PTMG segments is equal to 650 (see Table 2.1). Therefore, there is a large asymmetry in composition since 88.5% in weight of the material is PA12.

2.1.2 PA12 - Homopolymer

PA12 is a thermoplastic material which has excellent impact resistance and therefore it is found in various applications. Like most aliphatic polyamides, PA12 has been thoroughly characterized by X-ray, infrared, and differential scanning calorimetry ([132] and references there in). PA12 crystals can be found in different forms depending on the condition of crystallization. The main crystal form obtained from the melt at atmospheric pressure is the γ-form (hexagonal), which

	a [Å]	b [Å]	c [Å]	α [°]	β [°]	γ [°]
γ - monoclinic	9.38	32.2	4.87	90	121.5	90
γ - hexagonal	4.7	31	4.7	90	120	90
γ - pseudo hexagonal	9.58	31.9	4.79	90	120	90
α - monoclinic	9.8	32	8.5	90	65	90

Table 2.2: Crystalline lattice parameters of various polymorphs of PA12 [135]

has the amide plane twisted out of the polymethylene plane by ca. 60° [133]. The γ'-form is an imperfect form which is found in the melt-quenched PA12; it has a similar X-ray diffraction pattern as the γ-form. It is supposed to consist of small or poorly defined γ crystallites. The α-form can be obtained by precipitation from a phenol-ethanol solution or by slow crystallization from the melt above 500 MPa, whereas the α'-form is a stable form at high temperatures ($\geq$ 100°C-120°C) [134].

The γ'-form can be slowly annealed into the γ-form above $\backsim$110°C, while the α-form does not undergo this transformation. The γ-form is the common form at room temperature and can be transformed into α' above 120°C due to the breakage of hydrogen-bonded sheets. The γ'-form can also be annealed to the α'-form at high temperatures through a recrystallization process. The lattice parameters (a, b, c, α, β, γ) of PA12 are given in Table 2.2 for the most common crystalline forms.

The pure PA12 polymer selected in this work has a comparable molar mass ($M_n \backsim 20000$, $M_w \backsim 40000$) as the 7033 SA. Therefore the difference in the behavior of the two polymers is directly linked to the presence of PTMG in the block copolymer.

2.1.3 3533 SA - Multiblock copolymer

As discussed in the previous chapter, additives are usually incorporated by means of a masterbatch. In the industrial blend, the masterbatch carrier is a soft multiblock copolymer and 3533 SA is chosen to play this role. Hence, the 7033 SN polymer product (SN accounts for presence of additives) is a blend where the dispersed phase is the masterbatch carrier.

3533 SA is also made of PA12 and PTMG segments, however their length as well as their proportion differ from the 7033 SA (see Table 2.1). The synthesis route for the two materials is similar: 3533 SA is also obtained by polycondensation of functionalized PA12 and PTMG segments. Hence, an index of polydispersity (I_p) in weight of 2 is also expected. An additional polydispersity in the molecular composition because of the presence of PTMG segments of various lengths is also supposed to be present.

The 3533 SA nomenclature follows the same rules as for the case of the 7033 SA

presented previously. The grade number refers to the number of the "hard" and "soft" blocks and SA refers to the absence of additives. Due to the higher content of PTMG (ratio-wise) and to the smaller length of the PA12 segments, the 3533 SA is less viscous and "softer" than the 7033 SA.

One of the hypotheses for the delamination phenomenon is the presence of a two-phasic structure (macrophase). As was discussed in the Chapter 1, an important parameter in the morphology development is the viscosity ratio of the dispersed phase and the matrix phase. In order to verify whether the Pebax ® 3533 forms a two-phasic structure with Pebax ® 7033, two extreme masterbatch grades of 3533 SA were selected: 3533 RDG 242 and 3533 RDG 246. Although both are chemically very similar, their viscosity is quite different, probably because they have a different molecular mass.

2.2 Methods

In order to investigate the morphology development in Pebax, various experimental techniques are needed to encompass a large variety of length scales. These techniques will be briefly presented here, together with the sample preparation method.

2.2.1 X-ray scattering

X-ray scattering experiments give information about the smaller length scales present in the material. Typically wide angle X-rays scattering (WAXS) experiments - in transmission - are used to obtain data related to the crystalline lattice of the material. From small angle X-rays scattering (SAXS) experiments, one deduces information about a somewhat larger length scale (for instance the thickness of lamellae in semi-crystalline materials). The SAXS and WAXS apparatus used consists of a 18 kW rotating-anode X-ray generator (Brucker Ax, Ibaraki Pref, Japan) with a graphite crystal monochromator to obtain a CuK.α beam with a wavelength of 0.154 nm, and a one-dimensional position sensitive proportional counter (psPC) with line focus optics. In order to get 2D WAXS patterns, an imaging plate was introduced [136]. With the current set-up the q-range for SAXS was from 0.07 nm^{-1} to 1.4 nm^{-1}. For WAXS-experiments, the angle 2θ ranged from 5° to 30°. These experiments were performed at Kyoto University, Japan, in the laboratory of polymer mechanics.

Samples for WAXS were prepared by pressing a pellet between two glass plates at 200°C. Subsequently, the samples and the glass plates were cooled down to room temperature. The resulting films have an average thickness of about 0.4 mm (range from 0.3 to 0.6 mm). For SAXS, thicker samples were needed and

therefore another preparation route was followed. Pellets were melted at 200°C and an appropriate mold was filled under the action of gravity. Subsequently, the samples were cooled down to room temperature. The resulting sample thickness was about 2.5 mm.

Since the apparatus is not a synchrotron source, long accumulation times have to be used (at least 30 minutes). Keeping the polymer at high temperatures for a long time could cause some degradation. However, at the length scale probed here, no effect of degradation was observed: there was no difference between measurements before and after long time annealing. Due to the low intensities provided by the SAXS setup, a slit was required to enhance the beam intensity. This improves the time resolution but it has the drawback of giving a scattering profile slightly different from what one would obtain with a pin-hole system. Therefore, the air background had to be removed and the data had to be smoothed and corrected by means of a desmearing process before any further analysis could be performed.

In the analysis of the WAXS-patterns the air scattering background is first removed from the raw data. The profile of the sample, contains a mixture of amorphous halos and crystalline peaks. Gaussian curve fitting can be performed on the peaks in order to obtain information such as degree of crystallinity (area of crystalline peak divided by total area), the peak position and the width at half-height. The raw SAXS profiles were smoothed and desmeared before any further analysis was performed.

2.2.2 Rheology

Rheological experiments give information about the mechanical behavior of the material investigated. Typically, the elastic (G') and loss moduli (G") are obtained, using oscillatory shear. Both temperature and oscillation frequency can be tuned during the experiment. Using the time-temperature superposition, a few experiments allow to characterize the material behavior by drawing a so-called master curve. It should be mentioned that such a superposition does not necessarily apply to block copolymers since each block has its own shift factor. However, in the material under study here the time-temperature superposition works since a component is clearly in excess. In a similar way, the Cox-Merz equivalence enables the extrapolation of the viscosity at high shear rate from the oscillatory data.

Samples were prepared by heating the pellets to a temperature of 200°C in a Collin Plate Press and by pressing the two hot plates together at a pressure of 100 bar for 4 minutes. This procedure produces plates with a typical thickness of 1 mm that are of sufficient quality for rheological measurements.

Rheological measurements have been performed on a Dynamic Stress Rheometer (DSR Rheometrics) using a parallel plate geometry (25 mm). For all measurements, a gap thickness of 900 μm was used. Measurements have been carried out

under nitrogen atmosphere in order to minimize degradation as much as possible. After loading the sample in the rheometer at the desired temperature, a period of 5 minutes was allowed in order to homogenize the temperature in the sample. After this waiting time, the measurement was started. It has been verified that all tests were conducted in the linear strain regime.

2.2.3 Optical experiments

Rheo-optical experiments have been performed using a Linkam CSS450 system (Linkam Scientific Instruments, UK). The Linkam shearing cell consists of two highly polished parallel quartz windows, with the bottom plate that can rotate under the control of a stepper motor. Small angle light scattering (SALS) as well as microscopy experiments have been conducted on this device.

The SALS setup used in this work consists of a 10 mW polarized HeNe laser (model no. 1125P, Uniphase, USA, having a wavelength of 632.8 nm) , the Linkam shearing cell, a projection screen and a CCD camera, which is connected to a frame grabber. Light coming from the laser is subsequently sent through a polarizer, the sample and an analyzer which is 90° rotated with respect to the first polarizer (HV-configuration). The scattered light is visualized on a semi-transparent screen. A schematic overview of the SALS setup is shown in Figure 2.2. A high resolution 10-bit camera (Pulnix) is used to record the images, after which the image is digitized (at resolution of 1300 x 1030 pixels) with the help of the frame grabber card (Coreco) mounted on the PC. The SALS patterns have been analyzed using the KU Leuven-SALSSOFTWARE developed for that purpose.

In the microscopy experiments (OM), the Linkam shearing cell was directly mounted under an optical microscope (Leitz Laborlux 12 Pol S). A CCD camera (Hamamatsu Digital Camera C4742-95) was also added to the setup in order to record the images in a numerical format. Samples were prepared according to the following protocol. Pellets of predried polymer (drying under vacuum at 60°C and stored in a desicator in the presence of silica gel) were loaded in the Linkam cell and brought at high temperature (200°C for 7033 material and 210°C for PA12). The gap was then reduced to 100 μm, the gap width at which SALS and OM experiments were performed. About 5 minutes were allowed for the sample to relax from the compression before any measurements were started.

2.2.4 Differential scanning calorimetry

Differential Scanning Calorimetry (DSC) is a technique which allows an accurate temperature control, as well as an accurate heating/cooling rate. Various phenomena that occur within polymers, such as phase changes, imply modification of the heat capacity and/or release (absorption) of energy by an exothermic

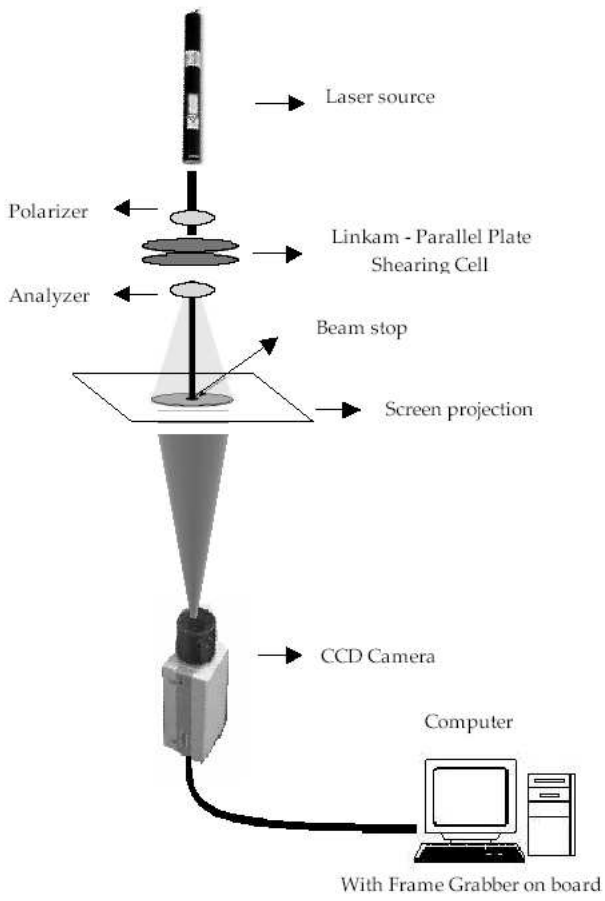


Figure 2.2: SALS setup

(respectively endothermic) process. In this study DSC measurements have been performed to obtain information on the transition temperatures in the materials and to estimate their crystallinity. A Perkin-Elmer Diamond DSC has been used which operated under N_2 atmosphere to avoid degradation of the material. The cooling rate ranged from $1°C.min^{-1}$ to $100°C.min^{-1}$ and the heating rate was set at $40°C.min^{-1}$.

Samples were prepared by slicing pellets of polymer, the thus obtained thin films were put in an aluminum pan and sealed.

2.2.5 Transmission electron microscopy

Transmission Electron Microscopy (TEM) is a powerful tool that allows an image magnification up to 600 000 times (value depending on the apparatus). It is convenient for direct observation of the morphology at a scale that is inaccessible to optical microscopy. In the blend study, use was made of the conventional transmission electron microscopy technique of stained ultra thin sections (see Chapter 5). The morphology of the blends was investigated with a JEM-2000FX (JEOL Co., Ltd.) electron microscope at an acceleration voltage of 120 kV. These experiments were performed at Kyoto University, Japan.

Thin sections of the polymer were cut by means of a Reichert ultracut E ultramicrotome, equipped with a cryogenic sectioning ultramicrotomy, with a diamond knife at -80°C. Thin films were then stained using osmium tetroxide (OsO_4) vapor, which preferentially stains soft domains (i.e. PTMG), at room temperature for one hour.

Chapter 3

Influence of the thermal history on the morphology of Pebax

Pebax ® is a multiblock copolymer which can exhibit quite a variety of microstructures. Hence, it is important to investigate the temperature dependence of the microstructure in detail. In this chapter, the important transition temperatures, such as the melting and order-disorder temperature will be determined. Next, the morphology evolution during various thermal histories will be studied. An attempt will be made to give a structural interpretation.

3.1 Transition temperatures

The Pebax ® material has been investigated in the past, but most often the focus was only on its semi-crystalline state [137–139]. Therefore, the morphology of this material above T_m remains unknown. Since the 7033 SA is a multiblock copolymer, one expects segregation between the PA12 and PTMG segments. Such a segregation can potentially lead to organization of matter at a very local scale. This has already been observed in other multiblock copolymer systems such as for instance TPUs (Thermoplastic Polyurethane) that are known to present a microphase separating behavior [140–142]. The ordered structures that result from this segmental repulsion usually have a period of the order of the polymer chain dimensions. Many patterns have already been observed such as for instance, lamellar, hexagonal-packed cylinder, or body-centered cubic phases [11]. These

morphologies are stable, depending on the composition of the block copolymer. The morphologies accessible in such multiblock copolymers have been extensively studied [3, 6, 143–146]. However, less attention has been paid to highly asymmetric copolymers [117, 147], composition-wise, where phase separation in the molten state is not easily predictable.

Before investigating the morphology of 7033 SA at different temperatures, it is of importance to know the position of T_m and T_{ODT}. They clearly limit the range in which different morphologies are stable, as well as give an indication on the segregation power of the couple PA12/PTMG. In the temperature range of interest, i.e. from room temperature to the processing temperatures ($\approx 250°C$), PTMG remains amorphous. The transition temperatures in the PA/PTMG block copolymer should be related to those in PA12 but they are expected to be affected by the interactions between PA12 and PTMG segments.

Melting point - T_m

To determine T_m the samples were first melted at 200°C and then cooled down to room temperature at a specific rate. Rates of 1°C, 10°C and 100°C/min were used. When the sample was subsequently heated, T_m was derived from the resulting peak in the DSC thermogram, more specifically it was defined here as the temperature at which the heat flow drops back to the base line, i.e. the end of the peak. A typical DSC trace is shown in Figure 3.1. The T_m of 7033 SA was found to be 172°C, independent of the cooling rate. A secondary shoulder could be observed in the experiment with a cooling rate of 100°C/min. It could be associated to multiple endotherms, that are associated with the presence of imperfect lamellae in the sample as reported earlier for multiblocks as well as for homopolymers [142, 148–154]. Another explanation would be that the crystals first melt at a low temperature into a supercooled state which allows for fast recrystallization, and hence will result in two distinct peaks [155]. However, the investigation of the origin of the multiple endotherm has not been pursued further since it is out of the scope of this study.

The crystallization behavior was also probed with WAXS. When a molten sample was quenched in liquid nitrogen, two populations of lamellae (perfect and imperfect) were expected as in the sample that was cooled at 100°C/min in the DSC experiments. Figure 3.2 shows the intensity profiles at various temperatures after heating at 0.5°C/min between measurements. At low temperatures, a sharp crystalline peak is superimposed on the amorphous halo. The position of this peak corresponds to a q-value of 14.7 nm^{-1}. A fast quench has been reported to lead to the imperfect γ' crystalline form of PA12 [134]. Accordingly, the peak position is associated with the diffraction from the (001) plane. Other crystalline peaks of PA12 exist, but their lower intensity prevents them from appearing in

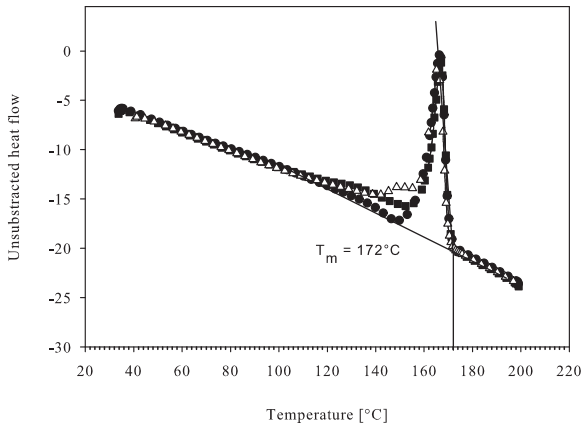


Figure 3.1: Pebax ® DSC traces during heating at 40°C/min, influence of cooling rate on crystallization • 1°C/min ■ 10°C/min △ 100°C/min

this fast screening experiment. The magnitude of the main peak starts to decrease at 160°C. From there on, the temperature increments were reduced in order to increase the resolution. When a temperature of 170°C was reached, the crystalline peak completely disappeared. This value of T_m is close to the value reported above (172°C). The difference of 2°C is reasonable, considering that the heating rate in DSC (40°C/min) was much faster than that in WAXS.

A second important characteristic temperature is the equilibrium melting temperature T_{m0}, i.e. the limiting melting temperature of a crystal of infinite thickness. The position of T_{m0} marks the thermodynamic transition between the molten and the semi-crystalline state. T_{m0} can be estimated from a plot of T_m versus the inverse of the thickness of the crystalline layer and extrapolating to an infinite layer thickness. The required value of the layer thickness of the crystals can be deduced from X-ray scattering experiments. The plot of T_m vs. thickness should be linear according to the Hoffman theory of crystallization [156]. This method is quite laborious, since it requires extensive measurements of crystal thickness. In order to overcome this difficulty the Hoffman-Weeks protocol has been followed [157] in the DSC measurements. It is based on the difference between the melting temperature T_m and the temperature used for crystallization T_c. Any crystallite formed at a temperature below T_{m0} has some imperfections that are locked in. Hoffman and Weeks defined a stabilization parameter ϕ, which is zero for perfect

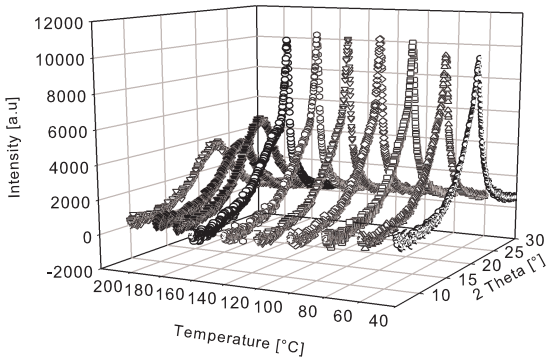


Figure 3.2: WAXS profile during a heating scan at 0.5°C/min

crystals and has a value of one for an unstable crystal full of imperfections. For the most stable crystallites T_m equals T_{m0}, for a completely unstable crystallite T_m equals T_c. A simple linear mixing law was assumed for T_m [157]:

$$T_m = T_{m0}(1 - \phi) + \phi T_c \tag{3.1}$$

Such a linear law implies that in a plot of T_m versus T_c, the so-called Hoffman-Weeks plot, T_m equals T_{m0} when the T_m line crosses the diagonal (T_m equals T_c). Although this method is based on a linear mixing rule, the value of T_{m0} obtained by this method and that derived from varying the crystal thickness yield very similar values [158]. Originally developed for homopolymers, the Hoffman-Weeks method has also been used successfully for multiblock copolymers [148, 159, 160]. The result for the present system is shown in Figure 3.3. The value of T_{m0} is calculated to be 184 ±1°C.

In literature, the equilibrium melting temperature of pure PA12 is reported to be 190°C [161]. Block copolymers [162] can be expected to melt at a lower temperature than the semi-crystalline homopolymer, an effect which is also observed in our case. Because of thermal motion and steric hindrance effects the second component in the multiblock prevents the formation of a more perfect crystalline structure which would have a higher melting point. Therefore, it is not surprising to find a lower T_{m0} for the Pebax ® than for the pure PA12.

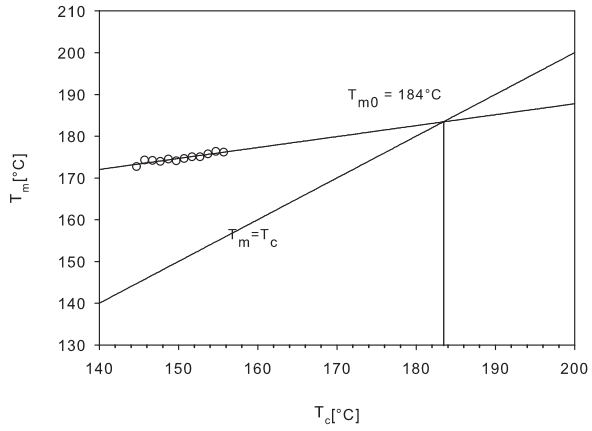


Figure 3.3: Hoffman-Weeks determination of T_{m0} (40°C/min)

Order-Disorder Transition Temperature - T_{ODT}

A well-known phenomenon in block copolymers is the existence of an order-disorder transition temperature (T_{ODT}), which marks the limit between organized and unorganized states in the phase diagram. Knowing this temperature is important because the presence of such a transition has some specific consequences. With a T_{ODT} above the T_m, even the molten material can have some structure, albeit on a very local scale. Various methods have been proposed to determine this order-disorder temperature [13–18]. Two of them have been used in this work: one based on rheometry, the other on SAXS. The first one has been proposed by Han et al. [15] and has proved to be adequate in determining T_{ODT} for other multiblock copolymers such as poly(ether-ester) multiblock copolymers [20–22]. The method is based on linear viscoelastic measurements: a change in the G' versus G" curves is expected at the temperature at which the microstructure changes. This temperature can then be regarded as T_{ODT}. Figure 3.4 shows plots of G' versus G" as a function of temperature for the system under consideration. Between 240°C and 185°C the curves coincide, indicating that no specific structure develops in the material. At 180°C a deviation can be observed, a feature that becomes even more pronounced at 178°C. It can be concluded that between 180°C and 185°C the material undergoes some change in microstructure. Since these temperatures are substantially higher than T_m (172°C), one can conclude that this transition temperature is associated with the T_{ODT}.

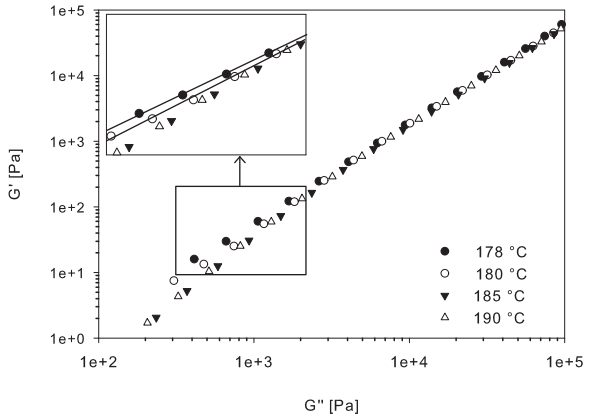


Figure 3.4: G' versus G" curves as a function of temperature

The other method to determine T_{ODT} is based on SAXS measurements. The material was first heated up to 200°C to erase the earlier thermomechanical history of the sample. Subsequently, it was quenched to 150°C and kept at this temperature for a period of 30 minutes, which was found to be more than sufficient to crystallize the material. Then, during 1 hour, the scattered X-rays are recorded in order to obtain the fully developed SAXS profile. Once the data acquisition was completed, the temperature was increased to 178°C at a heating rate of about 5°C/min. After waiting for 30 minutes, the scattering intensities were recorded for another 30 minutes in order to obtain the SAXS profile at this particular temperature. A similar protocol was applied at all subsequent temperatures. However, smaller temperature increments were used (1°C) in order to achieve the necessary temperature resolution to determine T_{ODT}.

The SAXS profiles resulting from this protocol are shown in Figure 3.5. At 150°C, a clear peak can be seen at q=0.32 nm^{-1}. It is associated with the crystalline order in the material [163, 164], more specifically with the lamellar spacing $2\pi/q =$ 19.6 nm. Up to temperatures of 182°C, a broad peak can be observed, its position shifting to smaller q-values with increasing temperature. It can be concluded from these measurements that a microphase-separated state has indeed developed in the material. At 182°C the peak shifts to q = 0.19 nm^{-1}, corresponding to a domain spacing of 32.7 nm. This value is larger than the lamellar spacing in the semi-crystalline state, an issue that will be addressed below. Above 185°C the

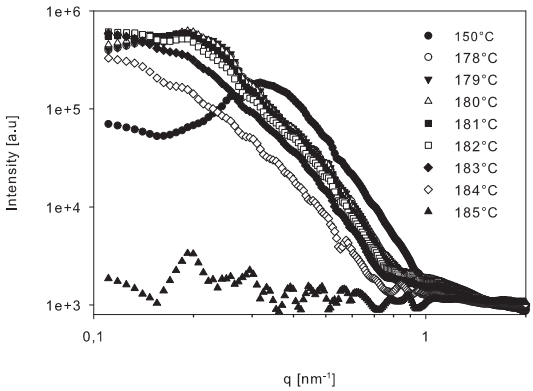


Figure 3.5: SAXS profiles evolution during heating scan. (●) Semi-crystalline ordered state (Other) Non crystalline ordered state (▲) Disordered state

scattering peak disappears. Based on these measurements, it can be concluded that the order-disorder temperature, as observed by SAXS, is between 184°C and 185°C, which is consistent with the rheological measurements. The segregation power that is driving the microphase separation above T_m (172°C) seems to be weak since the T_{ODT} is only 12°C above T_m, resulting in quite a small relative quench depth $\Delta T = (T_{ODT} - T_m)/(T_{ODT}) = 0.026$.

Temperature diagram

Based on the melting point and the order-disorder transition temperature, a schematic of the phase behavior can be drawn (Figure 3.6). At low temperatures, i.e. below T_m, the PA12 blocks are in the semi-crystalline state. Above T_{ODT}, on the other hand, the soft and hard segments are perfectly mixed and a single disordered phase is present. In between these two temperatures, a microphase separation is observed.

3.2 Morphology in the ordered states

The question arises whether the resulting microstructure depends on the thermal history to which the material has been subjected. Therefore, two different

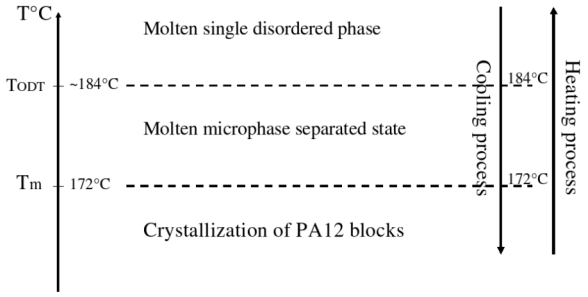


Figure 3.6: Schematic of the phase behavior

temperature protocols to reach the microphase-separated state have been compared. In a first one, the sample is crystallized and then it is heated towards the microphase-separated state region ('heating protocol'). Alternatively, the temperature interval in between T_m and T_{ODT} can also be reached starting by cooling from an unordered amorphous melt. This protocol will be denoted as the 'cooling protocol'.

Morphology generated by the heating protocol

In order to study the morphology development during the heating protocol, the material was first melted at 200°C and then cooled down at 30°C/min to 150°C, where it was allowed to crystallize. Subsequently the sample was heated up to a temperature between T_m and T_{ODT}. Two additional temperatures, 160°C and 170°C, that are not in the microphase-separated regime have been selected for comparison.
The resulting SAXS profiles at the various temperatures are shown in Figure 3.7. As for the crystallization at 150°C, the SAXS patterns were fully developed in less than 30 minutes, indicative of the structural rate of change. The height and position of the peak in the SAXS profile clearly depend on temperature. The peak position moves towards smaller q-values with increasing temperature, indicative of a larger characteristic length. At the same time, the intensity associated with the maximum becomes higher. The time evolution of these two parameters is shown in Figure 3.8.

As can be seen in Figure 3.8, the position of the peak decreases with temperature. Two different regimes can be distinguished, one below 170-172°C (which has been identified above as the T_m) and a second regime above. In the lower temperature

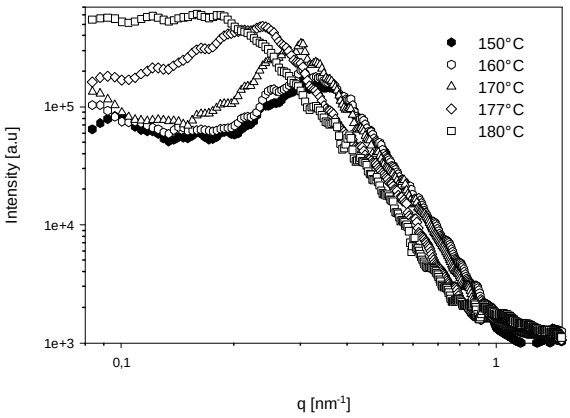


Figure 3.7: SAXS profiles as a function of temperature while heating

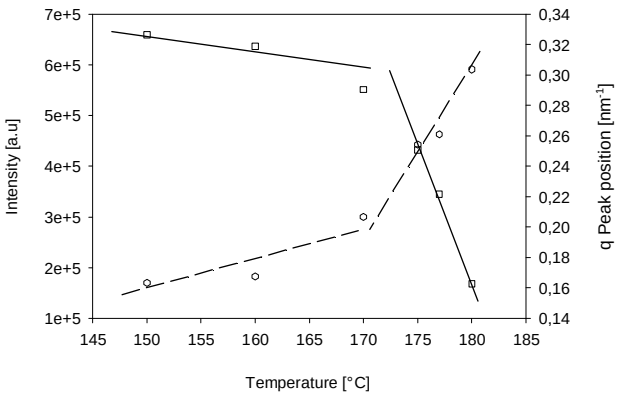


Figure 3.8: (○) I_m and (□) q_m as a function of temperature

region, q decreases slowly which means that the domain spacing increases gradually. This change can mainly be attributed to thermal expansion. Above the melting point of the PA12 block, the domain spacing increases so drastically that it cannot be attributed to thermal expansion only. It is a fingerprint of a change in the morphology of the material. The intensity increase, on the other hand, can be explained as follows: two contributions control the scattering level and they work in opposite directions. First, the mean squared electron density fluctuations $\langle \eta^2 \rangle$ decrease due to the melting, and thus lower the intensity. Outweighing the previous contribution, the intensity decrease is compensated by an increase of ξ^3, with $\xi = 2\pi/q_m$ being the characteristic size of a structure (q_m: position of peak).

Morphology generated by the cooling protocol

When the temperature is lowered from 200°C to 185°C, slightly above the T_{ODT} (184°C), no scattering (other than background) is recorded, as can be seen in Figure 3.9. Upon further cooling down to 175°C, i.e. within the temperature interval between T_{ODT} and T_m, a peak emerges. The time evolution of the SAXS profiles at 175°C is displayed in Figure 3.10. An incubation time of a few hours is required for a significant peak to emerge, it requires 20 hours to reach the steady state. In addition, the peak position does not change as a function of time during the cooling protocol, indicative of a spinodal phase separation process and clearly different from the evolution seen in the morphology development after the heating protocol.

Once the structure was fully developed at 175°C, the temperature was lowered to 150°C in order to let the material crystallize. The resulting steady state profile is added on Figure 3.9. It should be mentioned that the lack of smoothness of the curve is a consequence of data treatment and is not a real feature.

In Figure 3.11, the steady state SAXS (3.11a) and WAXS (3.11b) profiles, generated by means of the heating and cooling protocols discussed above, are compared. As no crystallized PA12 segments are present at 175°C, the WAXS patterns at these temperatures only show an amorphous halo. The WAXS profile at 150°C is indicative of the crystalline lattice and does not depend on the thermal histories applied to the sample, the difference being that the sample for the heating protocol was cooled immediately to 150°C whereas in the cooling protocol it was first cooled to temperatures in the microphase-separated regime. Three peaks can be distinguished in the corresponding WAXS profile. They are very similar to those of the γ' lattice for PA12 [135]. One can attribute the small peak at $2\theta \approx 6°$ to the 020 plane, the peak located at $2\theta \approx 12°$ to the next order 040, and the main peak $2\theta \approx 22°$ to the 001 plane of the dominant γ' form.

The SAXS pattern at 175°C, i.e. in the microphase-separated state, is clearly dependent on the thermal history. The peak resulting from the heating protocol

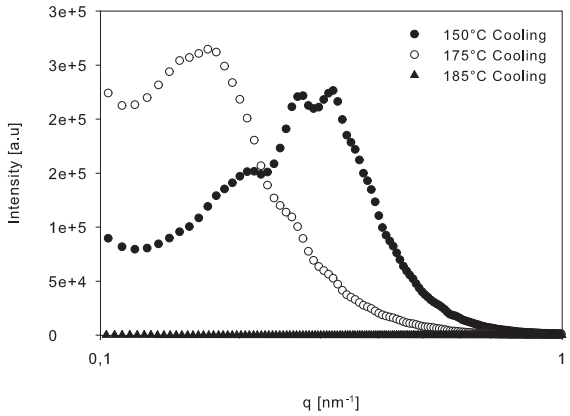


Figure 3.9: Background subtracted SAXS profiles recorded after cooling (1°C/min) from the disordered melt

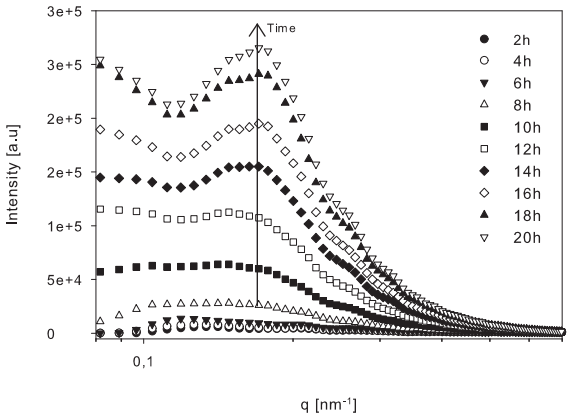


Figure 3.10: Kinetics of ordering at 175°C from the melt as followed by SAXS

has a larger intensity and its position is located at a larger q value (Figure 3.11). This implies a smaller domain spacing and hence a smaller structure size, when the structure is formed during melting of the PA12. The smaller size also results in a larger scattering power. The microphase-separated state obtained by heating from an initial semi-crystalline state is better defined than the one obtained from an initial amorphous melt. By heating, the domain size (31.3 nm) grows somewhat with respect to that in the semi-crystalline state (22.0 nm), but the thermal energy is not sufficient to expand it to the size of the microstructure that develops during cooling from the melt (45.0 nm).

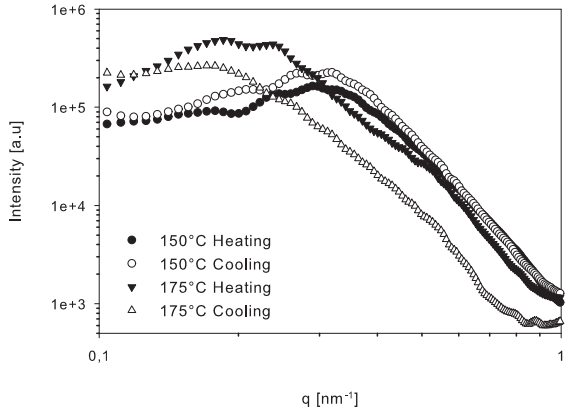
3.3 Investigation of the morphologies

To obtain more information about the structures, several methods are used to analyse the SAXS profiles. The choice of the equations and models applied to the SAXS profiles should be based on an indication about the morphology of Pebax. Hence, prior to the SAXS analysis, an attempt to directly observe the morphology is made. On such a small length scale, optical microscopy is not suitable and for that reason, transmission electron microscopy experiments are performed.

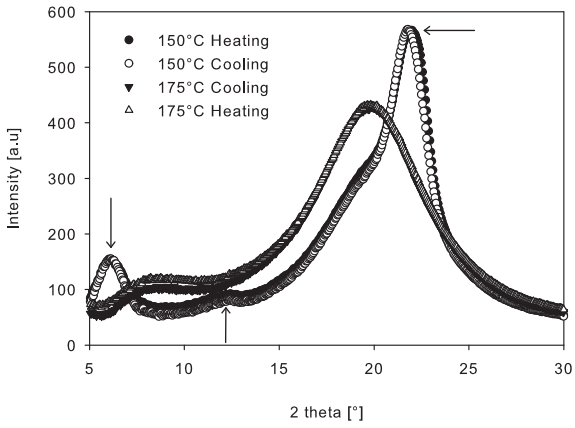
Direct observation of the morphology

It should be mentioned that, since in-situ experiments are not possible when using TEM, the sample has to be quenched in order to freeze the morphology. For the microphase-separated state, it implies to get out of its temperature stability range, and nothing insures that no change in its morphology will occur during quenching. Therefore, the TEM observation is only done for the crystalline state. After quenching, in order to avoid deformation during the cutting of thin film, the sample has to be brought much below its glass transition temperature. Furthermore, the preparation of polymers samples usually requires additional treatments to enhance the electron density contrast. For these reasons, the real structure and the observed structure may in fact be relatively different, and as a consequence TEM images of polymers should be taken as an indication of the structure and complemented with other investigation techniques.

In the case of 7033 SA, since the two blocks are made of H, C, O, and N atoms, the electron density difference between two polymers and thus the natural contrast is very weak. To enhance the contrast, ruthenium oxide (RuO_4), in the gaseous phase, is chosen to be the staining agent. Because of its high electron density, this molecule limits the transmission of the electron through the sample. Semi-crystalline material can be considered as a biphasic system where one phase allows a fast diffusion of particles (amorphous phase) while the other restrains strongly



(a)



(b)

Figure 3.11: (a) SAXS (b) WAXS profiles obtained by heating and cooling protocols

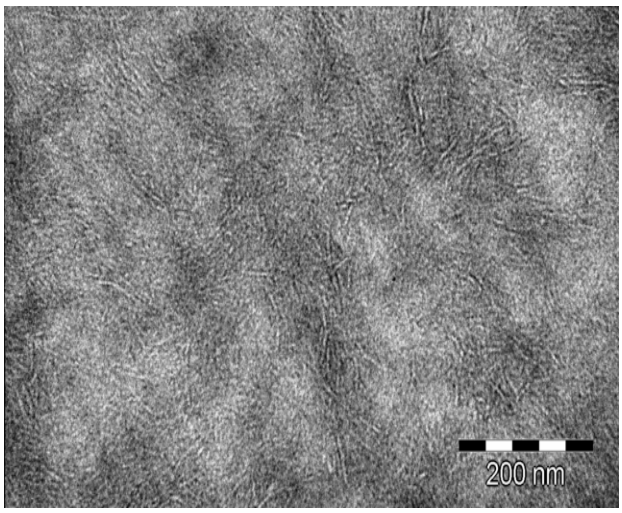


Figure 3.12: Crystallized 7033 SA observed by TEM after RuO_4 staining

the diffusion because of its compactness (crystalline phase). Due to this selectivity, one can expect the RuO_4 to diffuse faster in amorphous regions, and hence these regions will appear in black. Figure 3.12 presents the TEM image obtained on a 7033 SA allowed to cool down to room temperature. One can observe the alternation of black (and white) layers which are the amorphous layers, and respectively the crystalline ones. This clearly shows that the structure of 7033 SA in the organized state is lamellar. From this remark, the further SAXS analyses consider lamellar-like morphologies only.

Correlation function analysis

For a stack, typically of crystalline lamellae, the one dimensional correlation function $\gamma_1(r)$ of the electron density fluctuation perpendicular to the main face of a stack of crystals can be calculated according to the following Equation [165]:

$$\gamma_1(r) = \frac{\int_0^\infty q^2 I(q) \cos(qr) dq}{\int_0^\infty q^2 I(q) dq} \tag{3.2}$$

This equation is based on the assumption of a zero interphase thickness. This assumption can be verified by considering the Porod region of the plot $\log I(q)$

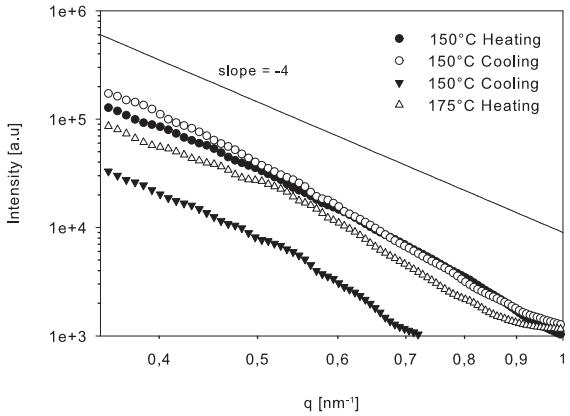


Figure 3.13: Plot of the SAXS profiles (heating and cooling, crystal and microphase) in the Porod region

vs. log q, which should yield a straight line with a slope equal to -4. A negative deviation from the linear relationship at high q values indicates a diffuse interface. In Figure 3.13, the Porod region of the semi-crystalline and microphase-separated states obtained by both the heating and the cooling protocols are shown. The slopes of the curves are slightly steeper than -4, especially at 175°C. It is possible to evaluate from this the interphase thickness with the help of different models (see [154]), although their relevance is questionable here. On average, the interphase thickness was found to be less than 2.5 nm.

The 1D correlation functions, based on a sharp interface, are shown in Figure 3.14(a and b). From these curves morphological data can be extracted. The position of the first peak, d in Figure 3.14a, provides the domain spacing. The thickness of one of the phases can be deduced by performing a linear regression on the curve at low r and intersecting this line with $y = \gamma_{minimum}$. The position of the intersection, d_a in Figure 3.14a, then corresponds to this thickness [165]. Additional information about the structure is required to assign this thickness to the appropriate phase. In the semi-crystalline state the percentage of semi-crystalline material can be calculated from either the heat of fusion obtained from DSC, or from the amount of scattering attributed to the semi-crystalline phase in the WAXS profiles. The degree of crystallinity is typically calculated from WAXS profiles, i.e. the ratio: crystalline peak area/profile total area [166]. For the ma-

Table 3.1: Length-scales and invariant of the biphasic system for the different thermal protocols. 1D account for data extracted from one-dimension correlation length

	Lamella/phase A thickness [nm] 1D	d [nm] 1D	Invariant Q
150°C - heating	5.4	17.1	7532
150°C - cooling	6.0	17.5	8213
175°C - heating	6.7	25.4	8564
175°C - cooling	7.7	30.2	3324

terial under investigation the degree of crystallinity was found to be 30% of PA12 and consequently constitutes the smaller fraction. Indeed, in Table 3.1 it can be seen that at 150°C the lamellar thickness is about one third of the domain spacing. Based on this result, the semi-crystalline PA12 phase can be assigned to the phase which has the smallest dimension.

At 175°C, the correlation length of the microphase-separated state (Figure 3.14b) is less well defined than in the semi-crystalline state (Figure 3.14a). The phase thickness can be estimated, however the available data do not allow to discriminate without doubt between the PA12 rich and the PTMG rich phase.

Total scattered intensity

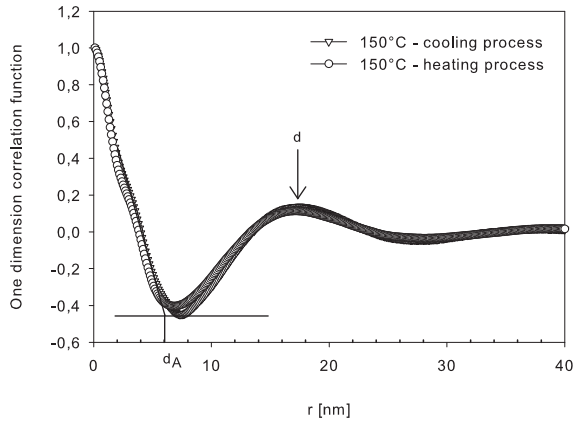
Additional information can be deduced from the total scattered intensity Q, also called the scattering invariant [167]:

$$Q = \frac{1}{2\pi^2} \int_0^\infty q^2 I(q) dq \propto \phi_1 \phi_2 (\rho_1 - \rho_2)^2 \tag{3.3}$$

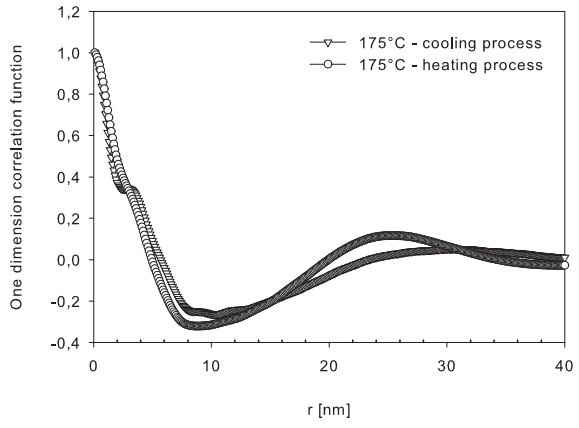
The invariant is linked to the difference in electronic density between the two phases, $\rho_1 - \rho_2$, as well as to the volume fractions of the two phases: ϕ_1 and ϕ_2. The results of this calculation are also shown in Table 3.1. The values are quite similar, except for the microphase-separated state obtained by the cooling process, where it is substantially smaller. This smaller value indicates that the microphase-separated state formed from the melt is less well defined than the one obtained from the heating protocol.

Fitting of models

Another approach to extract data from SAXS measurements consists in fitting some models to the SAXS profiles. The various morphologies accessible to multi-block copolymers have been described by Leibler [6] and for each of them, small



(a)



(b)

Figure 3.14: One dimension correlation function (a) Semi-crystalline state (b) Microphase-separated state

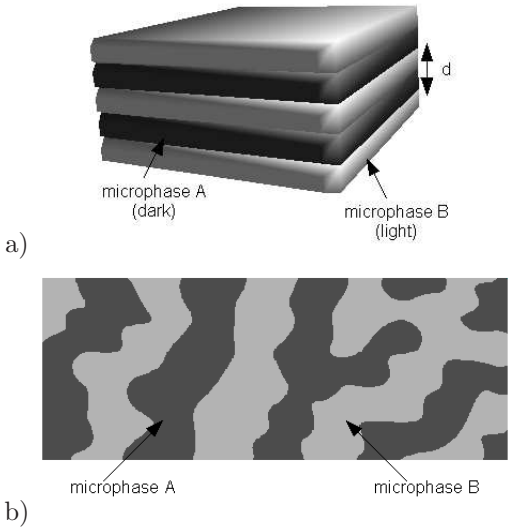


Figure 3.15: SAXS profiles as a function of temperature - Representation of the scattering models a) Lamellar model b) Random periodic [140]

angle X-ray scattering models have been developed. In the present case, since the morphology is lamellar-like, only two models that are thought to be representative for the material under study will be used. They are the lamellar model, and a random periodic model which depicts coarsely defined morphologies (see Figure 3.15). Details about the background of these models can be found elsewhere [140]. First, the models will be briefly presented and afterward, it will be investigated whether they can predict the occurring morphology in Pebax ®.

Lamellar morphology

Since a crystalline structure usually arranges in lamellae, the lamellar model is a popular model when describing polymer morphology. Indeed, the packing of the chains resulting from the crystallization tends to form a planar surface. Taking into account the thermal histories discussed before, it is seen that at 150°C, Pebax ® is in the semi-crystalline state. Hence, it might be possible to describe the structure by means of this lamellar model. The scattered intensity is defined as follows [140]:

$$I(q) = \frac{I_0}{q^4}\left[\frac{1 - A^2B^2 - A(1-B^2)\cos\Psi_A - B(1-A^2)\cos\Psi_B}{1 + A^2B^2 - 2AB\cos(\Psi_A + \Psi_B)}\right] \qquad (3.4)$$

where $A = \exp(-q^2\frac{\sigma_A^2}{2})$, $B = \exp(-q^2\frac{\sigma_B^2}{2})$, $\Psi_A = qd_A$ and $\Psi_B = qd_B$

with σ_A being the standard deviation of the Gaussian distribution of the thickness d_A of lamellae A (idem for B) and I_0 a normalization factor. This model has five parameters, from which the lamellar thickness and its standard deviation can be deduced. The domain spacing d is obtained by addition of the two lamellar thicknesses ($d = d_A + d_B$). It is important to note that this model assumes infinite lamellae (Figure 3.15a), a situation not occurring in practice.

Random periodic model

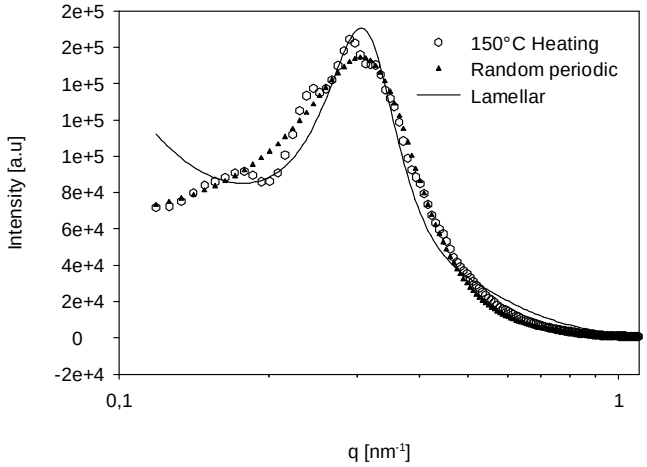
Considering a model consisting of an alternation of phases (coarsely defined shape), another model that could be used is the Teubner-Strey model which was initially developed for micro-emulsions. It describes a random two-phase morphology characterized by a long range order (Figure 3.15b). In this model, the scattered intensity is written as the following three parameter model:

$$I(q) = I_0[(\xi^{-2} + \frac{4\pi^2}{d^2})^2 + 2(\xi^{-2} - \frac{4\pi^2}{d^2})q^2 + q^4]^{-1} \tag{3.5}$$

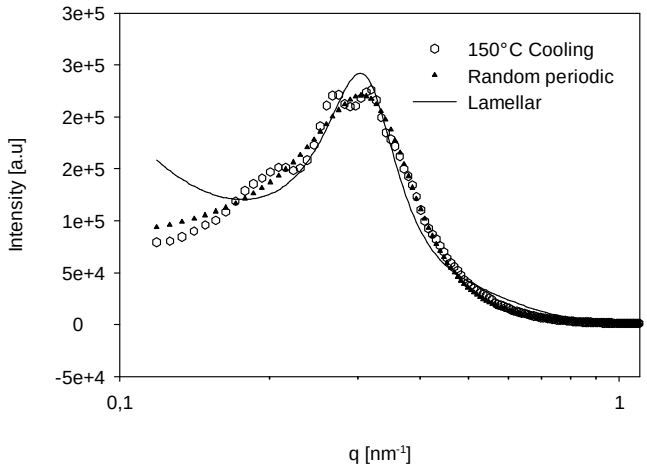
where ξ is the correlation length of the long range order, d is the domain spacing and I_0 a normalizing factor.

These two models are applied to the SAXS profiles obtained in the aforementioned cooling and heating protocols. The semi-crystalline state as well as the microphase-separated state are both considered. In order to discriminate between the models, one should see whether the theoretical curves match the experimental ones. In addition, the relevance of the obtained parameters should also be taken into account. The experimental data and their theoretical counterparts are shown in Figure 3.16.

As can be seen from the superposition of experimental and theoretical data, the lamellar model does not fit perfectly the curves at low q where an upturn in intensity is expected by the model. Looking at the fitting parameters, summarized in Table 3.2, the reason becomes clear. Indeed, in the four cases, the standard deviation of the lamellae A thickness is quite high and meanwhile the lamellae B appear to be monodisperse since their standard deviation is equal to zero. From a physical point of view, such a monodispersity of the layer thickness is very unlikely. Nevertheless, the phase thicknesses values are comparable and follow the same trend as what was found performing the correlation function analysis. Therefore, the morphology of Pebax ® in the semi-crystalline and in the microphase-separated state cannot be described as an ideal (plane) lamellar arrangement. This explains

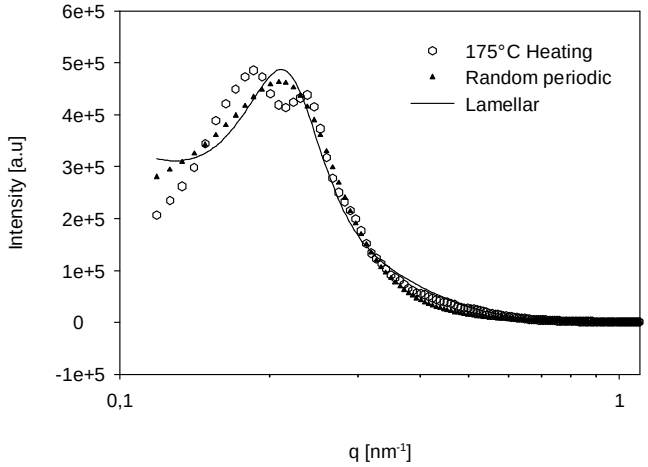


a)

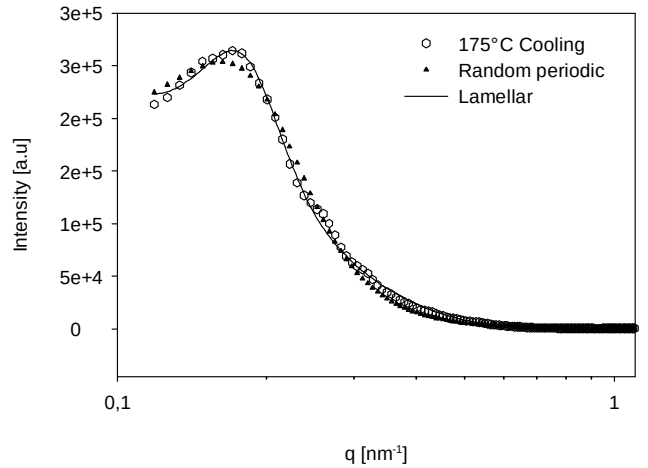


b)

Figure 3.16: SAXS profiles fitted by lamellar and random periodic models - a) 150°C heating protocol b) 150°C cooling protocol



c)



d)

Figure 3.16: SAXS profiles fitted by lamellar and random periodic models - c) 175°C heating protocol d) 175°C cooling protocol

Table 3.2: Fitting parameters for the ideal lamellae model

	Ideal lamella			
	d_A[nm]	d_B[nm]	σ_A[nm]	σ_B[nm]
150°C - heating	14.1	4.2	5.3	0.0
150°C - cooling	13.6	4.9	5.3	0.0
175°C - heating	18.8	6.7	8.1	0.0
175°C - cooling	20.9	7.7	10.5	0.0

Table 3.3: Fitting parameters for the random periodic model

	Random periodic	
	ξ [nm]	d [nm]
150°C - heating	8.7	19.2
150°C - cooling	9.5	19.5
175°C - heating	12.2	27.9
175°C - cooling	10.9	33.7

why the random periodic model also appears to decently fit the data, though a small discrepancy at low q is observed (see Figure 3.16). The parameters of this model are shown in Table 3.3. The domain sizes estimated from the fits are similar to the domain sizes estimated from lamellar model or the correlation function analysis. However, this model gives additional a new information, that is the distance up to which long range order exist. It is found to be relatively short since its value is of the order of one or two thinnest layer thickness. No real long range order prevails. Since the length of segments and the total chain length are polydisperse, the absence of long range order was expected. An organization that runs on a large scale is easier to obtain when the chains are similar.

To summarize the information obtained from the application of these two scattering models, it is clear that the Pebax ® organization is lamellar, although not perfect and well ordered. The lamellae are not organized parallel to one another but rather in a disordered pattern. This is true for the microphase-separated state as well as for the semi-crystalline one. The structure responsible for the scattering is found to have a poor organization in the sense that no long range order exists.

3.4 Structural interpretation

Based on the analysis of the X-ray patterns, the following picture of the structure can be deduced. The semi-crystalline state is relatively simple to depict since

PA12 crystals have been extensively studied. Adding amorphous PTMG does not radically change the crystal structure. The chain folding is estimated to one fold and the crystal form presents a mix of γ and γ' lattices (lattice data being based on reference [135, 147]). The number of folds in the crystal is estimated as follows. First, the length of a stretched segment of PA12 of molecular mass of 5000 g/mol was found to be equal to 41.1 nm. If the whole segment was involved in a crystalline lamella, a lamellar thickness of 5.7 nm - average value of the lamella thickness - as reported in Table 3.1 would imply that the chain was folded 6 times. This is, however, unlikely since the amorphous phase represents about 70% of the material which clearly proves that a large amount of PA12 is still amorphous. The 30% crystallinity then suggests that PA12 segments, on average, are only folded once.

The fact that crystallization in Pebax ® is similar to the one observed in pure PA12 indicates that the material can be seen as one semi-crystalline phase exclusively made of PA12 and at least one amorphous made of a mixture of amorphous PA12 and PTMG. Concerning the microphase-separated state, the two phases can be seen as one rich in PA12 and one rich in PTMG. Based on the values given in Table 3.1, it can be stated that the length scales involved in the semi-crystalline state are almost independent of the thermal history of the samples since all length scales and volume fractions are comparable. However, the length scale (e.g. domain spacing) in the microphase-separated state (175°C) clearly depends on the thermal history (domain spacing of $\backsim$25 nm versus $\backsim$30 nm). In addition, as was already explained above, the time needed to reach the equilibrium state at this temperature was also very different.

The above measurements suggest a morphology on a local scale, as illustrated in Figure 3.17. The semi-crystalline state consists of alternating layers composed of PA12 segments stacked together (crystalline layers) and layers composed of an amorphous PA12 + PTMG mixture. The crystalline and amorphous layers are not of monodisperse thickness, and hence the values found are only averages. The microphase-separated state has a larger spacing than the crystalline one. The domain spacing is much larger than expected on the basis of the pure PA12 and PTMG phases. Also, at 150°C the thickness of the crystalline lamellae of the multiblock (5.8 nm) is lower than that of pure PA12 (8 nm) [134]. These two arguments suggest that the crystal in the multiblock is less stable, and this is expected because of the presence of the PTMG segments. The final size of the microphase-separated state was also found to depend on the thermal protocol followed. The thermal expansion of the material alone cannot explain the difference in size between the semi-crystalline and microphase-separated state. The major contribution has to come from the unfolding of the PA12 chains in the microphase-separated state. The unfolding may increase the density of links between PA12 chains and PTMG chains along the interface, which in turn thickens both PA12-rich and PTMG-rich layers. Indeed the fraction of chain folding which exists

within the crystalline lamellae is progressively decreasing during heating and does add its effect to the thermal expansion. This is relevant since it does not occur systematically in such transitions [168]. The morphology of layers rich in PA12 may be stabilized by inter-chain bonding between PA chains, which in turn stabilizes the PTMG-rich layers.

In the disordered single phase above T_{ODT}, PA12 segments and PTMG segments are effectively mixed. There are some thermal concentration fluctuations in this phase which cause only a weak SAXS intensity as shown in Figure 3.5. The inter-chain hydrogen bonding of PA12 segments can be expected to be significantly weakened above T_{ODT}.

Concerning the difference in size obtained for different thermal protocols, one can assume that the hydrogen bonding can be relevant. Indeed, when the semi-crystalline state is heated above T_m, a fast reorganization of the structure is observed. During the phase transition, the role of hydrogen bonding, which occurs between PA12 segments is not very clear. In some cases, hydrogen bonding was found to control the packing [169]. One can anticipate that a short length scale reorganization of hydrogen bonding may be sufficient for the phase transition from the semi-crystalline state (i.e. pre-existing ordered-state) to the microphase-separated state. Thus the transition will occur relatively quickly. Possibly the hydrogen bonds within the PA12-rich domains hinder the growth of domain spacing between PA12-rich and PTMG-rich domains. In the resulting microphase-separated state the two phases remain well segregated. On the other hand, inducing microphase-separation by cooling requires some degree of ordering to develop in a more or less homogeneous phase. The segregation power induced by lowering temperature is not very large so that the disorder-to-order transition occurs relatively slowly. The ordering also seems to involve a spinodal growth and a reorganization of the hydrogen bonding over large length scales, which may be an additional reason for the slow ordering.

3.5 Conclusions

The morphology of Pebax ®, a PA12/PTMG block copolymer, has been investigated by means of small and wide angle X-ray scattering. This material displays an order-disorder transition temperature. The structural investigation focuses on the region between this temperature and the melting temperature. The order-disorder transition occurs at a temperature slightly higher than T_m, by about 12°C. Therefore the microphase separation, which takes place between a PA12 rich and a PTMG rich phase, is a weak segregation. Indeed, starting from the disordered state observed above T_{ODT}, and bringing the sample at a temperature in between T_m and T_{ODT} results in a very slow organization of the material. In contrast, the crystallization has obviously a relatively strong segregation power.

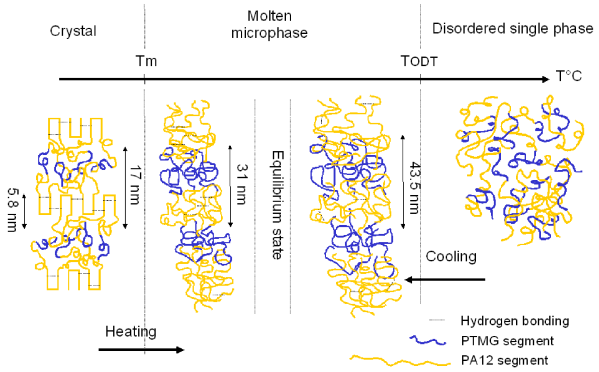


Figure 3.17: Summary of the different morphologies

It was also found that both the semi-crystalline and micro-separated structures have polydisperse thicknesses and that their nature in term of composition is similar. Moreover, the morphology in the two states is found to be lamellar with a poorly defined organization. Therefore starting with a semi-crystalline state, the existence of a microphase proceeds more from internal reorganization than microphase separation. While heating below T_{ODT}, crystalline lamellae are melting, and the PA12 segments unfold which leads to a steep increase in the domain spacing. The segments do not fully mix and the melt remains phase segregated. Above the T_{ODT} the system is in a homogeneous melt.

Chapter 4

Influence of the thermomechanical history on the crystallization of Pebax

In this chapter the crystallization of Pebax ® 7033 SA is studied. Since the crystallizable component is polyamide 12, the crystallization of a homopolymer of similar molecular mass is studied as well. Optical microscopy (OM) and small angle light scattering (SALS) are used to investigate the crystallization of the materials. The SALS technique allows to obtain insight in the very first stages of crystallization. The OM technique on the other hand allows to study the later stage, by direct observation of the crystalline morphology. Both techniques enable a quantitative measurement of the kinetics associated with the crystallization. The chapter is divided in four parts. First, the model used is presented and secondly its pratical use is presented. Then, the effect of crystallization temperature on the kinetics and morphology is discussed. Finally, the study of the effect of flow on the crystallization behavior is presented.

4.1 Extracting data from light scattering experiments

Whereas with OM the morphology is directly observed, SALS measurements only give an indirect view of the structure development. Hence, in order to extract structural information out of these experiments, a model is needed to describe the

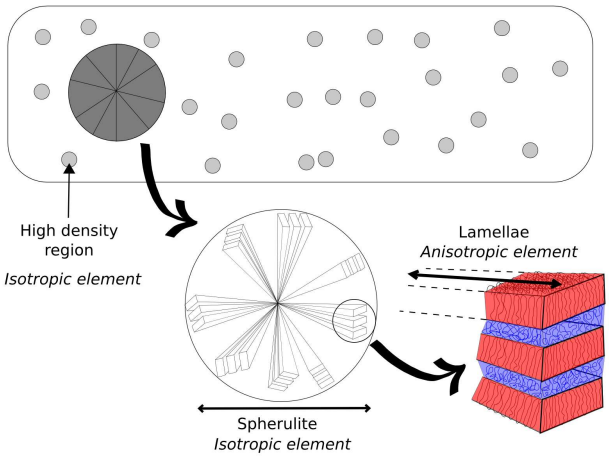


Figure 4.1: Light scattering elements found in polymer crystallization

evolution of the patterns. Here in this paragraph the model to be used will be introduced.

Polymers tend to form spherulites when they crystallize. The presence of such spherulites induces light scattering. Three different contributions can be distinguished. The first one is related to the difference in density within the material which leads to an isotropic scattering pattern. Indeed, regions of high density will have a polarizability slightly different from those of low density regions. The second contribution comes from the anisotropy generated by crystalline lamellae. A lamella being a three-dimensional object where one direction is much longer than the others, light passing through will be polarized differently depending on its direction. Finally, the last contribution to light scattering is due to the presence of spherulitic organization, i.e. their disposition in space, which could be isotropic or anisotropic depending on the structure formed. A schematic of the various elements involved in light scattering is shown in Figure 4.1.

4.1.1 Stein-Wilson theory [170]

Stein and Wilson proposed the following model to separate the isotropic and anisotropic contributions. In this model, each scattering element is supposed to be of cylindrical symmetry and can be described by two polarizabilities, $\alpha_{\parallel}$ and $\alpha_{\perp}$, respectively parallel and perpendicular to the axis of the element. Writing the anisotropy as $\delta = \alpha_{\parallel} - \alpha_{\perp}$ and the mean polarizability fluctuation as $\eta = \alpha - \overline{\alpha}$

(with $\alpha = (\alpha_{\parallel} + 2\alpha_{\perp})/3$ and $\overline{\alpha}$ the mean value of polarizability), Stein and Wilson made the following hypotheses:

- anisotropy fluctuations are independent of the mean polarizability fluctuations,
- orientation fluctuations are random,
- the scattered intensity has a spherical symmetry.

The first and last hypotheses are satisfied in the case of spherulites obtained via quiescent crystallization. Concerning the randomness of the orientation fluctuations, there is a certain degree of order in the system (a lamella is oriented radially), but since lamellae are randomly organized inside a spherulite this condition holds in a first approach. This method has been used extensively to describe the crystallization of polymers, in the quiescent and in the flow-induced state. A general overview of this approach in the study of polymer crystallization can be found in a review by Baert et al. [171].

Light scattering measurements can be obtained in 2 modes. When experiments are performed in a crossed polarizer configuration (HV), only light that has undergone a polarization shift will be transmitted. Hence, only orientation-related issues will emerge in the pattern. In a parallel polarizer configuration (VV) both isotropic and anisotropic contributions will be present. Stein and Wilson calculated the resulting patterns (or intensities I) for both configurations [170]:

$$I_{VV} = K[\langle\eta^2\rangle \int_0^{\infty} \gamma(r) \frac{\sin(qr)}{qr} 4\pi r^2 dr + \frac{4}{45}\overline{\delta}^2 \int_0^{\infty} f(r) \frac{\sin(qr)}{qr} 4\pi r^2 dr] \quad (4.1)$$

$$I_{HV} = \frac{K}{15}\overline{\delta}^2 [\int_0^{\infty} f(r) \frac{\sin(qr)}{qr} 4\pi r^2 dr] \quad (4.2)$$

f(r) is the orientation distribution function $f(r) = (3\langle\cos\theta_{ij}\rangle - 1)/2$ of the anisotropic elements, θ_{ij} being the angle made by elements i and j, $\gamma(r)$ is defined as the correlation function of the polarizability fluctuation, that can be expressed by: $\gamma(r) = \langle\eta_i\eta_j\rangle_r/\langle\eta^2\rangle$, and K is a scaling factor for the intensity.

When examining Equation 4.1, it can be seen that it contains 3 contributions: the isotropic scattering ($\langle\eta^2\rangle$ being the mean polarizability fluctuation or the density fluctuation), the anisotropic scattering (expressed by $\overline{\delta}^2$) and the spherulite scattering ($\frac{\sin(qr)}{qr} 4\pi r^2$). Since the HV set-up blocks out isotropic contributions, the HV intensities indeed only contain anisotropic and spherulite contributions.

The main achievement of the theory is the prediction of the pattern obtained from spherulites scattering. From Equations 4.1 and 4.2, one can expect an annular pattern in VV and a four lobes pattern in HV.

In order to extract the isotropic contribution (or the density fluctuation) one needs to perform the following operation:

$$I_{VV} - I_{HV} = K\langle\eta^2\rangle \int_0^\infty \gamma(r)\frac{\sin(qr)}{qr}4\pi r^2 dr \tag{4.3}$$

Stein, Koberstein and Russel [172] defined, based on the above Equations, two invariants: Q_η associated with density fluctuations and Q_δ associated with orientation fluctuations. Both properties are defined as:

$$Q_\eta = \int_0^\infty (I_{VV} - \frac{4}{3}I_{HV})q^2 dr \propto \langle\eta^2\rangle \tag{4.4}$$

$$Q_\delta = \int_0^\infty I_{HV} q^2 dr \propto \overline{\delta}^2 \tag{4.5}$$

Since the integration is made over the whole q range, i.e. the whole range of length scales, invariants are by definition independent of the geometry of the scattering elements and therefore of the spherulitic diameter.

In order to interpret the invariants, it is also useful to understand the underlying physical parameters. These parameters being $\langle\eta^2\rangle$, the mean value of the polarizability fluctuations, and $\overline{\delta^2}$ the mean value of the anisotropy. The scattering characteristics of a biphasic system can be written as [173]:

$$\langle\eta^2\rangle = \phi_{sph}(1-\phi_{sph})(\overline{\alpha}_{sph} - \alpha_{am}) \tag{4.6}$$

$$\overline{\delta^2} = \phi_{sph}\delta^2_{sph} \tag{4.7}$$

ϕ_{sph} being the volume fraction of spherulites, $\overline{\alpha}_{sph}$ the mean polarizability of spherulites being itself a combination of the amorphous and crystalline polarizabilities (α_{am} and α_{cr} respectively):

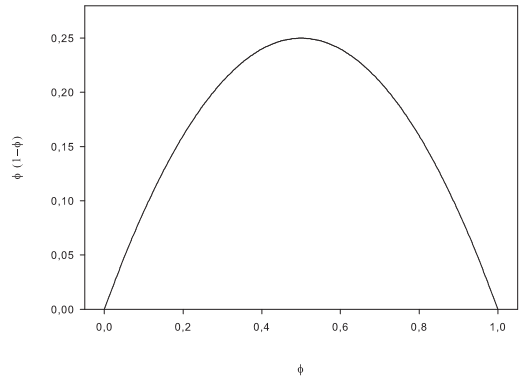


Figure 4.2: Expected evolution of the density invariant for a constant amount of 'defects'

$$\overline{\alpha}_{sph} = \phi_{cr,sph}\alpha_{cr} + (1 - \phi_{cr,sph})\alpha_{am} \tag{4.8}$$

where $\phi_{cr,sph}$ is the crystalline volume fraction for spherulites.

It is important to note that the notation used here is related to crystalline (cr) and amorphous (am) regions, however the equations are more general and they are also valid for any biphasic system that fulfills the model hypotheses. In a first approach, one can assume $\overline{\alpha}_{sph}$ to be constant. It would correspond to a structure of polarizability α_{cr} were the relative amount of defects (amorphous part) is constant. This assumption leaves the density invariant Q_η to be exclusively dependent on the product $\phi_{sph}(1 - \phi_{sph})$. Therefore, during the growth of the structures, it is anticipated that the evolution of this invariant is similar to Figure 4.2. As will be shown further in this chapter, density invariant measurements indeed exhibit this feature.

As for the calculation of $\overline{\alpha}_{sph}$, it is possible to write δ_{sph} as a linear combination of crystalline (δ^0_{cr}) and amorphous (δ^0_{am}) anisotropies:

$$\delta_{sph} = \phi_{cr,sph}\delta^0_{cr}f_{cr,sph} + (1 - \phi_{cr,sph})\delta^0_{am}f_{am,sph} \tag{4.9}$$

with $f_{cr}(r)$ and $f_{am}(r)$ the orientation functions of crystalline and amorphous regions.

Here one can assume the relative amount of 'defects' to be constant during structure growth. Therefore, $\phi_{cr,sph}$ can be considered to be constant. Since the others parameters of δ_{sph} are dependent on the nature of the phases, and because the nature of the phases does not vary, these parameters can also be considered to be constant. As a result, $\overline{\delta^2}$ is only dependent on ϕ_{sph}. This implies that the orientation invariant Q_δ will behave as $\phi_{sph}(t)$. In the case of crystallization, the evolution of crystallinity is found to follow a sigmoidal behavior. Schematically, $\phi_{sph}(t)$ is expected to increase slowly, then quickly and finally slowly again until it reaches a certain value. As will be seen further, such a behavior is indeed observed for the orientation invariant.

4.2 Application of the Stein-Wilson model in a case study

In this section, it will be shown how the model presented in section 4.2 can be used to extract morphological data from SALS experiments. The results obtained here will form the basis for a systematic study of the effect of the thermomechanical history on the crystallization of Pebax ®. Where possible, the SALS data will be complemented with optical microscopy images.

Experimental procedure

Using the setup described in chapter 2, the analysis of the SALS patterns was carried out with the SalsSoftware developed for that purpose. The calculation of the invariants has been performed with a program written in Python. The intensity as a (function of q) was calculated over the whole pattern (360°). The value of q was determined by simple scaling (1 pixel on camera = x μm on the screen), knowing the screen-sample distance.

$$q = \frac{4\pi}{\lambda} \sin(0.5\ arctanh(\frac{d_{pixelscreen}}{d_{distancesamplescreen}})) \tag{4.10}$$

To calculate the invariants, the first image (t = 0), which corresponds to a molten state was subtracted in order to remove the background scattering.

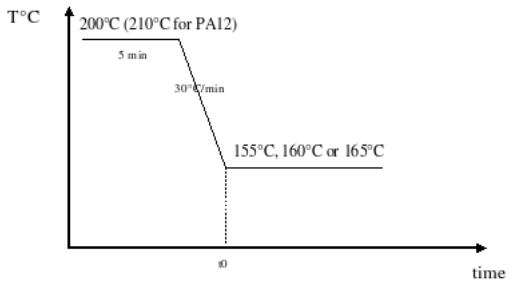


Figure 4.3: Isothermal quiescent crystallization protocol - Temperature profile

Scattering patterns

The protocol used in these experiments consists of first pressing polymer pellets in a hot-melt press at 200°C for 5 minutes. The film obtained is about 1 mm thick. Then, the film is put in the Linkam shear cell and heated to 200°C after which the gap is reduced to 100 μm. From that point on, the real thermal protocol begins (see figure 4.3). The material is subsequently melted for 5 minutes to erase any thermomechanical history, after which the sample is cooled down as fast as possible (technically 30°C/min) to the desired isothermal crystallization temperature. The light scattering setup does not yet allow simultaneous measurement of VV and HV intensities. Hence, first the VV measurements were performed. When the experiment was finished, the temperature was raised to 200°C for 5 minutes prior to the HV measurements.

Figure 4.4 shows a typical SALS pattern recorded during isothermal crystallization of Pebax ® 7033 SA at 165°C. Both HV and VV experiments are presented. The VV measurements show roughly a circular symmetry, indicating isotropic structures that do not have any preferential orientation through the volume. For spherulites observed in HV a four lobes pattern is expected. As can be seen in Figure 4.4 (HV 900 sec) these four lobes are not really distinguishable, which is consistent with the extremely low contrast within the spherulites in crossed polarizer microscopy experiments. However, an azimuthal plot of the HV intensities (see Figure 4.5) indicates that a four-fold symmetry is indeed present. Since the measurement is noisy, the median curve is added to the plot. The median is the line above and below which there is an is equal number of points. Compared to the mean value, it avoids to give importance to points of extreme values, and hence is suitable to correctly visualize the scattering distribution.

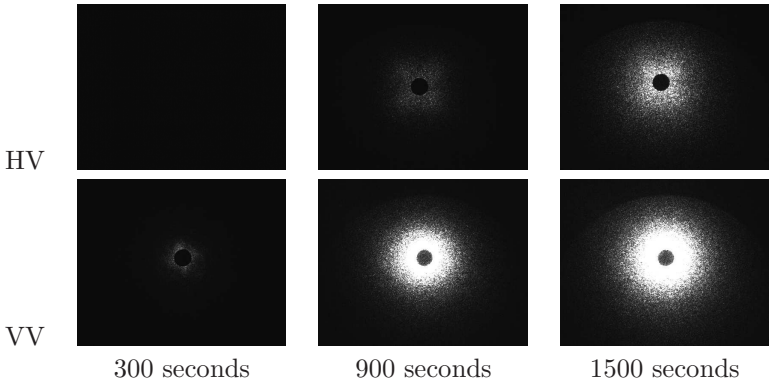


Figure 4.4: Evolution of SALS pattern of Pebax ® 7033 SA at 165°C.

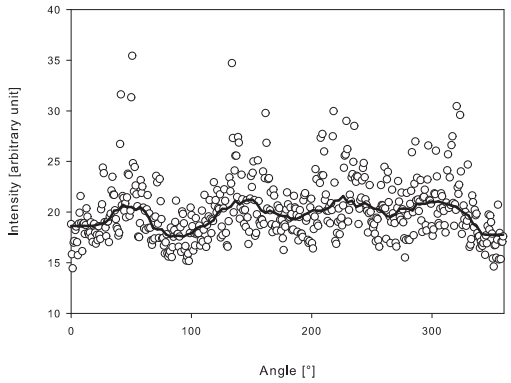


Figure 4.5: Azimuthal plot of HV pattern of Pebax ® 7033 SA at 165°C - (○) Intensity average (∼) median curve.

Invariant analysis

In order to study the early stages of crystallization, the scattering invariants have been calculated, as described in section 4.1.1. Figure 4.6 shows the typical evolution of the invariants as a function of time. As can be seen, the two invariants almost start to increase simultaneously. This is not universal since in many cases a delay between the onset of growth of the density and orientation invariants has been reported [174, 175]. As was discussed earlier, the density invariant is determined by the scattering contrast between the growing semi-crystalline phase and the surrounding amorphous melt. On the other hand, the orientation invariant is determined by the internal crystalline scattering contrast, a simultaneous increase is not guaranteed and requires specific material characteristics. It suggests that the crystallizable segments (in this case PA12 segments) pack and give rise to higher density regions. From these regions, spherulites eventually start to grow, leading to an increase in anisotropy. It is tempting to believe that these high density regions act as nucleating sites prior to crystalline growth, this issue will be addressed later. The evolution of the invariants can be explained as follows:

Based on Equation 4.1, the increase of the invariant of the density fluctuations ($\langle\eta^2\rangle$) is affected by three factors:

- an increase in the polarizability fluctuations, hence in the difference $\overline{\alpha}_{sph} - \alpha_{am}$;
- an increase in volume fraction ϕ_{sph} because of an increase of the size of the high density regions;
- an increase in volume fraction ϕ_{sph} because of an increase of the number of high density regions.

An increase in polarizability fluctuations would mean that the density difference between the regions of the material increases. Although there is no evidence, this phenomenon is not very likely to contribute substantially to the invariant evolution since the possible values of the density are limited to the density of the amorphous phase and to the density of the semi-crystalline phase, which differ by only a small amount. The increase in the size of the high density regions can also be neglected because a significant increase of their sizes would mean that lamellae are starting to grow, which would in turn affect the anisotropic invariant. Therefore, the increase of the number of high density regions seems to be the most plausible interpretation.
The increase of the anisotropic fluctuations ($\overline{\delta}^2$) can be understood as either an increase of ϕ_{sph} or δ (see Equation 4.1). Unfortunately, these values are not known at this point. It can only be said that the growth of lamellae and hence the increase in the number of anisotropic elements will contribute to the observed increase of anisotropic invariants.

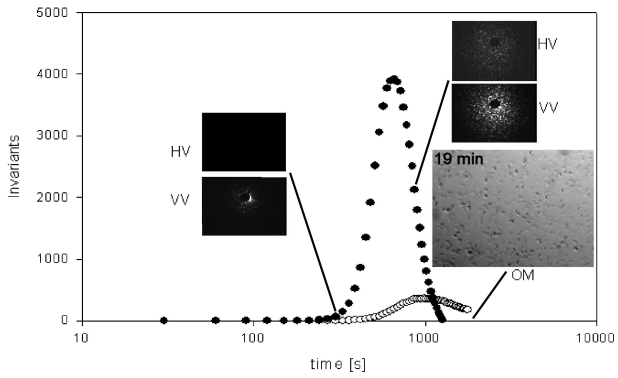


Figure 4.6: Evolution of fluctuations invariants during 7033 SA crystallization at 165°C - (•) Density invariant (○) Orientation invariant

Before the density invariant starts to decrease, the orientation invariant start to increase more than before. This again seems to be a generic characteristic of various polymeric systems [174, 175]. These changes in the slopes of the curves for the invariants reflects the growth of lamellae that overwhelms the formation of high density regions. During crystalline growth, the isotropic fluctuations are transformed in growing lamellae which anisotropically scatter the light, hence the isotropic contribution is decreasing. To this effect, another one can potentially be added. When half of the volume is occupied by high density regions, a further increase of their number mechanically decreases the scattering because the density difference becomes less ($Q \propto \phi(1-\phi)$ - see Figure 4.2). From a certain time on, the anisotropy will start to decrease. This part of the curve is most likely due to a too intense scattering at small angles, caused by the relatively big spherulites. Part of the scattering light is blocked by the beamstop which naturally reduces the amount of light recorded by the camera. Hence, the use of this region of the graph is doubtful and will be omitted in the further discussion.

Reproducibility of the measurements

Reproducibility with the same sample

Since it is known that the material is sensitive to degradation at high temperatures, it is important to check whether experiments can be performed on the same sample for a certain number of times without changing the crystallization characteristics. Indeed, multiple experiments on the same sample are sometimes required for a

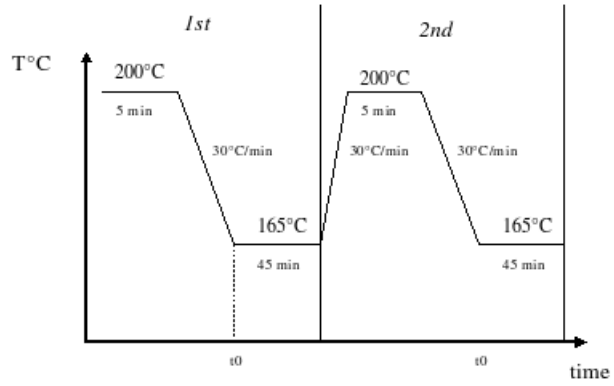


Figure 4.7: Thermal protocol for reproducibility with respect to time (1^{st} correspond to VV followed by the HV measurement, 2^{nd} to VV and HV, etc.)

complex protocol or in order to save material. The following protocol is applied (Figure 4.7). First, the sample is melted at 200°C during 5 minutes in order to erase any thermo-mechanical history. Then, the sample is cooled down to 165°C and is crystallized for 45 min. Crystallization is observed by means of light scattering with a VV setup. Afterward the sample is heated up again to 200°C and consecutively annealed for 5 minutes. Another crystallization of the sample at 165°C is performed and observed in a HV setup. This ends the first experiment after which the second experiment on the same sample can start following the same protocol.

Figure 4.8 shows the density and orientation invariants after different runs. The results from various runs almost superimpose, although some minor differences can be observed. From this figure, it can be concluded that the reproducibility on the same sample is acceptable. The peak positions differ by 8% around the mean value.

Sample to sample reproducibility

Because several samples are needed, the reproducibility between different samples should also be investigated. For that purpose, the isothermal crystallization protocol of 7033 SA at 165°C (see Figure 4.7) is applied to three samples.

Figure 4.9 shows the invariants of the different samples. The curves do not completely match. The peak positions differ by 15% around the mean value. It can be concluded that the reproducibility is low. Hence, if more accurate values are re-

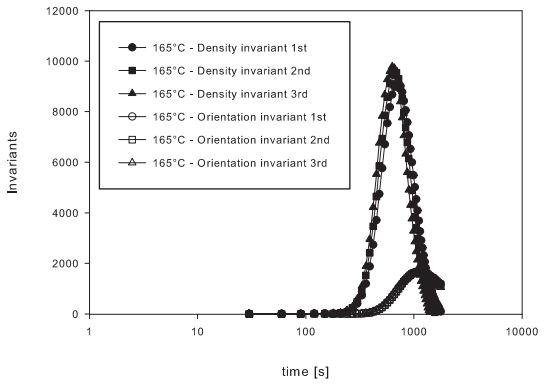


Figure 4.8: Reproducibility with time - Invariants during crystallization of 7033 SA at 165°C

quired, more experiments have to be performed. This result is not surprising since the material contains traces of catalyst that are not homogeneously distributed among the pellets. However, it is important to note that in this work we are investigating the effects of the thermomechanical history. Hence, only if the parameters are shifted by a sufficiently large amount the effects of thermomechanical history could be detected.

Now that the tools have been defined to extract data from light scattering experiments, a systematic investigation of the effects of the thermomechanical history on crystallization can be performed. Both quiescent, as well as flow-induced crystallization experiments will be performed using both SALS and OM. Since the crystallizable block with the Pebax ® material is PA12, a comparison between the crystallization behavior of the Pebax ® and a PA12 of similar molecular weight will be presented.

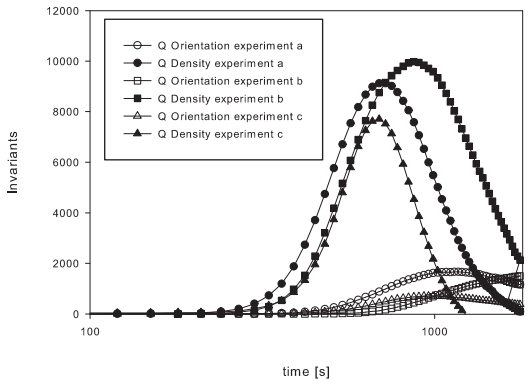


Figure 4.9: Sample reproducibility - Invariants during crystallization of 7033 SA at 165°C

4.3 Quiescent crystallization

4.3.1 Effect of temperature - Optical microscopy

Protocol for the study of quiescent crystallization

The protocol used here, see Figure 4.10, is the simplest protocol that can be applied for studying crystallization. The first step at 200°C consists of erasing the thermomechanical history of 7033 SA for about 5 minutes (at 210°C for a PA12, a higher temperature is needed here since T_m is higher). Then the polymer is cooled down to the crystallization temperature as fast as possible (30°C/min in a Linkam apparatus).

Figures 4.11 and 4.12 show snapshots of a crystallization experiment at 155°C. On these figures, the diameter of the spherulites as a function of time can be measured easily and hence a rather good accuracy of the growth rate can be expected. However, measuring the nucleation density is not very straightforward since different layers of spherulites are overlapping and hence only estimated values will be presented. Finally, induction times will also be shown. These are defined as the time at which spherulites appear. This is clearly a qualitative measure of the timescale for crystallization. Note that no polarizers have been used, the reason being that, when crossed polarizers are present, the clarity of the image is reduced. For some reasons, probably due to the imperfections of crystals, the edges

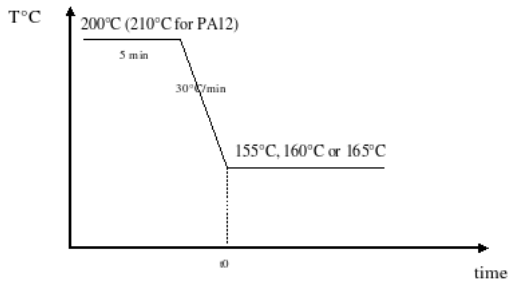


Figure 4.10: Isothermal quiescent crystallization protocol - Effect of temperature

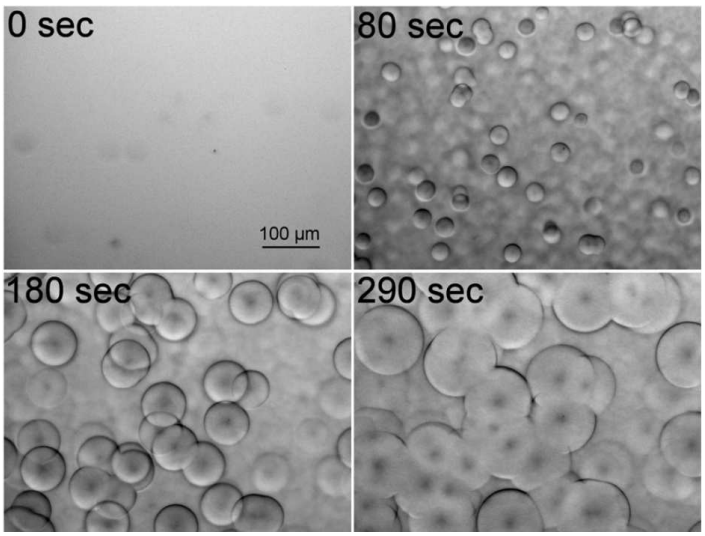


Figure 4.11: Isothermal crystallization of PA12 at 155°C

of spherulites in the HV mode can hardly be distinguished from the background. From these figures, it can be seen that the morphology development occurs as in a conventional polymer. The differences between the Pebax ® and the PA12 are quite clear. At the same temperature, more and hence smaller spherulites are observed in Pebax ® than in PA12. These data are quantified in the following section.

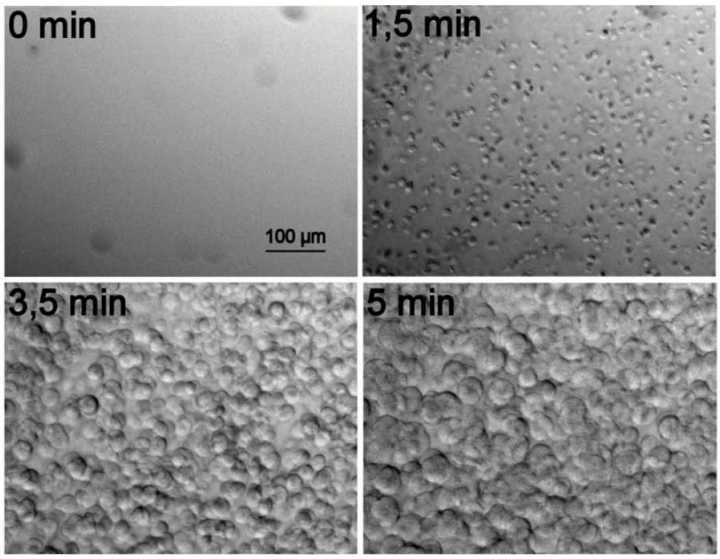


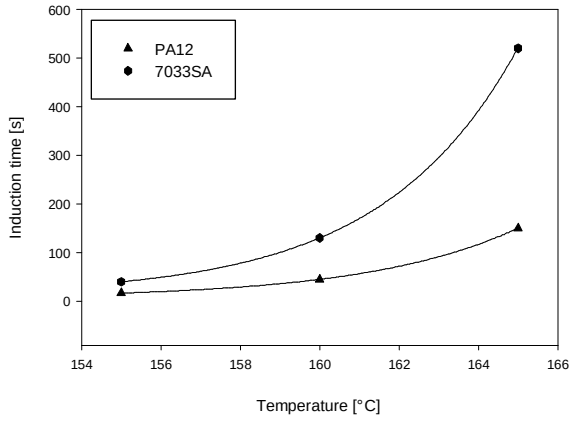
Figure 4.12: Isothermal crystallization of 7033 SA at 155°C

Effect of temperature on quiescent crystallization

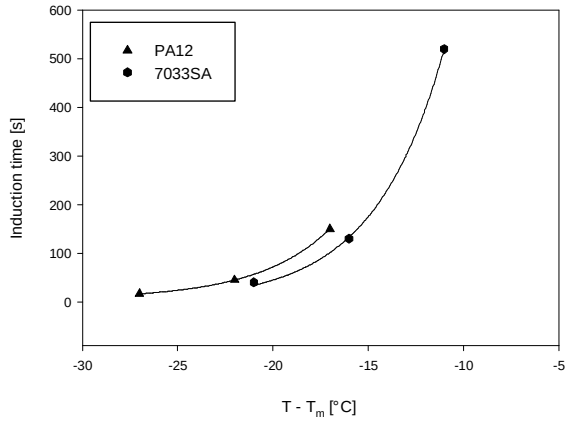
Since crystallization is usually very dependent on the thermal history of the material, an understanding of the crystallization phenomenon requires the consideration of the effect of temperature. The OM technique allows to get a good overview of the kinetics of crystallization, so it is first discussed here.

The timescale for crystallization is quantified in figure 4.13a in which the induction times are shown for the two polymers as a function of temperature. As can be seen, PA12 crystallizes faster than Pebax ®. However, in order to make a meaningful comparison between the two materials, one should compare them at the same degree of supercooling ($T - \mathrm{T_m}$). Such a rescaling will have a significant effect on the data representation. Results for the induction times as a function of this reduced temperature are presented in figure 4.13b. As can be seen on this figure, for a given reduced temperature, the crystallization kinetics of Pebax ® is, within experimental error, more or less the same as for PA12.

In order to characterize the crystallization further, the growth rate of the spherulites is measured. This quantity is determined by following the diameter of spherulites as a function of time. A typical result of such an experiment is shown in Figure 4.14. As can be seen, the diameter initially increases linearly with time. The constant slope is taken as the growth rate G. It should be noted that, while only



a)



b)

Figure 4.13: Induction time of isothermal crystallization of Pebax ® 7033 SA and PA12 a) regular scale b) reduced scale

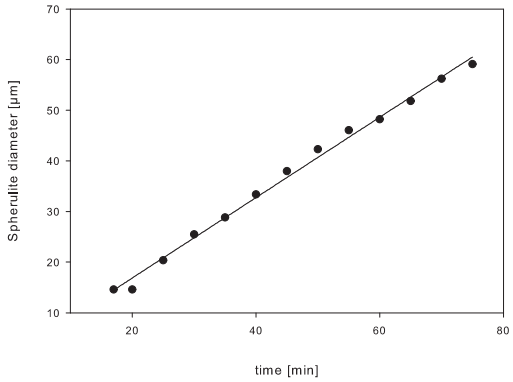
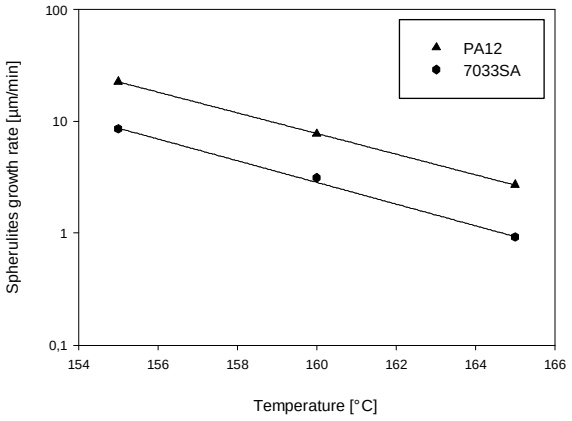


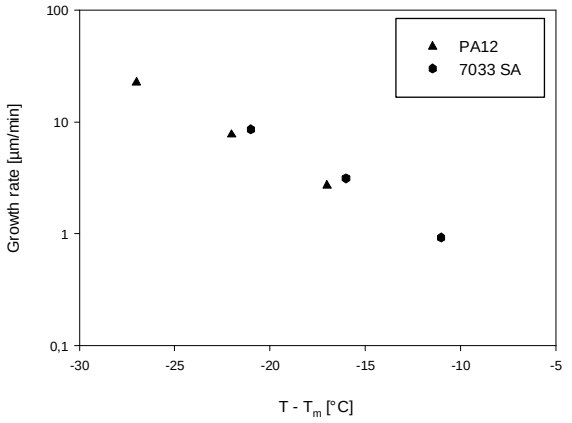
Figure 4.14: 7033 SA spherulites diameter as a function of time at 165°C

the linear region is shown, the spherulites diameter levels off later when they bump into each other. Figure 4.15a shows G as a function of temperature. Since temperatures investigated here are closer to the T_m than to the T_g, the thermodynamical effect dominates. Therefore, it can be observed that a lower temperature increases the growth rate. In other words, the thermal agitation at high temperature slows down the speed at which lamellae and spherulites grow. Comparing the two polymers, the growth rate for PA12 seems to be faster. As in the case of the induction time, a fair comparison can only be achieved when the polymers are plotted at the same degree of supercooling. This is done in Figure 4.15b. It is seen that the growth rates of the pure PA12 and the Pebax ® (i.e. the PA12 blocks in the Pebax) almost superimpose. Hence, under these conditions, spherulites in the multiblock - which consist of 88% in weight of PA12 - grow at a similar speed as the ones of the homopolymer.

Finally, an attempt is made to determine the nucleation density. This estimation is based on counting the number of spherulites formed. As already mentioned above, it is not a very accurate measurement since spherulites are overlapping. The results are presented in Figure 4.16a. The number of spherulites present in PA12 is lower and much more reproducible than for the 7033 SA. These two remarks point at the same cause, the presence of impurities in the 7033 SA material. Most probably, catalyst traces or other products from the synthesis that can be found in 7033 SA will contribute to heterogeneous nucleation. Therefore, 7033 SA has a higher number of nucleation sites. Additionally, since the impurities are not necessarily well dispersed, some regions of the material may present a high nucleation



a)



b)

Figure 4.15: Growth rate during isothermal crystallization of Pebax ® 7033 SA and PA12 a) regular scale b) reduced scale

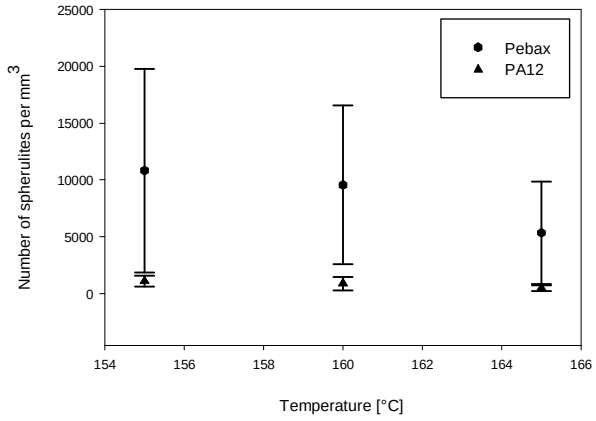
density whereas some other regions are potentially free of impurities and hence only homogeneous nucleation is observed, which accounts for a lower nucleation density. In the temperature range under investigation, the number of spherulites per volume unit for PA12 is almost independent of temperature, in agreement with other investigations [161]. On the other hand, the nucleation density of the 7033 SA seems sensitive to the temperature, although the low reproducibility of this measurement does not allow to assert it. The investigation of impurities being out of the scope of this work, it will not be discussed further. Finally, the nucleation density of the two polymers is plotted on a reduced scale in Figure 4.16b. However, since the trend was clear in Figure 4.16a, it does not provide additional valuable information.

4.3.2 Effect of temperature - Small angle light scattering

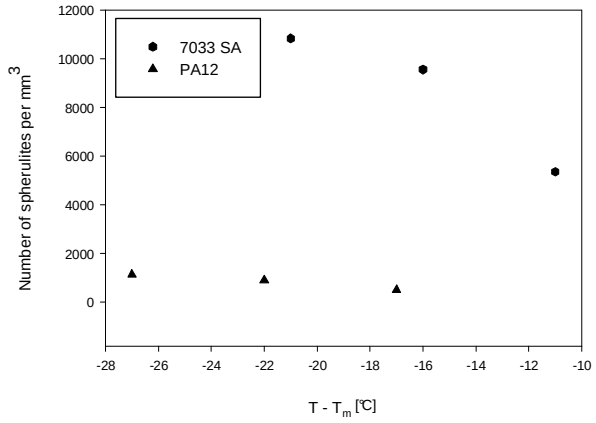
Before starting to address the effect of shear on the early stages of the crystallization, the effect of temperature is studied. According to the protocol shown in Figure 4.10, investigation of the quiescent isothermal crystallization was performed at three temperatures. The temperatures are chosen to provide a sufficient experimental time window. In a given polymer, when closer to T_m than to T_g, a decrease in crystallization temperature will increase the speed of the crystallization process. Hence, it can be expected that the density invariant peak will shift to smaller times with decreasing temperature. Since 7033 SA contains amorphous polytetramethylene glycol (PTMG), one can expect a slower crystallization in Pebax ® at given temperature than in neat PA12, as was observed in OM experiments. Indeed, PTMG segments soften the material and make T_m lower, thus the degree of supercooling is less for the multiblock than for the homopolymer. Hence, in Pebax ® the density invariant peaks are expected to occur later than in PA12.

PA12

Experimental results, shown in Figure 4.17, clearly indicate that the lower the temperature the faster the high density regions appear in PA12. The trend is very similar to what was observed by means of optical microscopy. As can be seen in Figure 4.18, the induction times obtained from OM experiments superpose better with the inflection point of the orientation invariant than with the peak position of the density invariant. Therefore, later on when the crystallization kinetics are compared, the inflection point of the orientation invariant is taken as the characteristic crystallization time. The agreement between the OM and SALS experiments implies that the time where spherulites are observed is similar to the one where lamellae (anisotropic elements) become longer and more numerous. This evidence supports the fact that high density regions are linked to nuclei. It should



a)



b)

Figure 4.16: Number of spherulites of Pebax ® 7033 SA and PA12 as a function of temperature a) regular scale b) reduced scale

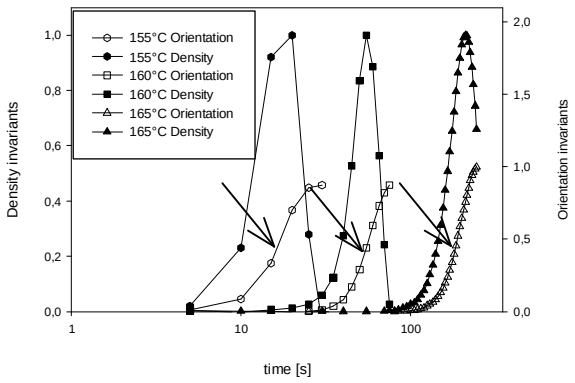


Figure 4.17: Influence of temperature - Invariants during crystallization of PA12

be stressed that the difference in invariant peak position is not related to errors due to the use of different samples. Indeed, a change of 5°C in crystallization temperature affects the peak position more strongly than expected from sample-to-sample variations (see section 4.2). Concerning the global shape of the curves, the data are similar at the three temperatures investigated here (e.g. position of orientation invariant with respect to density invariant). It indicates that the process is not fundamentally changed by temperature.

Pebax ® 7033 SA

The results on the Pebax ® (Figure 4.19) appear to be very similar to those on PA12. The position of the peaks shifts to smaller times when the temperature is lower, whereas the global shape of invariants remains the same. The main difference between the two polymers is their kinetics, peaks occurring earlier for the PA12 sample as compared to Pebax ®. This result is in agreement with OM experiments in which spherulites appear earlier and grow faster in PA12 than in Pebax ®. When the induction time estimated from OM experiments is compared with the inflection point of the orientation invariant, (Figure 4.20), a similar result to what was observed for PA12 is obtained, and their values are similar. This confirms that the density fluctuations and their transformation into anisotropic elements is of great importance in the crystallization process. When plotted on a relative temperature scale, it is clear that the kinetics of quiescent crystallization

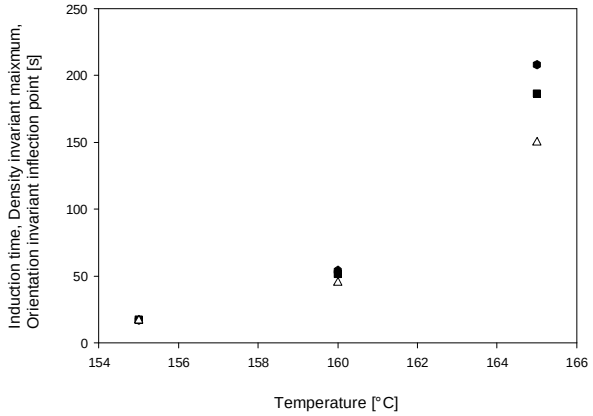


Figure 4.18: Comparison of (△) the induction time, (●) the position of the maximum of the density invariant and (■) the position of the inflection point of the orientation invariant for PA12

of the PA12 and of the Pebax ® are similar (see Figure 4.21). Hence, the fundamentals mechanisms are not different for the homopolymer and the copolymer under consideration.

4.3.3 Discussion on quiescent crystallization of PA12 and 7033 SA

It is found that the kinetics of static crystallization for 7033 SA and PA12 are similar. For the same degree of supercooling, the kinetics of 7033 SA and of PA12 are almost identical. On this relative scale, for the two polymers, the induction time and the growth rate of spherulites are of a comparable value. This is not very surprising since Pebax ® consists of 88% (in weight) of PA12, and since the two molecules studied here are of similar molecular mass (20 000 g/mol). The morphology of the semi-crystalline state is also very similar. However, the local arrangement is different. Though Maltese crosses are found in PA12 spherulites, in 7033 SA no such features are observed. This appears to be due to the presence of too many defects within the crystalline lamellae. These defects are supposed to be the amorphous regions (PA12 and PTMG) trapped in the lamellae. Finally, the nucleation behavior is the major difference between PA12 and 7033 SA. Indeed, the nucleation of 7033 SA is difficult to reproduce and the number of spherulites

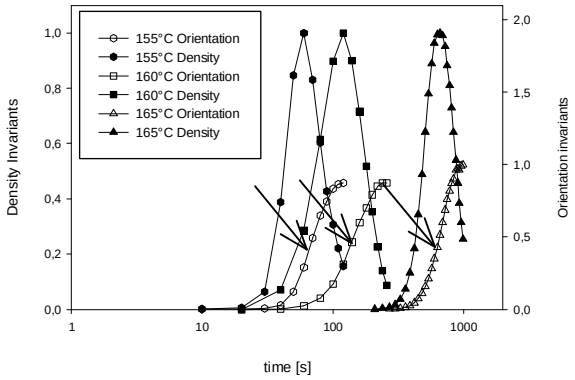


Figure 4.19: Influence of temperature - Invariants during crystallization of Pebax ® 7033 SA

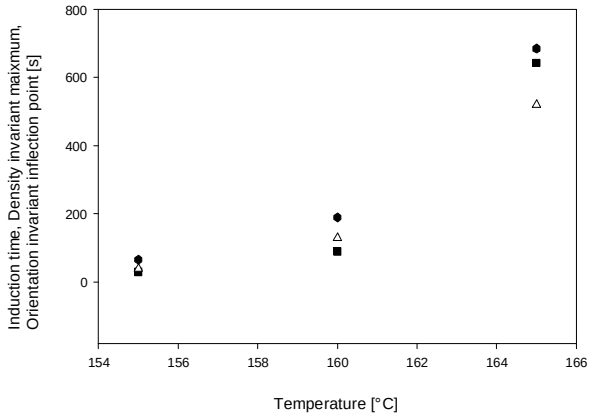


Figure 4.20: Comparison of (△) the induction time, (●) the position of the maximum of the density invariant and (■) the position of the inflection point of the orientation invariant for 7033 SA

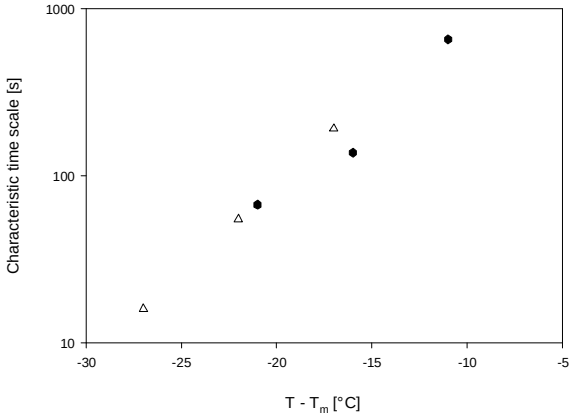


Figure 4.21: Comparison of the characteristic crystallization time on a reduced scale, obtained by SALS for (△) PA12 (●) 7033 SA

formed is much larger than the number of spherulites formed in PA12. This clearly indicates that, in the 7033 SA, heterogeneous nucleation is dominating. Impurities, such as catalyst traces, present in the material are thought to be responsible of such a behavior. They act as nucleation agents and thus increase the number of spherulites. In addition, their heterogeneous dispersion makes the crystallization a less reproducible process.

Concerning the density fluctuations observed by SALS, it is still debated whether they constitute the nuclei of the spherulites. The present work suggests a link. Indeed, if we compare the induction times as a function of temperature observed by OM (Figure 4.13), they appear to be very similar to the positions of the inflection point of the orientation invariants calculated from SALS experiments (see Figures 4.18 and 4.20). To be more precise, the induction time is always somewhat smaller than the position of the peak and corresponds roughly to the beginning of the increase of the orientation invariant.

4.4 Crystallization under shear

During processing, polymers are sometimes subjected to quite extreme flow conditions. Shear can have a profound effect on the crystallization process, ranging

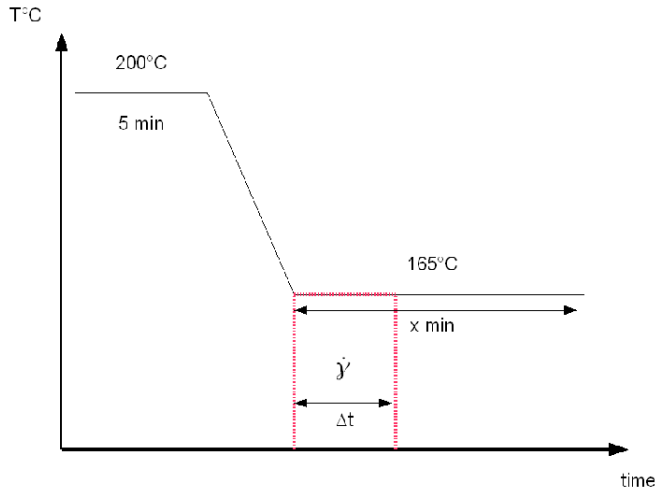


Figure 4.22: Thermal and shear protocol for the study of the effect of shear on crystallization

from an increase in nucleation rate to even modification of the crystalline morphology (see section 1.4). At present, however, no studies on the effect of flow on the crystallization of segmented multiblocks such as Pebax ® seem to have been conducted. Here, the experimental protocol developed by Janeschitz-Kriegl has been adopted [176].

The material is first heated to 200°C for 5 min to erase the thermomechanical history, after which the sample is cooled at 30°C/min to the desired crystallization temperature. Once the crystallization temperature is reached, a short shear pulse is applied. This protocol is depicted in Figure 4.22. The shear rate and the shearing time can be varied independently. A constant total strain γ (i.e., shear rate x shearing time) of 50 is chosen. The effect of shear flow on the crystallization process is investigated again with optical microscopy and SALS.

4.4.1 Effect of shear - Optical microscopy

Crystallization of PA12 under shear is observed as follows. At low shear rate, typically 1 s^{-1}, spherulites randomly appear in the material (Figure 4.23). When shear is applied, their number is slightly increased (6900 compared to 5500 /mm^3) and the time at which they appear is more or less the same (130 s). No particular change in the spherulites growth is seen after cessation of shear. However, at high

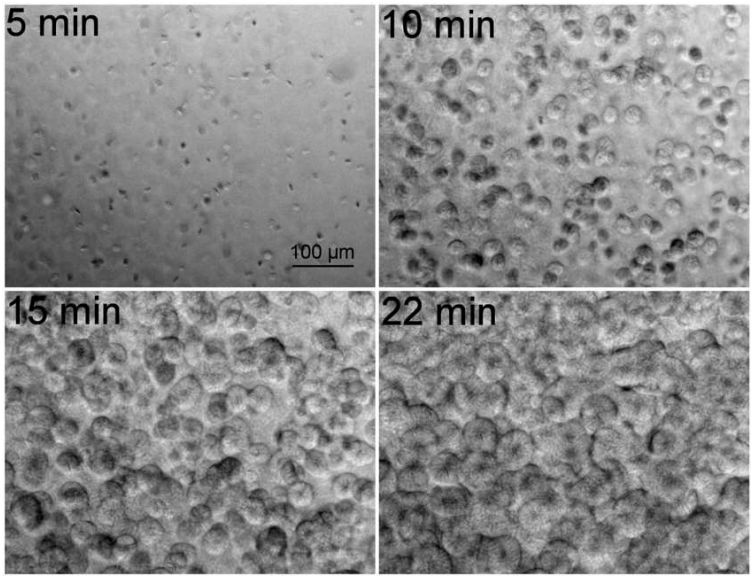


Figure 4.23: PA12 crystallization after 1 s^{-1} shear during 50 s ($\gamma = 50$) at 165°C

shear rates (50 s^{-1}) while spherulitic structures are still observed, their disposition in space is radically different. A typical crystallization picture at a high shear rate is shown in Figure 4.24. It can be seen that initially they nucleate in a row, parallel to the shear flow. After some time, random nucleation also occurs, hiding partially the previous organization. The density of nucleation greatly increases (at 30 s^{-1} and reaches about 28 000 /mm^3). However, it should be noted that at high shear rates, typically above 50 s^{-1}, it becomes difficult to properly count the number of spherulites, hence no value is given further.

In the case of the crystallization of Pebax ®, a different behavior is observed. While, in the shear rate range from 1 s^{-1} to 10 s^{-1} (Newtonian plateau to transition region), a dispersion of spherulites is observed, it does not appear to have a particular organization such as nucleation in rows. An example of crystallization after shear is presented in Figure 4.25. The nucleation density seems to be less affected by the shear as it remains around 3800 /mm^3.

The shear dependency of the nucleation density of PA12 and Pebax ® is shown in Figure 4.26. The trend explained previously is very clear on this figure. The more the PA12 is sheared, the more numerous are the spherulites, whereas the 7033 SA appears less affected by the flow.

It is thought that the difference in behavior may be due to a temperature effect.

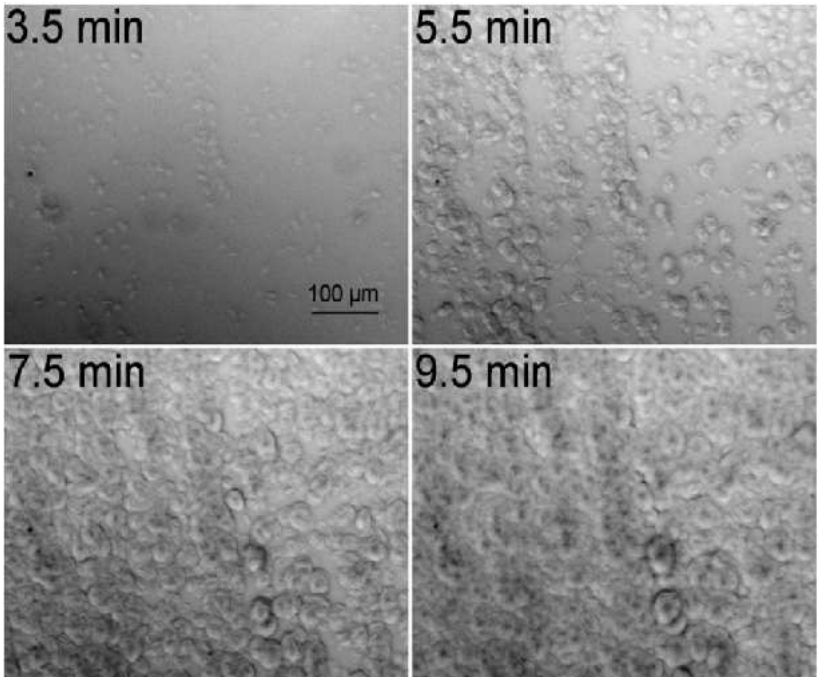


Figure 4.24: PA12 crystallization after 50 s^{-1} shear during 1 s ($\gamma = 50$) at 165°C

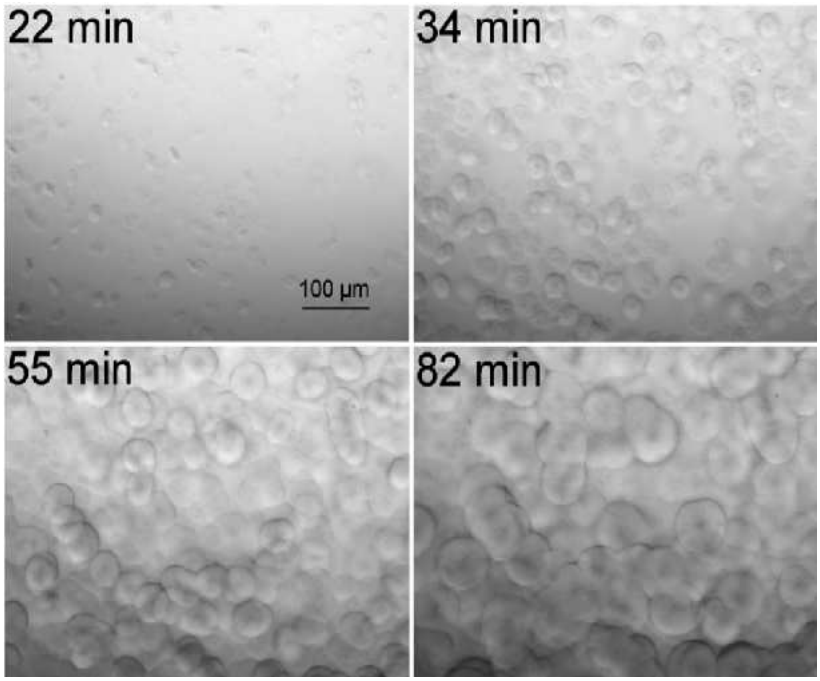


Figure 4.25: Pebax ® crystallization after 10 s^{-1} shear during 5 s ($\gamma = 50$) at 165°C

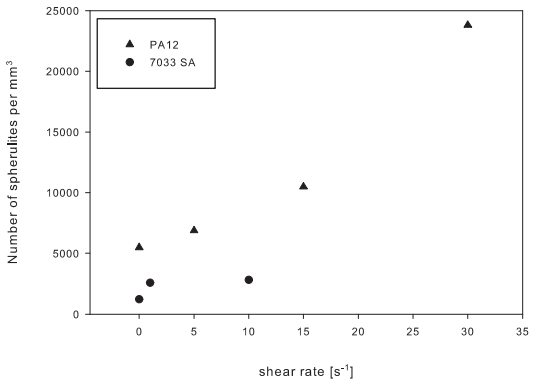


Figure 4.26: Nucleation density as a function of shear rate at 165°C ($\gamma = 50$)

Because the sensitivity to flow was investigated at the same temperature (165°C), it is relevant to perform one more set of experiments where the reduced temperature of PA12 will match the one of 7033 SA. To achieve such a comparison, either the crystallization of PA12 can be performed at higher temperatures or the one of 7033 SA can be done at lower temperatures. This basic consideration would make the PA12 measurement an obvious choice since experiments are more reliable. However, practically the crystallization of PA12 at 176°C takes an extremely long time. Therefore, to check whether the discrepancy in sensitivity to flow is due to a different degree of supercooling, the additional set of experiments was finally chosen to be performed with Pebax ® at 156°C. The nucleation density of the two materials, at the same degree of supercooling, are compared as a function of shear rate in Figure 4.27. The number of nuclei in PA12 is drastically enhanced when the shear rate is increased. This feature is commonly observed in many homopolymer systems and is associated with the flow-induced orientation of the chain. The probability of achieving the energetically stable unit cell conformation is clearly smaller in the random coil state in quiescent conditions than when oriented by flow. For the 7033 SA material, the effect of shear rate on the nucleation density is negligible, at least in the conditions studied here. Despite the fact that the imposed shear flow orients the segmented multiblock, no significant additional nuclei are created.

Based on rheological data (linear viscoelastic measurements), the longest relaxation time at this particular temperature is estimated to be 1 second for both

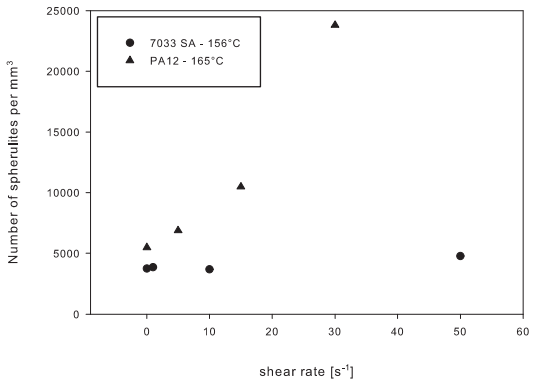


Figure 4.27: Nucleation density as a function of shear rate for the same degree of supercooling ($\gamma = 50$)

PA12 and 7033 SA. Hence, the Deborah number De - a measure typically used to determine the onset of molecular orientation (see for instance [177]) - exceeds a value of unity at shear rates above 1 s^{-1}. On this basis, an enhanced nucleation density would be expected in both polymers. As can be seen in Figure 4.27, this is not the case for 7033 SA. The reason for this phenomenon is not fully clear at present but is most probably related to the presence of catalyst traces that serve as heterogeneous nuclei.

4.4.2 Effect of shear - Small Angle Light Scattering

The influence of shear on crystallization was also studied by means of SALS, and here also the two materials are compared at the same degree of supercooling. Although the Stein-Wilson model discussed before may be no longer valid when the material is sheared, it was used in order to get an insight in the early stages of crystallization.

The total kinetics of the crystallization process after different shear histories is shown in Figure 4.28. Only the orientation invariant is shown here, since the inflection point on this curve is used as the characteristic crystallization time. As can be seen, flow does not have an effect on the crystallization time scale, since within experimental error, all curves superimpose. A comparison between the characteristic time scales defined as the inflection point of the orientation invariant

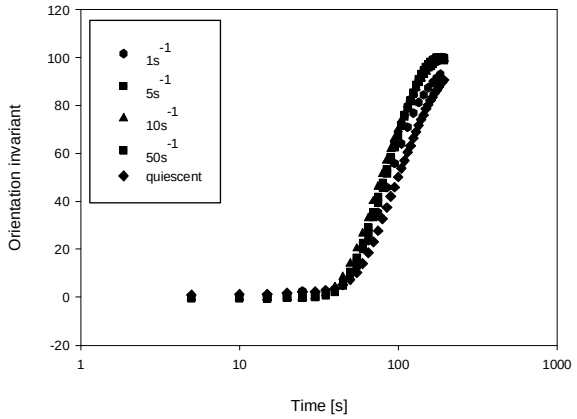


Figure 4.28: Crystallization of Pebax ® at 165°C - SALS orientation invariants as a function of shear rate ($\gamma = 50$)

as a function of shear rate for 7033 SA and PA12 is shown in Figure 4.29. In this figure, it can be seen that the effect on the kinetics is more pronounced on the homopolymer since the characteristic time scale decreases substantially with shear rate.

The dependence of the characteristic crystallization time for PA12 as a function of shear rate is roughly comparable with the dependence of its nucleation density on shear rate. This indicates that the subsequent growth rates of PA12 crystals are not significantly influenced by the preceding flow, as could be expected. Hence, from the data, it can be concluded that the increase in crystallization speed in PA12 is essentially dominated by the increase in nucleation density. In the case of 7033 SA, the characteristic crystallization rate is independent of the shear conditions, at least in the experimental window studied here. This is consistent with the absence of a shear effect on the nucleation density.

4.4.3 Conclusions on the effect of shear on crystallization of PA12 and 7033 SA

In this chapter, both the quiescent and shear-induced crystallization of the Pebax ® and a pure PA12 of equal molar mass were studied by means of optical microscopy and SALS.

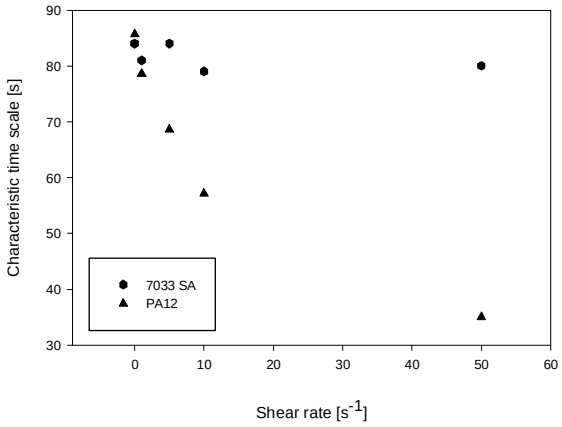


Figure 4.29: Crystallization of Pebax ® at 165°C - Peak position as a function of shear rate ($\gamma = 50$)

In the quiescent case, at a given temperature, PA12 kinetics is faster than the one of 7033 SA. This phenomenon is explained by the difference in the degree of supercooling, which directly comes from the presence of amorphous PTMG segments. However, at the same degree of supercooling the behaviors of the two polymers are very similar, both regarding the spherulitic growth rates as well as the total kinetics. The spherulitic morphology, however, is less developed in the block copolymer because of the presence of the PTMG segments that introduce defects in the crystalline ordering.

After application of flow, the situation becomes different. In the case of PA12, flow increases both the nucleation density and the global kinetics of the process. In the case of 7033 SA, flow did not have a significant effect on the nucleation density possibly because of the presence of a large amount of heterogeneous nucleation sites. The total kinetics of the crystallization process was not enhanced by flow, at least under the conditions studied here. It is thought that the large amount of heterogeneous nucleation sites is responsible of this lack of sensitivity. Another issue is the role played by the amorphous PTMG segments. They are thought to make the chains stretched by the shear quickly change back to their coil conformation. Several influences of the PTMG can be seen. First, the PTMG does not make hydrogen bonds and thus when a PTMG chain is stretched parallel to a PA12 chain, there is no extra stabilization that would be expected with two

parallel PA12 chains. Additionally, PTMG segments are more rubber-like, and therefore they continuously "pull" the PA12 segments which make them lose the orientation given by the flow.

This difference explains partially why the nucleation in rows is less easily observable with the 7033 SA because of smaller relaxation times. The mechanism underlying this particular arrangement of spherulites is clearly shear-dependent and hence the 7033 SA is less sensitive to it. Explanation of the row nucleation remains a puzzling problem. Indeed, the distance between nuclei in the same row is much larger than the polymer chain length, which implies the existence of a structure correlated over a few chains. Since in our experiments the nucleation occurs much after the cessation of flow, it is possible to exclude some hypotheses. Usually particles align under flow because doing so they reduce the friction with the liquid, and since there is no flow during nucleation, such an explanation is not valid. Moreover, the time required for nucleation being larger than the relaxation time of the polymer, the chains should have relaxed to their coil conformation when the nucleation starts. This is correct, providing that all the chains have a similar length. However, if a small amount of very long chain is present, and in a very small quantity to be not detected by means of rheology, the relaxation time of such chains may exceed the nucleation time. This hypothesis has the advantage to explain the existence of an elongated structure where the spherulite can develop and hence nucleate in rows, and it also explains why the distance between two consecutive spherulites can be superior than the average chain length. A proper study with a mixture of well defined short and long length chains would be required to verify this hypothesis.

Chapter 5

Study of 7033 SA blends

As discussed in chapter 1, one of the hypotheses of the delamination observed in injected Pebax ® pieces is based on the fact that Pebax ® 7033 SN consists of two immiscible components: the main 7033 material and a softer masterbatch carrier. This supposed immiscibility might lead to a weak cohesion. In order to evaluate the blend character, the effects of viscosity ratio and concentration on the morphology will be evaluated in this chapter.

5.1 Brief material description

The materials used in this study are the 7033 SA and 3533 polymers presented in chapter 2. The 7033 SA is the major component, the 3533 is incorporated by mixing the two polymers in an extruder. Various blends were prepared by simply changing the grade/viscosity of the 3533 or by varying its amount. Some other blends were made with 3533 which contains the common additives used in the industrial material, such as UV and heat stabilizers. By convention, the denomination of blends containing additives is written "SN" (*vs* "SA" for materials containing no additives). A description of the samples can be found in Table 5.1. It needs to be stressed here that two types of 3533 SA will be studied; RDG 242 and RDG 246. The two types are similar in composition but have a different viscosity which will affect their behavior as masterbatch carrier in the mixture with Pebax ® 7033 SA. It should be noted that RDG refers to particulars batches of 3533 SA. The RDG 242 and RDG 246 have extreme viscosities - low and high - and therefore, when RDG is not mentioned a regular 3533 SA of average viscosity is considered.

Minor component	Amount	Additives	Characteristic
3533 SA	1%	No	
3533 SA	3%	No	
3533 SA	5%	No	
3533 SA	10%	No	
3533 RDG 242	5%	No	Higher viscosity
3533 RDG 246	5%	No	Lower viscosity
3533 SN	5%	Yes	

Table 5.1: Description of 7033 SA blends

5.2 Probing the blend character by means of rheology

Predicting the behavior of a mixture of two components is not an easy task. Many parameters, linked to the physical properties and to the chemical nature of the components, will play a role. Among these features, the most important one is the miscibility of the two materials. When two components are totally miscible the obtained material behaves as a homogeneous material and most of the properties can be described by a simple mixing rule. However, in the case of partial miscibility or total immiscibility, a phase morphology is observed. In that case, the new material is classified as a blend. The next section investigates whether the masterbatch carrier used in industry can be considered to be fully miscible with the 7033 material.

5.2.1 Probing the blend character

Using rheological measurements, it is possible to detect whether a mixture behaves like a heterogeneous or a homogeneous material. Palierne developed a model to decribe the viscoelastic response of an immiscible polymeric mixture [178]. A simplified version of it, for a monodisperse particles size distribution and a constant interfacial tension during oscillatory measurements, is shown here:

$$G'_{Mixture}(\omega) = G'_{Matrix}(\omega)\frac{1+3\phi H(\omega)}{1-2\phi H(\omega)} \tag{5.1}$$

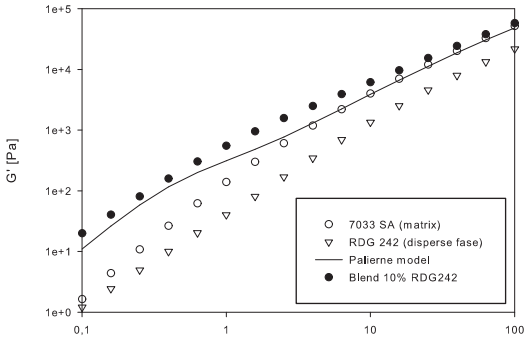
$$H(\omega) = \frac{[G'^*_d(\omega) - G'^*_M(\omega)][19G'^*_d(\omega) + 16G'^*_M(\omega)] + \frac{4\alpha}{R}[5G'^*_d(\omega) + 2G'^*_M(\omega)]}{[2G'^*_d(\omega) + 3G'^*_M(\omega)][19G'^*_d(\omega) + 16G'^*_M(\omega)] + \frac{40\alpha}{R}[G'^*_d(\omega) + G'^*_M(\omega)]} \tag{5.2}$$

with α the interfacial tension, R the droplet radius, ϕ the volume fraction of dispersed phase, and $G'^{*}_{M}(\omega)$ and $G'^{*}_{d}(\omega)$ the complex shear moduli of the matrix and the dispersed phase. When a small amount of an immiscible polymer is added to another polymer, a droplet matrix structure is formed. The storage moduli of such a mixture will be higher than those of the pure polymer alone. The reason behind this phenomenon is that the droplets will deform because of the imposed shear. This will change the interfacial area and allows for the storage of elastic energy. For instance the storage moduli of the mixture G'_{Mixture} can then be written as:

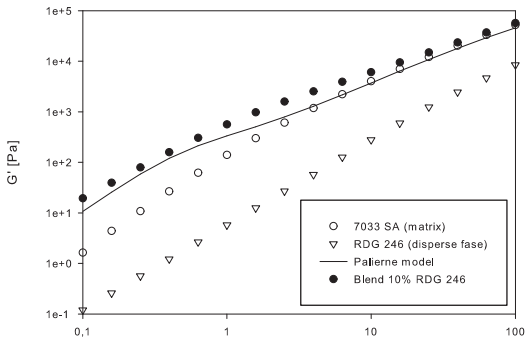
$$G'_{Mixture} = G'_{Components} + G'_{Interface} \tag{5.3}$$

with $G'_{\text{Components}}$ a linear combination depending on the concentration of each component and $G'_{\text{Interface}}$ the storage moduli induced by the presence of an interface. Therefore, the non-linear increase in G'_{Mixture} with respect to the native material is an indication that the two components are partially immiscible and hence is a fingerprint for the existence of a dispersed phase. Hence, such a behavior points towards real blend behavior. From these kinds of experiments, parameters such as interfacial tension and/or miscibility can thus be obtained.

In order to investigate whether a blend of 3533 and 7033 can be treated as an immiscible polymer blend, blends containing 10% of RDG were prepared. This relatively high concentration is chosen to obtain a sufficient rheological response of the interphase. Both high viscosity RDG 242 and low viscosity RDG 246 were used to cover the grade range of 3533. The response to flow of 7033 SA alone, as well as the response of the RDG polymers alone were also recorded. The results of these rheological measurements are shown in Figure 5.1. As can be seen in these figures, the response of the blends appears to be more complex than a linear combination of the two components alone. It indicates that the mixture is indeed a two-phasic blend, i.e. the components are only partially miscible. An attempt to fit the simple Palierne model, presented above, is also added to these figures. It is seen that the simple Palierne model cannot capture the response of the material since the fits do not match the blends curves. It can either mean that the interfacial tension is not constant and/or that the dispersed droplets are not monodisperse in size. Although the latter cause is more probable, based on this experiment only it is still difficult to discriminate the exact cause of the discrepancy. Hence, a direct visualization by means of optical microscopy will be of help. The interfacial tension cannot reliably be calculated from these experiments, another technique is required (see further).



a)



b)

Figure 5.1: Response of the blend to oscillatory flow a) 10% RDG 242 b) 10% RDG 246

5.2.2 Droplet relaxation

Since the interfacial tension determines the shape of the interface, observing at the deformation of a droplet gives valuable information. In fact, provided that the droplets are directly observable, it is easy to calculate the interfacial tension (see Equation 5.12). In order to obtain large droplets, blends based on RDG 242 and RDG 246 with a high content of dispersed phase (10%) were prepared. To obtain the interfacial tension, droplet relaxation experiments have been performed. Prior to the measurement, the samples were pre-sheared at 0.25 s^{-1} for 200 s in order to obtain droplets of convenient size for OM observation. For that purpose the blends were inserted in a Linkam shear cell. Based on the relaxation time of the droplets and the knowledge of the final radius of the droplet, the interfacial tension can be calculated as:

$$\tau = \frac{\eta_m R}{\Gamma} \tag{5.4}$$

where τ is the relaxation time, η_m the viscosity of the droplet material, R the radius of the droplet and Γ the interfacial tension.

As shown for instance by Vinckier [179] this value of the relaxation time properly describes the droplet relaxation provided that the imposed deformation is not too high. An example of such an experiment is shown in fig 5.2 for the RDG 242 blend. A clear interface can be seen in this figure, pointing towards a real blend character of this blend system. The relaxation of different droplets is monitored as a function of time and the results are fitted with an exponential curve. The result is shown in Figure 5.3, the relaxation can indeed be described by a simple exponential curve. From these measurements, the average interfacial tension can be calculated to be 0.54mN/m. This value is relatively small compared to values obtained for conventional polymer blends that are typically one order of magnitude higher. This is not surprising since the 7033 and the 3533 are chemically similar in nature.

In the case of RDG 246, optical microscopy is not capable of obtaining droplet images either because the droplets are too small or the refractive index in low or because the RDG 246 is fully miscible with the 7033 SA. Considering that it was previously found in rheological experiments that the RDG 246 response to flow presents a blend character, one can conclude to the non-miscibility of RDG 246 and 7033 SA. The droplets are too small to be observable by OM. However, estimation of the interfacial tension of RDG 246 blend is still possible. It can be achieved it by comparing the critical capillary number of the two RDG blends. Indeed, the critical capillary number is a known function of p (see Figure 1.10),

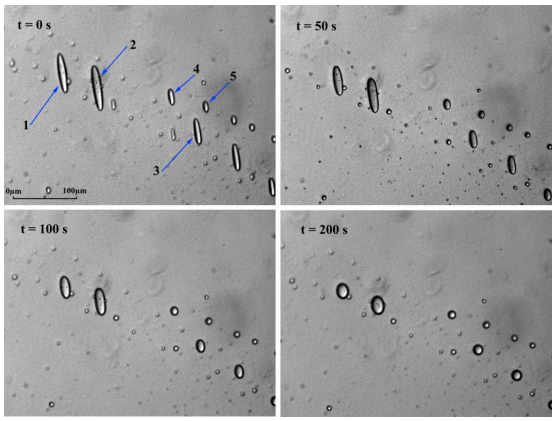


Figure 5.2: Relaxation of RDG 242 droplets in 7033 SA matrix

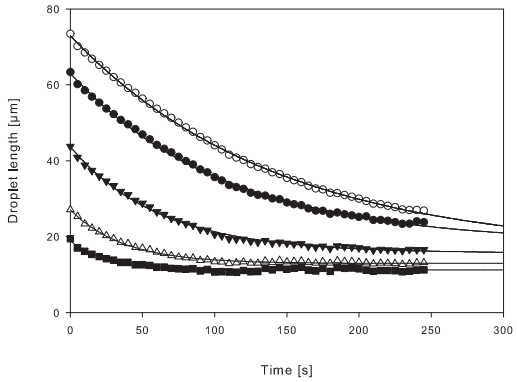


Figure 5.3: Droplets relaxation of the blend 10% RDG 242 after cessation of flow

and the measurement of p can be done by means of rheology (see further). From Figure 1.10, the ratio A of the two critical capillary number is obtained.

$$Ca_{RDG242\ crit} = A\ Ca_{RDG246\ crit} \tag{5.5}$$

$$\frac{\eta_m \dot{\gamma} R_{RDG242}}{\Gamma_{RDG242}} = A\ \frac{\eta_m \dot{\gamma} R_{RDG246}}{\Gamma_{RDG246}} \tag{5.6}$$

Providing that the measurement of radius of the droplets is done at the same shear rate, and that this shear rate is high enough to reach the critical capillary number, i.e. droplets are broken during shear, the Equation 5.6 can be reduced to:

$$\frac{R_{RDG242}}{\Gamma_{RDG242}} = A\ \frac{R_{RDG246}}{\Gamma_{RDG246}} \tag{5.7}$$

Since the values for RDG 242 are already known, only R_{RDG246} has to be measured. This can be done by means of SALS experiments. It has been shown elsewhere [127] that extracting the correlation length from a Debye-Bueche plot of the intensity, see Equation 5.8, allows to approximated the radius of the droplet by Equation 5.9.

$$I(q)^{-0,5} = \frac{1}{A^{0,5}} + \frac{\xi^2}{A^{0,5}} q^2 \tag{5.8}$$

$$R^2 \simeq 10\xi^2 \tag{5.9}$$

In experiments where the samples were pre-sheared for 1000 s in order to reach steady state, at 5 s^{-1}, it was found that ${\xi^2}_{RDG242}/{\xi^2}_{RDG246} \simeq 7.0$. As a consequence, the interfacial tension of RDG 246 blend is calculated to be about 0.20 mN/m. Such a low value was expected since this material forms much smaller droplets than RDG 242, less than 5μm. It should mentioned that in this calculation, the ratio A of the two critical capillary numbers was taken equal to 1 since the viscosity ratio of the RDG242 and of the RDG246 blends (measured further) leads to the same value of Ca_{crit}.

5.2.3 Viscosity ratio measurements

Determination of the viscosity ratio

As was mentioned in chapter 1, the viscosity ratio between the matrix and the dispersed phase is of importance since it defines to a certain extent the blend response to flow. Hence, a first step is the measurement of the viscosity of the different 3553 samples. Dynamic measurements have been performed and, as was done for other TPEs [180], the Cox-Merz analogy applied to calculate the steady state viscosity. The results are shown in Figures 5.4, 5.5 and 5.6 in which the viscosity is shown at different temperatures.

From these data, the viscosity ratios of RDG 242 and RDG 246 *vs* 7033 SA at different temperatures can be easily determined. Results are shown in Figure 5.7. Over the frequency (shear rate) range of 0.1 to 100 s^{-1}, it appears that both blends have a more or less constant viscosity ratio. However, as can be seen in Figure 5.7 the blend consisting of RDG 242 has a larger viscosity ratio than the blend based on RDG 246. This difference is substantial and this will drastically influence the break-up behavior of the different blends.

Additionally, from these measurements, it is also possible to predict the rheological behavior of the neat 7033 SA and RDG polymers at higher shear rates. To do so, one has to construct the master curve of each polymer for a given reference temperature. An example of such a master curve is shown for 7033 SA at 190°C in Figure 5.8. As can be seen in this figure, the experimental data superpose well when shifted by the appropriate shift factor a_T. In order to capture the behavior at various shear rates, a model that can describe the viscosity has to be used. One of the most simple models available is the three-parameter Ellis model [181]. In this model the viscosity is written as:

$$\eta = \frac{\eta_0}{1 + K(\dot{\gamma})^{1-n}} \tag{5.10}$$

where η_0 is the viscosity in the Newtonian regime, with K and n two constants independent of temperature. Since the shift factors are known, one can easily calculate $\eta_0(T)$, and hence the viscosity of the materials can be predicted at any temperature and shear rate.

Since blends based on RDG 246 have a lower viscosity ratio, it is anticipated that breaking-up of fibrils is easier to achieve in this blend than in the one based on RDG 242. This can be verified through a simple calculation of the break-up times.

Van Puyvelde et al. [182] demonstrated that the deformation-induced break-up in polymer blends seems to follow a general rule given by following scaling relation:

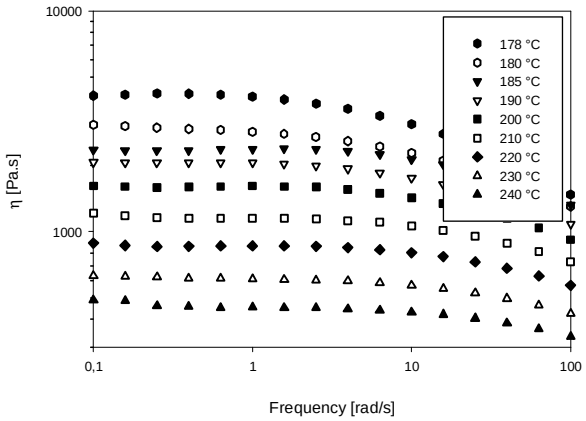


Figure 5.4: Viscosity of 7033 SA as a function of frequency at different temperatures

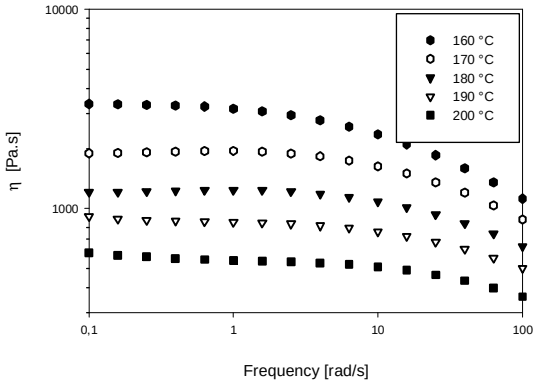


Figure 5.5: Viscosity of RDG 242 as a function of frequency at different temperatures

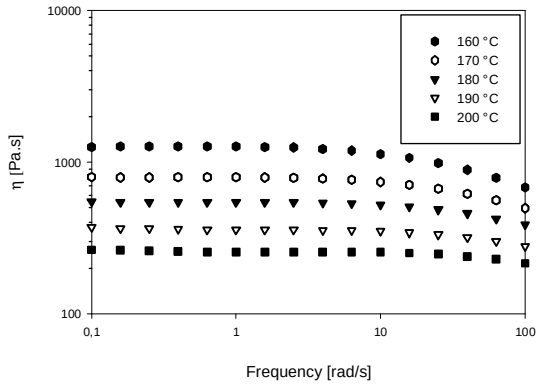


Figure 5.6: Viscosity of RDG 246 as a function of frequency at different temperatures

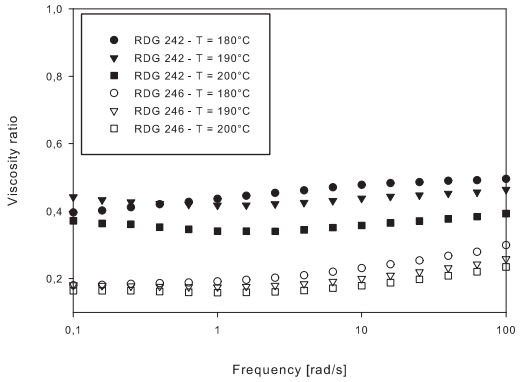


Figure 5.7: Viscosity ratio (dispersed phase / matrix) at various temperatures as a function of shear rate (frequency)

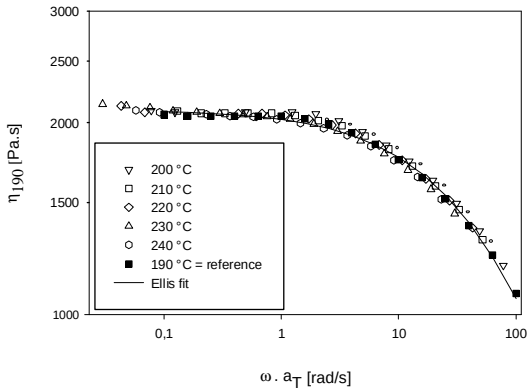


Figure 5.8: Viscosity master curve and Ellis fit of 7033 SA at 190°C

$$t_{B\ deform} \propto {C_a}^{2/3}\sqrt{p}/\dot{\gamma} \tag{5.11}$$

So far, this relation has been found to be experimentally valid for $1 < {C_a}^{2/3}\sqrt{p} < 10$. With the conditions fixed in the further calculations, the product ${C_a}^{2/3}\sqrt{p}$ is sometimes outside this experimental range. The minimum value is 0.12 and the maximum one 19. In a first approximation, Equation 5.11 will be considered to be valid. When shear flow is not strong enough to break up droplets, the elongated droplets will be under the form of fibrils. If the material is cooled slowly, before its solidification, Rayleigh instabilities will develop and will break up the fibrils in several droplets. The time needed for Rayleigh instabilities to break up a fibril can be estimated as [130]:

$$t_{B\ rayleigh} = \frac{\eta_m B}{\Gamma\Omega}\log(\frac{10^{23}\Gamma B^2}{T}) \tag{5.12}$$

where T is the temperature, B the radius of the fibril and Ω a known function of p [183].

Assuming that the interfacial tension does not have much influence on the deformation rate, the geometry of the elongated droplets can be easily calculated by means

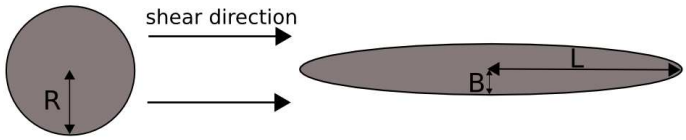


Figure 5.9: Scheme of a droplet deformed under flow

of the affine deformation theory [184], see Figure 5.9 and related Equations 5.13 and 5.14:

$$L = R\sqrt{1 + \frac{\gamma^2}{2} + \frac{\gamma}{2}\sqrt{4 + \gamma^2}} = long\ semi\ axis\ of\ deformed\ droplet \quad (5.13)$$

$$B = R^{3/2}L^{-0.5} = short\ semi\ axis\ of\ deformed\ droplet \quad (5.14)$$

By calculating the break-up times under various conditions, it is hence possible to predict the blend morphologies obtained after injection molding.

To simulate conditions close to the injection ones, relevant values of the parameters are chosen. High shear rates ($\dot{\gamma}$) of 100 and 1000 s^{-1} and a short injection time (t_{inj}) of 1 s are selected for that purpose. It thus sets the deformation strain (γ) at 100 and to 1000, see Equation 5.15.

$$\gamma = \dot{\gamma} * t_{inj} \quad (5.15)$$

The temperature is about 240°C. At such temperature and shear rate, the viscosity can be obtained from the rheological measurements. These values are shown in Table 5.2. The viscosity ratios are thus known, as well as the factor Ω in Equation 5.12. It therefore leaves the droplet radius R and the interfacial tension Γ as variables (contained in C_a).

The interfacial tensions previously found for RDG 242 and RDG 246, are 0.54 and 0.20 mN/m respectively. Figures 5.10 and 5.11 show the influence of the initial droplet radius on the break-up times for a shear rate of 100 s^{-1}. It is is seen that the deformation induced break-up time, though lower for RDG 242, is comparable

Polymer	η_0 [Pa.s]	η [Pa.s] at 100 s^{-1}	η [Pa.s] at 1000 s^{-1}
RDG 242	73	3.4	0.5
RDG 246	32	2.7	0.4
7033 SA	471	333	164

Table 5.2: Viscosity estimations at 240°C

for both blends. This result is not surprising since at high temperatures and high shear rates, the two RDG materials have a comparable low viscosity. For an injection time of 1s, it is clear that the shear is not able to break droplets with a radius superior to 0.8 μm. It is thus anticipated that, during the injection, such droplets will the be found under the form of fibrils. It is also seen that the Rayleigh break-up requires more than the injection time to occur, as a consequence of which after injection the fibrils remain. With these conditions of injection, one can expect to see fibrils in the injected piece.

In Figures 5.12 and 5.13, the influence of the initial droplet radius on the break-up times for a shear rate of 1000 s^{-1} is shown. Here, the deformation induced break-up time is always smaller than the injection time. It means that the deformation is large enough to break up the droplets of any size. This holds for the RDG materials under consideration here. Therefore, when applying such a high shear, no fibrils are expected to be present after injection.

Conclusions

Since a fibrillar morphology is supposed to weaken the material because it brings a discontinuity/interface over a large scale, and hence leads to delamination, it is of interest to avoid their formation in injected pieces. Several parameters can be manipulated, such as viscosity ratio, injection speed or cooling rate. Because only the polymer of the dispersed phase is susceptible to be modified, and since a low viscosity is required for easier incorporation of additives, the choice is rather limited. The experiments and the calculation show that two polymers of extreme viscosity at room temperature, behave in a very similar manner during injection. Therefore, it can be expected that changing the viscosity of 3533 grade will be inefficient. Only two choices are left to suppress the formation of fibrils. Either more time can be allowed to the material to cool down after injection, so that Rayleigh break-up can occur, or a higher shear rate should be used in order to let the excess of deformation break up the droplets. The first solution, while efficient, is probably not suited from an industrial point of view since it slows down the production rate. As a consequence, the latter one might be more suitable.

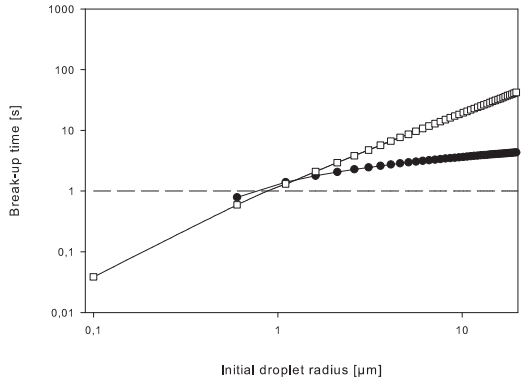


Figure 5.10: Break-up times of the blend 10% RDG 242 at 100 s^{-1} - $\Gamma = 0.5$ mN/m (•) Deformation induced break-up - from Equation 5.11 (□) Rayleigh instabilities induced break-up - from Equation 5.12 (− − −) Injection time

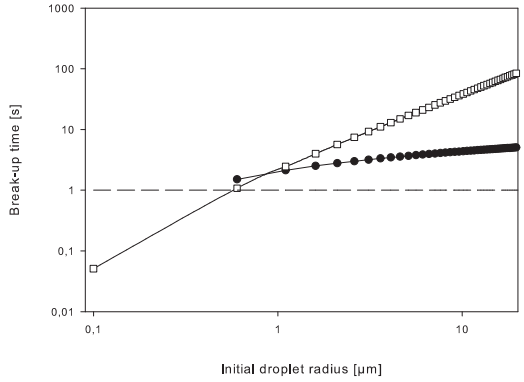


Figure 5.11: Break-up times of the blend 10% RDG 246 at 100 s^{-1} - $\Gamma = 0.2$ mN/m (•) Deformation induced break-up - from Equation 5.11 (□) Rayleigh instabilities induced break-up - from Equation 5.12 (− − −) Injection time

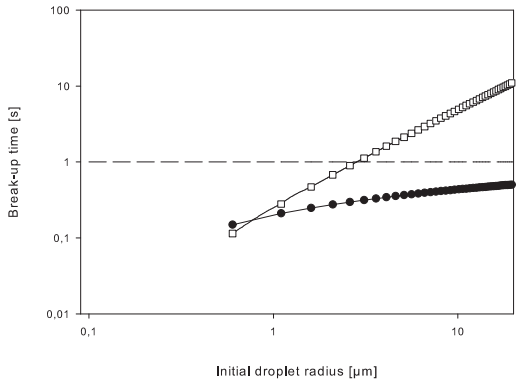


Figure 5.12: Break-up times of the blend 10% RDG 242 at 1000 s^{-1} - $\Gamma = 0.5$ mN/m (•) Deformation induced break-up - from Equation 5.11 (□) Rayleigh instabilities induced break-up - from Equation 5.12 (− − −) Injection time

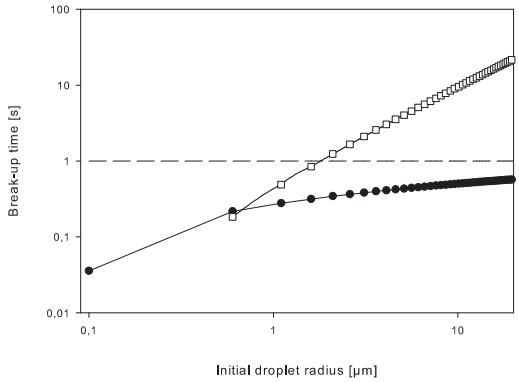


Figure 5.13: Break-up times of the blend 10% RDG 246 at 1000 s^{-1} - $\Gamma = 0.2$ mN/m (•) Deformation induced break-up - from Equation 5.11 (□) Rayleigh instabilities induced break-up - from Equation 5.12 (− − −) Injection time

5.3 Direct observation of the blends - Transmission electron microscopy

7033 SA and 3533 SA were found to be partially miscible, and Equation 5.12 shows that a small value of the interfacial tension implies a small value of the droplet radius. Therefore, the radius of droplets obtained by blending can be of relatively small size. Furthermore, it is expected that under shear, droplets will deform and become more narrow in the direction perpendicular to flow. The structure size can then be below the micrometer scale, and at such scale OM experiments are no longer suitable for direct observations. Therefore, it is relevant to pursue investigation by means of Transmission Electron Microscopy (TEM) which allows monitoring of smaller structures.

5.3.1 Discrimination of dispersed phase

TEM is a powerful tool to observe various morphologies or topologies. However the structure observed should have an electron density different from that of the surroundings so that a visual contrast can be obtained. In the case of polymers, in order to improve this contrast, a staining agent is required. The efficiency of the TEM technique, is thus bound to the use of a suitable staining agent. Two conditions should be fulfilled:

- the staining agent should not alter the morphology
- the staining agent should be selective and affect only one component

As a result of the first condition, the staining is usually done on the sample after the morphology one wants to observe has formed. The second condition can be more difficult to realize. A common way to stain selectively, is to use a molecule which will chemically react or bind to one of the components. However in the case studied here, the 7033 and 3533 materials are of the same chemical nature (PA12 and PTMG) and hence if a chemical reaction can occur with 7033, it can happen with 3533 as well. In order to solve this problem, another approach needs then to be found. Considering the blend of 7033/3533, the main difference between the two phases is the viscosity, i.e. the difference in chain length. This remark is of importance, because it means that diffusion of a particle through a network of 7033 chains (long length) will be slower than in a network of 3533 chains. If this is true, it would allow the use of non-reactive staining agent. In the TEM experiments presented in this chapter, the staining molecule is ruthenium oxide (RuO_4), a heavy electron loaded molecule, which can diffuse in the bulk of the polymer. The staining process is done in the gaseous phase, i.e. the sample to be stained is

left in a RuO_4 vapour for a certain amount of time and then taken out for the TEM experiment. It should be noted, that staining with such a diffusive molecule is delicate. Indeed, though the RuO_4 diffuses faster in 3533, it also diffuses into 7033. Too short exposition time of the sample to RuO_4 vapour ends in a weak contrast (concentration of RuO_4 is not much different in the two phases). Too long exposition time makes the material very opaque to the electron beam, and either a stronger beam is needed (risk of damaging the sample) or either thinner samples (difficult to obtain) are required.

As was shown in section 3.3, this staining method is based on the difference of diffusivity. Indeed, a semi-crystalline sample can be selectively stained in function of the density of its phases. Hence, RuO_4 appears to be a suitable staining agent for the study of the Pebax ® blends.

5.3.2 Observation of the blends

In this section, to prove the relevance of such approach, blends of 7033 SA + x% of 3533 SN, with x = 1,3,5,10 are monitored. The samples were first annealed at 200°C to remove the thermomechanical history, after which they were cooled down in liquid nitrogen and prepared for TEM. The images resulting from these experiments are shown in Figure 5.14. It is seen that a higher amount of dispersed phase (here 3533 SN) induces a higher coverage of the black spots by increasing their number and/or their size. This is again a proof that the RuO_4 allows to stain selectively the soft phase.

5.3.3 Observation of a sheared sample

In the previous section, it was found that the dispersed phase can be selectively stained and therefore direct observation by means of TEM is possible. The question arises whether it is possible to observe the effect of flow on the blend morphology. The current state of the technology, makes the dynamical measurement by TEM impossible, however, if the sample is frozen in a given state, later observations are still possible.

In an attempt to make qualitative estimations, a injected piece was made from a blend containing 5% of 3533 SN. In Figure 5.15 the TEM image obtained is shown. The black spots observed previously, i.e. the 3533 area, now present an elongated shape characteristic of droplets under flow. It should be noticed that the width of these structures is at most about 40 nm, which makes them impossible to monitor by means of OM.

In the quiescent state, by means of TEM it was observed that a 5% blend is made of a dispersion of $\approx$100 nm radius. Such droplets will deform into fibrils

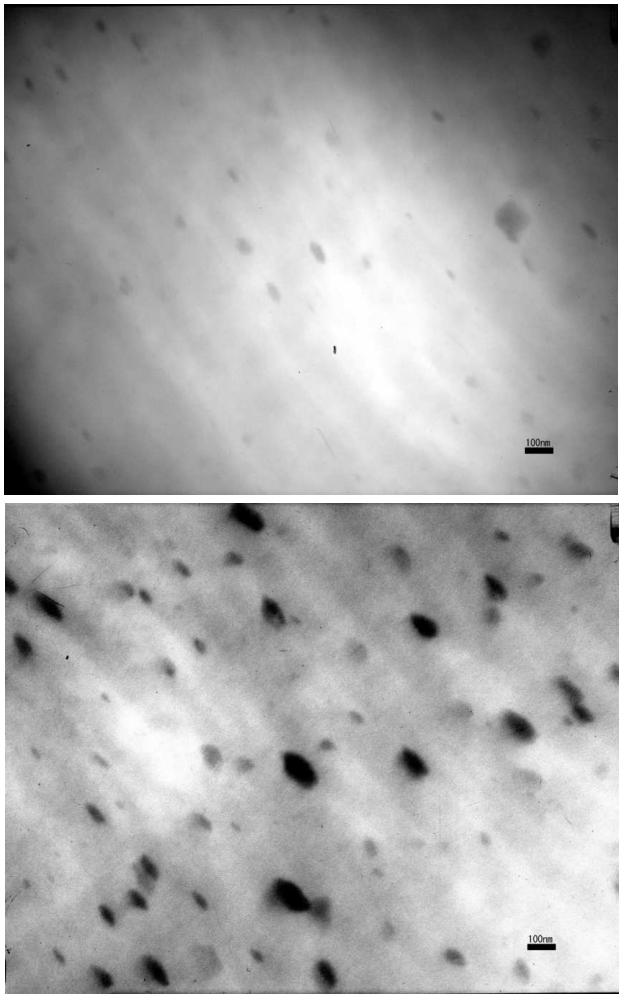


Figure 5.14: TEM images of 7033 SA + 3533 SA blends of various amount of 3533 a) 1% b) 3% c) 5% d) 10%

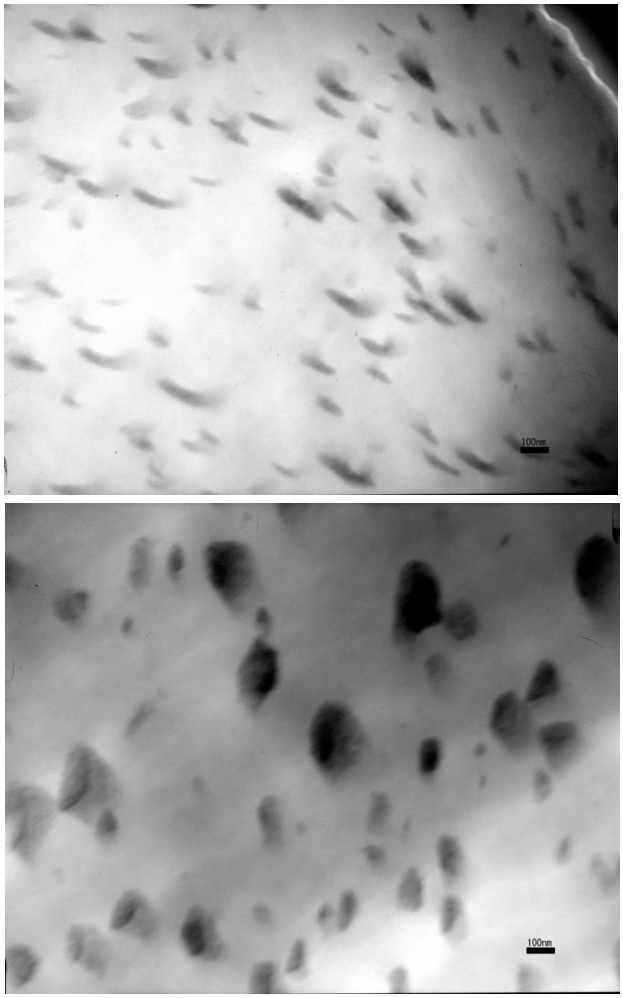


Figure 5.14: TEM images of 7033 SA + 3533 SA blends of various amount of 3533 a) 1% b) 3% c) 5% d) 10%

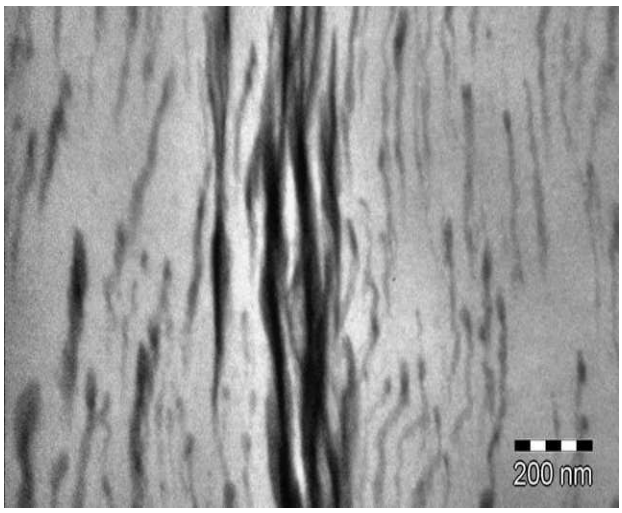


Figure 5.15: Injected piece of 7033 SA + 3% of 3533 SN observed by TEM after RuO_4 staining

under the effect of shear, and they may break up if the material is not frozen fast enough. Since the fibrils shown in Figure 5.15 have very different diameter it can be concluded that before injection at least two populations, in size, of droplets were present. The radius of the large droplets was logically higher than the diameter of the thick fibrils, and using Equation 5.12 a droplet radius of roughly 3 μm is found. For such a large droplet, about 10 s would be required to observe the Rayleigh instabilities induced break-up. Clearly the cooling was too fast and hence the fibril was frozen as such.

5.4 Conclusions

The mixtures of the 7033 SA with 3533 (SA, RDG or SN) were found to be partially miscible, but still formed a droplet dispersion. Since the two components are chemically similar, the interfacial tension is weak compared to truly immiscible blends. Therefore, the droplets are usually small and difficult to observe by means of microscopy. The characteristics of the material are such that no break-up of the droplets is predicted during injection, because of the shear rate. The expected morphology of the dispersed phase is hence fibril-like. However, providing that the glass transition of the material is not reached too quickly, it was also found that Rayleigh instabilities are susceptible to break the fibril. TEM and rheological

experiments show that the droplets are not monodisperse in size. As a consequence some droplets, the largest ones, will never have time to collapse and hence fibrils are still observed in the injected pieces.

Chapter 6

General conclusions

This study was focused on the influence of a thermomechanical treatment on the delamination phenomenon in industrial Pebax, a PA12/PTMG copolymer. The investigation was performed along two main axes. First, the morphologies that can develop due to the natural segregation between the blocks is considered to be a possible origin of delamination. Since the organization of the phase segregated microdomains is expected to be dependent on the thermomechanical history, an independent study of the effect of both thermal and mechanical treatments was performed. In chapter 3, the transition temperatures of the multiblock were measured, and the effect of the thermal history on the final morphology was investigated. In chapter 4, in an attempt to get closer to the industrial process, the effect of the mechanical history was studied. For comparison purposes, the pure PA12 homopolymer was also studied. Secondly, noticing that the real material is in fact a mixture of two chemically similar multiblocks, one can think that macrophase separation of the two multiblocks is another possible source of delamination. Based on this approach, the blend character of such a mixture and the morphology expected after injection molding were discussed in chapter 5.

Influence of the thermal history on the morphology of PA12/PTMG

For the study of the morphology of crystallizable multiblocks, usually three transition temperatures are found to be relevant: the glass transition temperature T_g, the melting point T_m, and the order-disorder transition temperature T_{ODT}.

- T_g being related to molecular movement, its measurement was performed by

means of differential scanning calorimetry and found to be 5°C.

- T_m being related to the crystalline structure, it was obtained by both differential scanning calorimetry and wide-angle X-ray scattering experiments. Its value is 176°C for PA12/PTMG block copolymer rich in PA12 and without additives.
- T_{ODT} being related to the segregation of the segments on a local scale, for which rheological and small-angle X-ray scattering experiments were performed. It was determined to be 184°C.

Since the T_{ODT} is higher than the T_m, it means that the material can be organized even in the molten state. As a consequence, one can distinguish three states for the Pebax, disordered, organized melt and semi-crystalline state. By means of x-ray scattering techniques the morphology of the structured states, their kinetics and their interdependence were investigated.

- The semi-crystalline state of PA12 is found to be comparable to PA12 with pseudo-hexagonal γ' as the principal crystalline form. It can be described as a coarsely lamellar organization.
- The exact morphology of the molten phase-separated state cannot be assessed, although it appears to be lamellar-like. The polydispersity in phase thicknesses and the very short length at which an order can be correlated makes such an analysis difficult.
- The crystallization of the PA12 segments is a fast process, and in the temperature range investigated, it appears to be independent of the thermal protocol applied. The segregation power of the crystallization is strong.
- The kinetics of the organization of the molten state is found to be accelerated when the previous state is an organized. Internal reorganization from the crystalline morphology enables such a fast appearance of an organized state.
- When cooled down from a disordered melt, the microphase separation in the melt can be described as a spinodal process. The emergence of the phase-separated structure is much slower than when obtained by heating from the semi-crystalline state.

The fact that, in quiescent state, the PA12/PTMG semi-crystalline state is similar to the PA12 homopolymer one, makes the parallel study of a neat PA12 relevant. Therefore, in the study of delamination as a consequence of shear-induced crystallization, a PA12 homopolymer with a molecular weight close to the PA12/PTMG was also considered. Since, the molten microphase separation was found to have slow kinetics and to have no substantial effect on the crystallization, it has not been considered in the further delamination investigation.

Influence of the thermomechanical history on the crystallization of PA12/PTMG

Prior to the study of shear-induced crystallization, the crystallization of PA12/PTMG and PA12 homopolymer in the quiescent state was investigated. In static conditions, the kinetics of crystallization are similar for the two materials when the degree of supercooling is the same. On such a relative scale, the induction time and the growth rate of spherulites are also comparable for both materials. Such a result was expected since the total amount of PA12 in the two polymers is similar, and since also their molecular weight is equal. Concerning the morphology, both materials exhibit a spherulitic structure. The morphologies appear to be the same, except that no Maltese crosses are found in PA12/PTMG spherulites. It is thought that this is due to the presence of defects within the crystalline lamellae, these defects are being linked to the amorphous regions (PA12 and PTMG) trapped in the lamellae. The main difference between the PA12/PTMG and the PA12 homopolymer lies in the nucleation behavior. The nucleation density of PA12/PTMG is found to be higher than the one of PA12 homopolymer, and the reproducibility of its measurement is poor. This suggests that heterogeneous nucleation is dominating in PA12/PTMG. Since impurities, such as catalyst traces, are present in the material, they are thought to be responsible for such a behavior. The heterogeneous dispersion of the impurities makes the experiments less reproducible.

Looking at the early stages of crystallization, the present work suggests a link between the density fluctuations observed by small-angle light scattering, and the nuclei that give rise to spherulites. The induction time as a function of temperature observed by optical microscopy and the position of inflection point of the orientation invariant calculated from small-angle light scattering experiments are almost the same. The crystallization of PA12/PTMG and PA12 homopolymer is thus described as follows:

- Cooling from the melt, high density regions appear throughout the volume. Some scattering is monitored in small-angle light scattering.
- Crystalline lamellae grow from the nuclei. During their growth lamellae consume the matter and hence 'absorb' high density regions. The density invariant decreases.
- Crystallization stops when two spherulites come in contact. The orientation invariant stagnates.

When a shear step is applied prior to crystallization, a difference in the crystallization process is observed. For the PA12 homopolymer, increasing the shear rate leads to two distinct effects.

- The nucleation density increases with shear rate. Since the chains align and stretch in the direction of the flow, they end up in a more favorable conformation to crystallize.

- At high shear rate, the nucleation proceeds in rows. Lines of spherulites are observed in optical microscopy. It is thought that a small amount of high molecular weight chains are present in the sample. They remain elongated for a long time sufficiently for nucleation to occur. Therefore, the crystallization initiates preferentially in the neighborhood of these chains. As a consequence, the spherulites appear in rows.

In the case of PA12/PTMG, the effect of shear on crystallization is different because of the presence of amorphous PTMG segments. They tend to bring the molecule back to the coil conformation. The crystallization being also controlled by the presence of impurities (heterogeneous nucleation), the effect of the flow is less noticeable.

- As a consequence, the nucleation density appears to be more or less insensitive to the shear rate. The number spherulites remains almost constant. No memory of the shear is present anymore when the nucleation occurs.

- It also implies that if high molecular weight chains are present, they are less likely to remain stretched. Therefore, on the contrary to PA12 homopolymer, no crystallization in rows is observed.

The information gathered in this study, concerning the influence of thermomechanical history on the crystallization process, shows that the morphology of PA12/PTMG is much less dependent on shear and that temperature only modifies the kinetics. In the limit of the conditions applied, it seems that the shear-induced crystallization is hardly the cause of delamination since the structure is not altered by the application of flow. A better option would be to consider a possible macrophase separation in the delaminating area.

Study of PA12/PTMG blends

The PA12/PTMG rich in PA12 was mixed with a small amount of PA12/PTMG rich in PTMG. The rheological experiments suggest that the two polymers are not fully miscible. As a result, the PA12/PTMG rich in PTMG is present under the form of droplets. Relaxation experiments on the droplets allowed to estimate the interfacial tension.

- As a consequence of the similar chemical nature of the polymers, the interfacial tension is small, about 10 times less than that for fully immiscible blends.

- Depending on the viscosity of the PA12/PTMG rich in PTMG under consideration, droplets can be too small for direct observation by means of optical microscopy.

Making use of the estimated interfacial tension and of the viscosity ratio obtained from rheological experiments, it becomes possible to calculate break-up times. One accounts for the break-up during shear and the other after cessation of shear. This allows predicting the dispersed phase morphology in an injected piece.

- Transmission electron microscopy and rheological experiments show that the droplets are polydisperse in size.

- When the material is quenched, most of the small droplets have time to break up. However, droplets bigger than a certain size become trapped in the fibril shape. Such a structure was observed by means of transmission electron microscopy on an injected piece.

The presence of fibrils within the blend is clearly a source of decohesion, since it brings a discontinuity in the matrix phase. The delamination phenomenon almost certainly originates from these morphologies. To prove this it would be worth to 'scan' over the thickness of sheared samples to study how a gradient of shear rate affects in the disposition of these fibrils/filaments. Looking at delaminating injected pieces by means of TEM, one can expect that either the fibrillar black areas will move to the high shear regions, following the shear gradient, or because fibrils are formed under shear, they can be formed and thus stabilized only in the vicinity of the high shear regions.

Suggestions for future work

In this work, a large range of morphologies has been identified for the PA12/PTMG block copolymers. Some were observed for the first time in this material. The presence of the PTMG segments makes the crystallization less sensitive to the shear imposed prior to crystallization. However far from industrial process conditions, for instance no elongational flow was applied, this suggest that the crystallinity of the PA12/PTMG rich in PA12 is hardly a source of weakening for the material since it is not much affected by flow. The last part of the study indicates that the mixing of PA12/PTMG rich in PA12 with its masterbatch carrier is imperfect,

and after injection, fibrils presence is expected. Such a morphology is suspected to weaken the material up to delamination.

An attempt to produce injected pieces that delaminate was made. On the four relevant parameters - mold and material temperatures, injection speed, and mold thickness - only the ones related to temperature could be modified in the laboratory. The mold thickness is about 1 mm and the injection speed is imposed by a piston under 4 bars pressure. These conditions appear to be not sufficient enough to induce delamination since its not observed for any of the samples prepared (mold temperature 35-50°C and polymer temperature 190-220°).

For future research on the delamination, recommendations can be formulated.

- Using injected pieces that delaminate, prepared by means of an industrial injection molding apparatus, one could follow the displacement or the morphology of the dispersed phase along the shear gradient. Such an experiment would also require the use of transmission electron microscopy since it enables the selective staining of the dispersed phase. It is anticipated that the fibrils will mainly be observed in the high shear region, close to the wall. This particular area allows the formation of fibrils as well as their fast cooling so that the fibrillar shape is maintained.

- In a practical manner, to avoid the formation of fibrils and most probably delamination as well, several parameters can be modified. First, more time could be given to the fibrils to break up by cooling down the mold at a slower rate. Second, making the dispersed phase droplets smaller would also allow the fibrils to break up faster. To do so, either the compatibility of the dispersed phase with the PA12/PTMG rich in PA12 should be increased, or the viscosity of the masterbatch carrier has to be decreased. These two options could be implemented during the synthesis of the masterbatch. Finally, one could change the processing conditions so that the masterbatch carrier is more finally dispersed. Increasing the shear rate during injection appears as an interesting choice.

The bibliography

[1] Schollenberger C.S. US PATENT 2,871,218, 1955.

[2] Schollenberger C.S., Scott H., and Moore G.R. *RUBBER CHEM TECHNOL*, 35:742, 1962.

[3] Fredrickson G.H., Milner S.T., and Leibler L. Multicritical phenomena and microphase ordering in random block copolymer melts. *MACROMOLECULES*, 25(23):6341–6354, 1992.

[4] Panyukov S. and Potemkin I. Phase diagram of microphase-separated multiblock copolymers. *PHYSICA A*, 249(1-4):321–326, 1998.

[5] Angerman H., Brinke G.T., and Erukhimovich I. Microphase separation in correlated random copolymers. *MACROMOLECULES*, 29(9):3255–3262, 1996.

[6] Leibler L. Theory of microphase separation in block copolymers. *MACROMOLECULES*, 13(6):1602–1617, 1980.

[7] Fredrikson G.H. and Milner S.T. Thermodynamics of random copolymer melts. *MACROMOLECULES*, 67(7):835–838, 1991.

[8] Kuchanov S. New results in weak segregation limit theory of block copolymers. *MACROMOL SYMP*, 252:76–89, 2007.

[9] Fredrickson G.H., Ganesan V., and Drolet F. Field-theoretic computer simulation methods for polymers and complex fluids. *MACROMOLECULES*, 35(1):16–39, Jan 2002.

[10] http://www.princeton.edu/∼polymer/block.html adapted from Matsen M.W. and Bates F.S. Unifying weak- and strong-segregation block copolymer theories. *MACROMOLECULES*, 29(4):1091–1098, 1996.

[11] Bates F.S. and Fredrickson G.H. Block copolymer thermodynamics: Theory and experiment. *ANNU REV PHYS CHEM*, 41:525–557, 1990.

[12] Hashimoto T. Time-dependent ginzburg-landau approach for microphase-separation kinetics of block polymers. *MACROMOLECULES*, 20(2):465–468, 1987.

[13] Hashimoto T., Ogawa T., and Han C.D. Determination of sharpness of order-disorder transition of block-copolymers by scattering methods. *J PHYS SOC JPN*, 63(6):2206–2214, 1994.

[14] Kim J.K., Lee H.H., Gu Q-J., Chang T., and Jeong Y.H. Determination of order-order and order-disorder transition temperatures of sis block copolymers by differential scanning calorimetry and rheology. *MACROMOLECULES*, 31(12):4045–4048, 1998.

[15] Han C.D., Baek D.M., Kim J.K., and Chu S.G. Rheological behaviour of block copolymers in the disordered state: effects of molecular weight and block length ratio. *POLYMER*, 33(2):294–305, 1992.

[16] Rosedale J.H. and Bates F.S. Rheology of ordered and disordered symmetric poly(ethylenepropylene) poly(ethylene) diblock. *J CHEM PHYS*, 92(10):6255–6270, 1990.

[17] Stuhn B., Mutter R., and Albrecht T. Direct observation of structure formation at the temperature-driven order-to-disorder transition in diblock copolymers. *EUROPHYS LETT*, 18(5):427–432, 1992.

[18] Wolff T., Burger C., and Ruland W. Synchrotron SAXS study of the microphase separation transition in diblock copolymers. *MACROMOLECULES*, 26(7):1707–1711, 1993.

[19] Ogawa T., Sakamoto N., Hashimoto T., Han C.D., and Baek D.M. Effect of volume fraction on the order-disorder transition in low molecular weight polystyrene-block-polyisoprene copolymers .2. order-disorder transition temperature determined by small-angle x-ray scattering. *MACROMOLECULES*, 29(6):2113–2123, 1996.

[20] Veenstra H., Hoogvliet R.M., Norder B., and Posthuma De Boer A. Microphase separation and rheology of a semicrystalline poly(ether-ester) multiblock copolymer. *J POLYM SCI POL PHYS*, 36(11):1795–1804, 1998.

[21] Huang J., Lisowski M.S., Runt J., Hall E.S., Kean R.T., Buehler N., and Lin J.S. Crystallization and microstructure of poly(l-lactide-co-meso-lactide) copolymers. *MACROMOLECULES*, 31(8):2593–2599, 1998.

[22] Wu S.S., Kalika D.S., Lamonte R.R., and Makhija S. Crystallization and melting and relaxation of modified poly(phenylene sulfide) .1. calorimetric studies. *J MACROMOLECULAR SCI PHYS*, 35(2):157–178, 1996.

[23] Leung L.M. and Koberstein J.T. DSC annealing study of microphase separation and multiple endothermic behavior in polyether-based polyurethane block copolymers. *MACROMOLECULES*, 19(3):706–713, 1986.

[24] Ryan A.J., Macosko C.W., and Bras W. Order-disorder transition in block copolyurethane. *MACROMOLECULES*, 25(23):6277–6283, 1992.

[25] Legge N.R., Holden G., and Schroeder H.E. *Thermoplastic elastomers: a comprehensive review*. Hanser Publishers, Munich, 1987.

[26] Deleens G. A new generation of thermoplastic elastomers, the polyether block amides. *SPE ANTEC*, page 419, 1981.

[27] *Internal data of Arkema*.

[28] Kumaraswamy G. Crystallization of polymers from stressed melts. *J MACROMOL SCI-POL R*, C45(4):375–397, 2005.

[29] Wunderlich B. *Crystal nucleation, growth, annealing*. Macromolecular physics Vol. 2. Academic Press, New York, 1976.

[30] Hoffman J.D. and Lauritzen Jr. J.I. Crystallization of bulk polymers with chain folding: Theory of growth of lamellar spherulites. *J RES NATL BUR STAND*, 65A:297–336, 1961.

[31] Pogodina N.V., Lavrenko V.P., Srinivas S., and Winter H.H. Rheology and structure of isotactic polypropylene near the gel point: quiescent and shear-induced crystallization. *POLYMER*, 42(21):9031–9043, 2001.

[32] Devaux N., Monasse B., Haudin J-M., Moldenaers P., and Vermant J. Rheooptical study of the early stages of flow enhanced crystallization in isotactic polypropylene. *RHEOL ACTA*, 43(3):210–222, 2004.

[33] Olmsted P.D., Poon W.C.K., McLeish T.C.B., Terril N.J., and Ryan A.J. Spinodal assisted crystallization in polymer melts. *PHYS REV LETT*, 81(2):373–376, 1998.

[34] Muthukumar M. Modeling polymer crystallization in interphases and mesophases in polymer crystallization III], journal = ADV POLYM SCI, year = 2005, volume = 191, number = , pages = 241-274,

[35] Janeschitz-Kriegl H., Ratajski E., and Wippel H. The physics of athermal nuclei in polymer crystallization. *COLLOID POLYM SCI*, 277:217–226, 1999.

[36] Strobl G.R. *The Physics of Polymers*. Springer, New York, 1997.

[37] Mandelkern L. *Crystallization of Polymers*. Cambridge University Press, 2004.

[38] Wunderlich B. *Macromolecular Physics*, volume 1-3. Academic Press, San Diego, 1976.

[39] Mandelkern L. *Crystallization of Polymers*. McGraw-Hill Book Co, New York, 1964.

[40] Hoffman J.D. and Miller R.L. Kinetics of crystallization from the melt and chain folding in polyethylene fractions revisited: Theory and experiment. *POLYMER*, 38(13):3151–3212, 1997.

[41] Sadler D.M. and Gilmer G.H. A model for chain folding in polymer crystals: rough growth faces are consistent with the observed growth rates. *POLYMER*, 25(10):1446–1452, 1984.

[42] Strobl G. From the melt via mesomorphic and granular crystalline layers to lamellar crystallites: A major route followed in polymer crystallization? *EUR PHYS J E*, 3:165–183, 2000.

[43] Vleeshouwers S. and Meijer H.E.H. A rheological study of shear induced crystallization. *RHEOL ACTA*, 35(5):391–399, 1996.

[44] Chai C.K., Auzoux Q., Randrianatoandro H., Navard P., and Haudin J-M. Influence of pre-shearing on the crystallisation of conventional and metallocene polyethylenes. *POLYMER*, 44(3):773–782, 2003.

[45] Pogodina N.V., Winter H.H., and Srinivas S. Strain effects on physical gelation of crystallizing polypropylene. *J POLYM SCI POLYM PHYS*, 37:3512–3519, 1999.

[46] Pogodina N.V., Lavrenko V.P., Srinivas S., and Winter H.H. Rheology and structure of isotactic polypropylene near the gel point: quiescent and shear-induced crystallization. *POLYMER*, 42(21):9031–9043, 2001.

[47] Andersen P.G. and Carr S.H. Crystal nucleation in sheared polymer melts. *POLYM ENG SCI*, 18(3):215–221, 1978.

[48] Lagasse R.R. and Maxwell B. An experimental study of the kinetics of polymer crystallization during shear flow. *POLYM ENG SCI*, 16(3):189–199, 1976.

[49] Sherwood C.H., Price F.P., and Stein R.S. Effect of shear on crystallization kinetics of poly(ethylene oxide) and poly(epsilon-caprolactone) melts. *J POLYM SCI POLYM SYMP*, 63(1):77–94, 1978.

[50] Kobayashi K. and Nasegawa T. Crystallization of sheared polymer melts. *J MACROMOL SCI B*, B4(2):331–345, 1970.

[51] Monasse B. Nucleation and anisotropic crystalline growth of polyethylene under shear. *J MATER SCI*, 30:5002–5012, 1995.

[52] Janeschitz-Kriegl H., Ratajski E., and Stadlbauer M. Flow as an effective promotor of nucleation in polymer melts: a quantitative evaluation. *RHEOL ACTA*, 42(4):355–364, 2003.

[53] Koscher E. and Fulchiron R. Influence of shear on polypropylene crystallization: morphology development and kinetics. *POLYMER*, 43(25):6931–6942, 2002.

[54] Jay F., Haudin J.M., and Monasse B. Shear-induced crystallization of polyproprylenes: Effect of molecular weight. *J MATER SCI*, 34:2089–2102, 1999.

[55] Duplay C., Monasse B., Haudin J.M., and Costa J-L. Shear-induced crystallization of polypropylene: Influence of molecular structure. *POLYM INT*, 48:320–326, 1999.

[56] Duplay C., Monasse B., Haudin J.M., and Costa J-L. Shear-induced crystallization of polypropylene: Influence of molecular weight. *J MATER SCI*, 35:6093–6103, 2000.

[57] Haudin J.M., Duplay C., Monasse B., and Costa J-L. Shear-induced crystallization of polypropylene. growth enhancement and rheology in the crystallization range. *MACROMOL SYMP*, 185:119–133, 2002.

[58] Monasse B. Polypropylene nucleation on a glass fire after melting shearing. *J MATER SCI*, 27:6047–6052, 1992.

[59] Tribout C., Monasse B., and Haudin J.M. Experimental study of shear-induced crystallization of an impact polypropylene copolymer. *COLLOID POLYM SCI*, 274(3):197–208, 1996.

[60] Hadinata C., Gabriel C., Ruellman M., and Laun H.M. Comparison of shear-induced crystallization behavior of PB-1 samples with different molecular weight distribution. *J RHEOL*, 49:327–349, 2005.

[61] Varga J. and Karger-Kocsis J. Rules of supermolecular structure formation in sheared isotactic polypropylene melts. *J POLYM SCI POLYM PHYS*, 34:657–670, 1996.

[62] Martins J.A., Zhang W., Carvalho V., Brito A.M., and Soares F.O. Evaluation of the sample temperature increase during the quiescent and shear-induced isothermal crystallization of polyethylene. *POLYMER*, 44(26):8071–8079, 2003.

[63] Watanabe K., Suzuki T., Masubuchi Y., Taniguchi T., Takimoto J., and Koyama K. Crystallization kinetics of polypropylene under high pressure and steady shear flow. *POLYMER*, 44(19):5843–5849, 2003.

[64] Hill M.J. and Keller A. Further studies on polyethylene crystallized under stress: Morphology, calorimetry and stress relaxation. *J MACROMOL SCI B*, B5(3):591–616, 1971.

[65] Samon J.M., Schultz J.M., Hsiao B.S., Seifert S., Stribeck N., Gurke I., Saw C., and Collins G. Structure development during the melt spinning of polyethylene and poly(vinylidene fluoride) fibers by in situ synchrotron small- and wide-angle x-ray scattering techniques. *MACROMOLECULES*, 32(24):8121–8132, 1999.

[66] Somani R.H., Yang L., and Hsiao B.S. Precursors of primary nucleation induced by flow in isotactic polypropylene. *PHYSICA A*, 304(1-2):145–157, 2002.

[67] Yang L., Somani R.H., Sics I., Hsiao B.S., Kolb R., Fruitwala H., and Ong C. Shear-induced crystallization precursor studies in model polyethylene blends by in-situ rheo-SAXS and rheo-WAXD. *MACROMOLECULES*, 37(13):4845–4859, 2004.

[68] Somani R.H., Yang L., Sics I., Hsiao B.S., Pogodina N.V., Winter H.H., Agarwal P., Fruitwala H., and Tsou A. Orientation-induced crystallization in isotactic polypropylene melt by shear deformation. *MACROMOL SYMP*, 185:105–117, 2002.

[69] Somani R.H., Yang L., Hsiao B., Sun T., Pogodina N.V., and Lustiger A. Shear-induced molecular orientation and crystallization in isotactic polypropylene: Effects of the deformation rate and strain. *MACROMOLECULES*, 38(4), 2005.

[70] Somani R.H. Structure development during shear flow induced crystallization of i-PP: In situ wide-angle x-ray diffraction study. *MACROMOLECULES*, 34(17):5902–5909, 2001.

[71] Nogales A., Hsiao B.S., Somani R.H., Srinivas S., Tsou A.H., Balta-Calleja F.J., and Ezquerra T.A. Shear-induced crystallization of isotactic polypropylene with different molecular weight distributions: in situ small- and wide-angle x-ray scattering studies. *POLYMER*, 42(12):5247–5256, 2001.

[72] Agarwal P.K., Somani R.H., Weng W., Mehta A., Yang L., Ran S., Liu L., and Hsiao B.S. Shear-induced crystallization in novel long chain branched polypropylenes by in situ rheo-SAXS and -WAXD. *POLYMER*, 36(14):5226–5235, 2003.

[73] Somani R.H. Shear-induced precursor structures in isotactic polypropylene melt by in-situ rheo-SAXS and rheo-WAXD studies. *MACROMOLECULES*, 35(24):9096–9104, 2002.

[74] Somani R.H., Hsiao B.S., Nogales A., Srinivas S., Tsou A.H., Sics I., Balta-Calleja F.J., and Ezquerra T.A. Structure development during shear flow-induced crystallization of i-PP: In-situ small-angle x-ray scattering study. *MACROMOLECULES*, 33(25):9385–9394, 2000.

[75] Kumaraswamy G., VerMa R.K., Kornfield J.A., Yeh F., and Hsiao B.S. Shear-enhanced crystallization in isotactic polypropylene. in-situ synchrotron SAXS and WAXD. *MACROMOLECULES*, 37(24):9005–9017, 2004.

[76] Moitzi J. and Skalicky P. Shear-induced crystallization of isotactic polypropylene melts: isothermal WAXS experiments with synchrotron radiation. *POLYMER*, 34(15):3168–3172, 1993.

[77] Goeschel U., Swartjes F.H.M., Peters G.W.M., and Meijer H.E.H. Crystallization in isotactic polypropylene melts during contraction flow: time-resolved synchrotron WAXD studies. *POLYMER*, 41(4):1541–1550, 2000.

[78] Li L.B. and de Jeu W.H. Shear-induced crystallization of poly(butylene terephthalate): A real-time small-angle x-ray scattering study. *MACROMOLECULES*, 37(15):5646, 2004.

[79] Kolb R., Kolb R., Seifert S., Stribeck N., and Zachmann H.G. Simultaneous measurements of small- and wide-angle x-ray scattering during low speed spinning of poly(propylene) using synchrotron radiation. *POLYMER*, 41(4):1497–1505, 2000.

[80] Pople J.A., Mitchell G.R., and Chai C.K. In-situ time-resolving wide-angle x-ray scattering study of crystallization from sheared polyethylene melts. *POLYMER*, 37(18):4187–4191, 1996.

[81] Marco Y., Chevalier L., and Chaouche M. WAXD study of induced crystallization and orientation in poly(ethylene terephthalate) during biaxial elongation. *POLYMER*, 43(24):6569–6574, 2002.

[82] Wolkowicz M.D. Nucleation and crystal growth in sheared poly(1-butene) melts. *J POLYM SCI POLYM SYMP*, 63(1):365–382, 1978.

[83] Abuzaina F.M., Fitz B.D., Andjelić S., and Jamiolkowski D.D. Time resolved study of shear-induced crystallization of poly(p-dioxanone) polymers under low-shear, nucleation-enhancing shear conditions by small angle light scattering and optical microscopy. *POLYMER*, 43(17):4699–4708, 2002.

[84] Ulrich R.D. and Price F.P. Morphology development during shearing of poly(ethylene oxide) melts. *J APPL POLYM SCI*, 20:1077–1093, 1976.

[85] Ma C.G., Chen L., Xiong X., Zhang J.X., Rong M.Z., and Zhang M.Q. Influence of oscillatory shear on crystallization of isotactic polypropylene studied by dynamic mechanical analysis. *MACROMOLECULES*, 37(24):8829, 2004.

[86] Floudas G., Hiliou L., Lellinger D., and Alig I. Shear-induced crystallization of poly(-caprolactone). 2. evolution of birefringence and dichroism. *MACROMOLECULES*, 33(17):6466–6472, 2000.

[87] Yoon W.J., Myung H.S., Kim B.C., and Im S.S. Effect of shearing on crystallization behavior of poly(ethylene naphthalate). *POLYMER*, 41(13):4933–4942, 2000.

[88] Bove L. and Nobile M.R. Shear flow effects on polymer melts crystallization: kinetics features. *MACROMOL SYMP*, 180:169–180, 2002.

[89] Bove L. and Nobile M.R. Shear-induced crystallization of isotactic poly(1-butene). *MACROMOL SYMP*, 185:135–147, 2002.

[90] Hobbs J.K. and Miles M.J. Direct observation of polyethylene shish-kebab crystallization using in-situ atomic force microscopy. *MACROMOLECULES*, 34(3):353–355, 2001.

[91] Elmoumni A., Winter H.H., Waddon A.J., and Fruitwala H. Correlation of material and processing time scales with structure development in isotactic polypropylene crystallization. *MACROMOLECULES*, 36(17):6453–6461, 2003.

[92] Keller A. and Kolnaar H.W.H. *Material Science and Technology: A Comprehensive Treatment*, volume 18, chapter Flow-induced Orientation and Structure Formation, pages 191–268. VCH Publishers, New York, 1997.

[93] Binsbergen F.L. Orientation-induced nucleation in polymer crystallization. *NATURE*, 211:516–517, 1966.

[94] Hill M.J. and Keller A. Direct evidence for distinctive stress-induced nucleus crystals in the crystallization of oriented polymer melts. *J MACROMOL SCI B*, B3(1):153–169, 1969.

[95] Odell J.A., Grubb D.T., and Keller A. A new route to high modulus polyethylene by lamellar structures nucleated onto fibrous substrates with general implications for crystallization behaviour. *POLYMER*, 19(6):617–626, 1978.

[96] Bashir Z., Odell J.A., and Keller A. High modulus filaments of polyethylene with lamellar structure by melt processing: The role of high molecular weight component. *J MATER SCI*, 19:3713–3725, 1984.

[97] Hsiao B.S., Yang L., Somani R.H., Avila-Orta C.A., and Zhu L. Unexpected shish-kebab structure in a sheared polyethylene melt. *PHYS REV LETT*, 94(117802), 2005.

[98] Monks A.W., White H.M., and Bassett D.C. On shish-kebab morphologies in crystalline polymers. *POLYMER*, 37(26):5933–5936, 1996.

[99] Bashir Z., Odell J.A., and Keller A. Stiff and strong polyethylene with shish kebab morphology by continuous melt extrusion. *J MATER SCI*, 21(11), 1986.

[100] Hay I.L. and Keller A. A study on orientation effects in polyethylene in the light of crystalline texture. *J MATER SCI*, 2(6):538–558, 1967.

[101] Keller A. and Machin M.J. Oriented crystallization in polymers. *J MACROMOLECULAR SCI PHYS*, 1(1):41–91, 1967.

[102] Peterlin A. *PURE APPL CHEM: MACROMOL CHEM*, 8:277, 1973.

[103] Pople J.A., Mitchell G.R., Sutton S.J., Vaughan A.S., and Chai C.K. The development of organized structures in polyethylene crystallized from a sheared melt, analyzed by WAXS and TEM. *POLYMER*, 40(10):2769–2777, 1999.

[104] Hamley I.W. Crystallization in block copolymers. *ADV POLYM SCI*, 148:113, 1999.

[105] Biemond G.J.E., Feijen J., and Gaymans R.J. Influence of polydispersity of crystallizable segments on the properties of segmented block copolymers. *POLYM ENG SCI*, 48(7):1389–1400, May 2008.

[106] Hamley I.W., Fairclough J.P.A., Terrill N.J., Ryan A.J., Lipic P.M., Bates F.S., and Towns-Andrews E. Crystallization in oriented semicrystalline diblock copolymers. *MACROMOLECULES*, 29(27):8835–8843, 1996.

[107] Nojima S., Kato K., Yamamoto S., and Tamaichi A. Crystallization of block copolymers. 1. small-angle x-ray scattering study of a .epsilon.-caprolactone-butadiene diblock copolymer. *MACROMOLECULES*, 25(8):2237–2242, 1992.

[108] Nojima S., Nakano H., Yamamoto S., and Ashida T. Crystallization of block copolymers: 3. crystallization behaviour of an var epsilon-caprolactone-butadiene diblock copolymer. *POLYMER*, 35(16):3479–3486, 1994.

[109] Nojima S., Nakano H., and Ashida T. Crystallization behaviour of a microphase-separated diblock copolymer. *POLYMER*, 34(19):4168–4170, 1993.

[110] Rangarajan P., Register R.A., Adamson D.H., Fetters L.J., Bras W., Naylor S., and Ryan A.J. Dynamics of structure formation in crystallizable block copolymers. *MACROMOLECULES*, 28(5):1422–1428, 1995.

[111] Rangarajan P., Register R.A., Fetters L.J., Bras W., Naylor S., and Ryan A.J. Crystallization of a weakly segregated polyolefin diblock copolymer. *MACROMOLECULES*, 28(14):4932–4938, 1995.

[112] Sauer B.B., Mclean R.S., Brill D.J., and Londono D.J. Morphology and orientation during the deformation of segmented elastomers studied with small-angle x-ray scattering and atomic force microscopy. *J POLYM SCI POL PHYS*, 40(16):1727–1740, 2002.

[113] Konyukhova E.V., Neverov V.M., Chvalun S.N., and Godovsky Y.K. Reversible stress-induced crystallization of the soft phase in polyblock thermoplastic elastomers under uniaxial tension. *POLYMER Science Series A*, 46(1):61–74, 2004.

[114] Angerman H.J. The phase behavior of polydisperse multiblock copolymer melts : (a theoretical study). *Ph.D. thesis, University of Groningen*, 1998.

[115] Shiomi T., Tsukada H., Takeshita H., Takenaka K., and Tezuka Y. Crystallization of semicrystalline block copolymers containing a glassy amorphous component. *POLYMER*, 42(11):4997–5004, 2001.

[116] Ryan A.J., Hamley W.I., Bras W., and Bates F.S. Structure development in semicrystalline diblock copolymers crystallizing from the ordered melt. *MACROMOLECULES*, 28(11):3860–3868, 1995.

[117] Quiram D.J., Register R.A., and Marchand G.R. Crystallization of asymmetric diblock copolymers from microphase-separated melts. *MACROMOLECULES*, 30(16):4551–4558, 1997.

[118] Quiram D.J., Register R.A., Marchand G.R., and Ryan A.J. Dynamics of structure formation and crystallization in asymmetric diblock copolymers. *MACROMOLECULES*, 30(26):8338–8343, 1997.

[119] Douzinas K.C. and Cohen R.E. Chain folding in ethylene-butylene-ethylethylene semicrystalline diblock copolymers. *MACROMOLECULES*, 25(19):5030–5035, 1992.

[120] Vasilev C., Reiter G., Pispas S., and Hadjichristidis N. Crystallization of block copolymers in restricted cylindrical geometries. *POLYMER*, 47(1):330–340, 2006.

[121] Chen H-L., Hsiao S-C., Lin T-L., Yamauchi K., Hasegawa H., and Hashimoto T. Microdomain-tailored crystallization kinetics of block copolymers. *MACROMOLECULES*, 34(4):671–674, 2001.

[122] Loo Y-L., Register R.A., and Ryan A.J. Modes of crystallization in block copolymer microdomains: Breakout, templated, and confined. *MACROMOLECULES*, 35(6):2365–2374, 2002.

[123] Tucker III Charles L. and Moldenaers P. Microstructural evolution in polymer blends. *ANNU REV FLUID MECH*, 34:177–210, 2002.

[124] Grace H.P. Dispersion phenomena in high viscosity immiscible fluid systems and application of static mixers as dispersion devices in such systems. *CHEM ENG COMMUN*, 14:225, 1982.

[125] Taylor G.I. The viscosity of a fluid containing small drops of another fluid. *P ROY SOC LOND A MAT*, A138:41–48, 1932.

[126] Taylor G.I. The formation of emulsions in definable fields of flow. *P ROY SOC LOND A MAT*, A146:501–523, 1934.

[127] Van Puyvelde P. Flow-induced morphology changes in immiscible polymer blends: A rheo-optical study. *Ph.D. thesis, Katholiek Universiteit Leuven*, 1999.

[128] Rumscheidt F.D. and Mason S.G. Particle motions in sheared suspensions XII. deformation and burst of fluid drops in shear and hyperbolic flow. *J COLLOID SCI*, 16(3):238–261, 1961.

[129] Rayleigh J.W.S. On the instability of jets. *P ROY SOC LOND A MAT*, 10:4–13, 1879.

[130] Tomotika S. On the instability of a cylindrical thread of a viscous liquid surrounded by another viscous fluid. *P ROY SOC LOND A MAT*, A150:322–337, 1935.

[131] Rossignol J.M. *Internal report Arkema*, 1988.

[132] Mathias L.J. and Greg J.C. Solid-state NMR investigation of nylon 12. *MACROMOLECULES*, 24(23):6114–6122, 1991.

[133] Arimoto H., Ishibashi M., Hirai M., and Chatani Y. Crystal structure of the γ-form of nylon 6. *J POLYM SCI PART A*, 3(1):317–326, 1962.

[134] Li L., Koch M.H.J., and de Jeu W.H. Crystalline structure and morphology in nylon-12: A small- and wide-angle x-ray scattering study. *MACROMOLECULES*, 36(5):1626–1632, 2003.

[135] Owen A.J. and Kollross P. A note on the crystal-structure of nylon-12. *POLYM COMMUN*, 24(10):303–306, 1983.

[136] Hashimoto T., Okamoto S., Saijo K., KimishiMa K., and Kume T. Time-resolved small-angle and wide-angle x-ray scattering apparatus using the imaging plate as a two-dimensional detector. *ACTA POLYM*, 46(6):463–470, 1995.

[137] Hatfield G.R., Guo Y., Killinger W.E., Andrejak R.A., and Roubicek P.M. Characterization of structure and morphology in two poly(ether-block-amide) copolymers. *MACROMOLECULES*, 26(24):6350–6353, 1993.

[138] Sheth J.P., Xu J., and Wilkes G.L. Solid state structure-property behavior of semicrystalline poly(ether-block-amide) Pebax thermoplastic elastomers. *POLYMER*, 44(3):743–756, 2003.

[139] Boublil H., Okoroafor E., Belhoucine M., Rault J., and Glotin M. Morphology of polyamide and polyether block amide blends. *POLYM ENG SCI*, 29(10):303–306, 1989.

[140] Laity P.R., Taylor J.E., Wong S.S., Khunkamchoo P., Norris K., Cable M., Andrews G.T., Johnson A.F., and Cameron R.E. A review of small-angle scattering models for random segmented poly(ether-urethane) copolymers. *POLYMER*, 45(21):7273–7291, 2004.

[141] Lee D., Lee S-H., Kim S., Char K., Park J.H., and Yoo H.B. Micro-phase-separation behavior of amphiphilic polyurethanes involving poly(ethylene oxide) and poly(tetramethylene oxide). *J POLYM SCI POL PHYS*, 41(20):2365–2374, 2003.

[142] Nichetti D. and Grizzuti N. Determination of the phase transition behavior of thermoplastic polyurethanes from coupled rheology/DSC measurements. *POLYM ENG SCI*, 44(8):1514–1521, 2004.

[143] Hamley I.W. and Castelletto V. Small-angle scattering of block copolymers in the melt, solution and crystal states. *PROG POLYM SCI*, 29:909–948, 2004.

[144] Cho J. Analysis of phase separation in compressible polymer blends and block copolymers. *MACROMOLECULES*, 33(6):2228–2241, 2000.

[145] Gabriëlse W., Soliman M., and Dijkstra K. Microstructure and phase behavior of block copoly(ether ester) thermoplastic elastomers. *MACROMOLECULES*, 34(6):1685–1693, 2001.

[146] Helfand E. and Lauritzen Jr. J.I. Theory of copolymer crystallization. *MACROMOLECULES*, 6(4):631–638, 1973.

[147] Li L., Séréro Y., Koch M.H.J., and de Jeu W.H. Microphase separation and crystallization in an asymmetric diblock copolymer: Coupling and competition. *MACROMOLECULES*, 36(3):529–532, 2003.

[148] Lewis C.L. and Spruiell J.E. Crystallization of 2-methyl-1,3-propanediol substituted poly(ethylene terephthalate). I. thermal behavior and isothermal crystallization. *J APPL POLYM SCI*, 100(4):2592–2603, 2006.

[149] Fougnies C., Damman P., Dosiere M., and Koch M.H.J. Time-resolved SAXS, WAXS, and DSC study of melting of poly(aryl ether ether ketone) (peek) annealed from the amorphous state. *MACROMOLECULES*, 30(5):1392–1399, 1997.

[150] Marigo A., Causin V., Marega C., and Ferrari P. Crystallization of the γ form in random propylene-ethylene copolymers. *POLYM INT*, 53(12):2001–2008, 2004.

[151] Rabiej S. On the origin of the multiple melting observed after isothermal crystallization of homogeneous ethylene/1-octene copolymers. *POLIMERY*, 49(6):414–423, 2004.

[152] Jeong Y.G., Jo W.H., and Lee S.C. Synthesis and structure and and thermal property of poly(trimethylene terephthalate-co-trimethylene 2,6-naphthalate) copolymers. *FIBER POLYM*, 5(3):245–251, 2004.

[153] Jokela K., Väänänen A., Torkkeli M., Starck P., Serimaa R., Löfgren B., and Seppälä J. Differential scanning calorimetry, small-angle x-ray scattering, and wide-angle x-ray scattering on homogeneous and heterogeneous ethylene-α-copolymers. *J POLYM SCI POL PHYS*, 39(16):1860–1875, 2001.

[154] Medellin-Rodriguez F., Phillips P., and Lin J.S. Melting behavior of high-temperature polymers. *MACROMOLECULES*, 29(23):7491–7501, 1996.

[155] Li Y.J., Yan D.Y., and Zhang G.S. Crystalline structure and thermal behavior of nylon-10,14. *J POLYM SCI POL PHYS*, 41(12):1422–1427, Jun 15 2003.

[156] Gedde U.W. *Polymers Physics*. Springer, New York, 1995.

[157] Hoffman J.D. and Weeks J.J. Rate of spherulitic crystallization with chain folds in polychlorotrifluoroethylene. *J CHEM PHYS*, 32(8):1723–1741, 1962.

[158] Bond E.B. and Spruiell J.E. The effects of atacticity and comonomer content and and configurational defects on the equilibrium melting temperature of monoclinic isotactic polypropylene. *J APPL POLYM SCI*, 81(1):229–236, 2001.

[159] Vannini M., Finelli L., Lotti N., Colonna M., Lorenzetti C., and Munari A. Thermal behavior and crvstallization kinetics of random poly(ethylene-co-2,2-bis[4-(ethylenoxy)-1,4-phenylene]propane terephthalate) copolyesters. *J POLYM SCI POL PHYS*, 43(12):1441–1454, 2005.

[160] Cao J., Su W., Wu Z., Liu J., Kitayama T., and Hatada K. Crystallization behaviour of poly(ether ether ketone)/poly(ether sulfone) block copolymer. *POLYMER*, 37(20):4579–4584, 1996.

[161] Plummer C.J.G., Zanetto J.E., Bourban P.E., and Manson J.A.E. The crystallization kinetics of polyamide-12. *COLLOID POLYM SCI*, 279(4):312–322, 2001.

[162] Flory P.J. and Mandelkern L. Melting of copolymers. *J POLYM SCI*, 21(98):345–348, 1956.

[163] Hamley I.W. Chain folding in crystallizable block copolymers. *ADV POLYM SCI*, 148:ADV POLYM SCI, 1999.

[164] Hsiao B.S. and Chu B. Small-angle x-ray scattering of polymers. *CHEM REV*, 101(6):1727–1761, 2001.

[165] Strobl G.R., Schneider M.J., and Voigtmartin I.G. Direct evaluation of the electron-density correlation-function of partially crystalline polymers. *J POLYM SCI POL PHYS*, 18(6):1343–1359, 1980.

[166] Kuchanov S., Pichugin V., and Brinke G.T. Phase behavior of weakly-segregated multiblock copolymers with two-scale periodic architecture. *MAKROMOLEKUL CHEM*, (12), 2006.

[167] Glatter O. and Kratky O. *Small Angle X-ray scattering*. Academic Press, New York, 1982.

[168] Ryan A.J., Fairclough J.P.A., Hamley I.W., Mai S-M., and Booth C. Chain folding in crystallizable block copolymers. *MACROMOLECULES*, 30(6):1723–1727, 1997.

[169] McKiernan R.L., Heintz A.M., Hsu S.L., Atkins E.D.T., Penelle J., and Gido S.P. Influence of hydrogen bonding on the crystallization behavior of semicrystalline polyurethanes. *MACROMOLECULES*, 35(18):6970–6974, 2002.

[170] Stein R.S. and Wilson P.R. Scattering of light by polymer films possessing correlated orientation functions. *J APPL PHYS*, 33(6):1914–1922, 1962.

[171] Baert J., Van Puyvelde P., and Langouche F. Flow-induced crystallization of PB-1: From the low shear rate region up to processing rates. *MACROMOLECULES*, 39(26):9215–9222, 2006.

[172] Koberstein J., Russel T.P., and Stein R.S. Total integrated light-scattering intensity from polymeric solids. *J POLYM SCI, POLYM PHYS ED*, 17:1719–1730, 1979.

[173] Debye P. and Bueche A.M. Scattering by an inhomogeneous solid. *J APPL PHYS*, 20:518–525, 1949.

[174] Pogodina N.V. and Winter H.H. Polypropylene crystallization as a physical gelation process. *MACROMOLECULES*, 31(23):8164–8172, 1998.

[175] Devaux N. Influence d'un cisaillement sur les premiers stades de la cristallisation du polypropylene. *Ph.D. thesis, Ecole des Mines de Paris*, 2003.

[176] Janeschitz-Kriegl H. *COLLOID POLYM SCI*, 281:1157, 2003.

[177] Acierno S., Coppola S., Grizzuti N., and Maffettone P.L. Coupling between kinetics and rheological parameters in the flow-induced crystallization of thermoplastic polymers. *MACROMOL SYMP*, 185:233–241, Aug 2002.

[178] Palierne J.F. Linear rheology of viscoelastic emulsions with interfacial tension. *RHEOL ACTA*, 29(3):1435–1528, 1990.

[179] Vinckier I., Moldenaers P., and Mewis J. Relationship between rheology and morphology of model blends in steady shear flow. *J RHEOL*, 40(4):613–631, 1996.

[180] Pozdzal R. and Rolaniec Z. Rheological properties of multiblock ether-ester copolymers. *KAUT GUMMI KUNSTST*, 52(10):656–662, Oct 1999.

[181] Macosko C.M. *Rheology, Principles, Measurements and Applications*. VCH Publishers, New York, 1994.

[182] Van Puyvelde P., Yang H., Mewis J., and Moldenaers P. Breakup of filaments in blends during simple shear flow. *J RHEOL*, 44(6):1401–1415, 2000.

[183] Janssen J.M.H. Dynamic of liquid-liquid mixing. *Ph.D. thesis, Technische Universiteit Eindhoven*, 1993.

[184] Elemans P.H.M., Bos H.L., Janssen J.M.H., and Meijer H.E.H. Transient phenomena in dispersive mixing. *CHEM ENG SCI*, 48:267–276, 1993.

List of publications

Publication in International Journal

- Tavernier B., Mewis J., Van Puyvelde P., Takenaka M., Ernst B. and Hashimoto T., *Effect of thermomechanical history on the crystallization of poly(ether-block-amide)*, POLYMER ENGINEERING AND SCIENCE 48(12):2418-2425 ,2008.

Congress Contribution

- Tavernier B., Hashimoto T., M. Takenaka, Mewis J. and Van Puyvelde P., *Morphological studies of polyamide-polyether multiblock copolymers*, 54th Annual Meeting of The Society of Polymer Science, Japan, Yokohama, Japan (2005).

Curriculum vitae

Bruno Tavernier was born in in 1980 in Saint Etienne, France. From 1998 until 2000 he attended the french preparatory courses to the Grandes Ecoles. In 2003 he obtained an engineering degree from the European Engineering School of Chemistry, Polymers and Materials Science in Strasbourg (FR) and a Master in Chemistry and Physics of Polymers, Materials and Surfaces from the University Louis Pasteur, Strasbourg (FR). The thesis involved development of fluorinated surfactant monolayers for biological applications.

In October 2003 he started his research as a PhD student at the laboratory of applied rheology and polymer processing of the department of chemical engineering at the Catholic University of Leuven.

He started working in the field of fuel cells membranes, at the National Institute of Advance Industrial Science and Technology (AIST) Tokyo, Japan in 2008.